UNIVERSITY OF CALIFORNIA
RIVERSIDE

Design and Construction of an Open Circulating Water Channel

A Thesis submitted in partial satisfaction
of the requirements for the degree of

Master of Science

in

Mechanical Engineering

by

Joseph Redenius

June 2019

Thesis Committee:
Dr. Marko Princevac, Chairperson
Dr. Monica Martinez
Dr. Sinisa Coh

The Thesis of Joseph Redenius is approved:

_____

_____

_____

Committee Chairperson

University of California, Riverside

ACKNOWLEDGEMENTS

I would first like to thank my advisor, Professor Marko Princevac, for trusting me with the water channel build and for all the advice he recommended to me with regards to not only this thesis project, but also my career goals. I would also like to thank Professor Monica Martinez for providing me with much needed advice and motivation and Professor Sinisa Coh for serving on my thesis committee as a last minute fill-in. I also want to acknowledge my graduate laboratory colleagues AmirHessam Aminfar, Masoud Ghasemian, Jeanette Cobian, Yair Sanchez, and Rosalinda Lopez for taking time out of their dissertations and research to support me with the water channel project, and all of the undergraduate students that also helped me with the design, drafting, and assembling. I also want to thank UCR's Mechanical Engineering Machine Shop, which include Matt McCormick, Steve Rightnar, and the student-volunteers, for their much needed help and general advice. I want to thank Taylor Cole, the former student who built the previous water channel, for all his expertise, and Riverside Machine Works for their fantastic work on welding and fabrication of the steel components. Lastly, I cannot thank my family and girlfriend enough for all the moral support and motivation. Through the ups and down, they inspired me every day to work hard and complete this project.

For my mother, Gloria; father, Randall; brother, Jon; and sister, Jocelyn.

Thank you for pushing me to be the best version of myself.

ABSTRACT OF THE THESIS

Design and Construction of an Open Circulating Water Channel

by

Joseph Redenius

Master of Science, Graduate Program in Mechanical Engineering
University of California, Riverside, June 2019
Dr. Marko Princevac, Chairperson

Obtaining field measurements of environmental flows provides invaluable data. However, these experiments are often difficult to repeat due to various uncontrollable factors such as background flows and surface topography. Furthermore, studying interactions between fluid dynamics and aquatic organisms in their natural habitat can be problematic since these locations are often inaccessible. Because of this, having the capability to perform and repeat hydrodynamic experiments in a controlled setting is essential because one can isolate and control these factors with relative ease of access. With this in mind, an open circulating water channel was designed and manufactured by the Laboratory for Environmental Flow Modeling at the University of California, Riverside. This channel will provide opportunities for students and researchers to study fluid behavior. The assembly was designed and optimized by integrating both fluid dynamic and mechanical design requirements of the system. The water channel consists of two settling tanks and a 13 foot long, 40 inch wide, 36 inch tall test section. One settling tank is fully transparent to enable measurements of stratified layer mixing by organism dynamics. The design process, calculations, fabrication, assembling, and future recommendations of the water channel are described in detail in this presentation.

Table of Contents

List of Figures

List of Tables

NOMENCLATURE

Upper Case Roman	Description
A	area
A_c	cross sectional area of Tank C
A_t	tensile stress area of bolt
BCM	Brittle Coulomb-Mohr
C	stiffness constant
CAD	Computer Aided Design
CFD	Computational Fluid Dynamics
E	elastic modulus
E_{flex}	flexural modulus
F_b	total tensile load on bolt
FEA	Finite Element Analysis
F_i	modified preload on bolt
F_p	preload on bolt
G	shear modulus
K	nut factor
K_h	bolt hole coefficient
LEFM	Laboratory for Environmental Flow Modeling
N	Brunt–Väisälä frequency
N_b	number of bolts
$NPSH_a$	net positive suction head available

$NPSH_r$	net positive suction head required
P	pressure, perimeter
P_{ext}	external load on bolt
PIV	Particle Image Velocimetry
PLIF	Planar Laser Induced Fluorescence
Q	volumetric flow rate
Re	Reynolds number
R_h	hydraulic radius
S	salinity
S_{uc}	ultimate compressive strength
S_{ut}	ultimate tensile strength
T	temperature
T	torque
U	mean free stream velocity
UNESCO	United Nations Educational, Scientific and Cultural Organization
V	volume
$V_{A,i}$	initial volume in Tank A
$V_{B,i}$	initial volume in Tank B
VFD	variable frequency drive
V_s	shear capacity of bolt

Lower Case Roman	Description
b	width
d	diameter
f	frequency
g	gravity
h	depth reference for density gradient
k_b	bolt stiffness
k_m	member stiffness
n_{bcm}	BCM factor of safety
n_e	number of slip resistant interfaces
n_p	proof stress factor of safety
n_{vm}	von Mises factor of safety
n_{vs}	shear safety factor
t	thickness
z	depth reference for density gradient

Greek	Description
$\delta\rho/\delta z$	density gradient
μ_f	coefficient of friction
v	Poisson ratio, kinematic viscosity
ρ	density
ρ_a	ambient density
ρ_A	freshwater density in Tank A
$\rho_{B,i}$	initial saltwater density in Tank B
$\sigma_1,\sigma_2,\sigma_3$	principal stresses
σ_b	bolt stress
σ_{flex}	flexural strength
σ_{proof}	proof strength
σ_{ucs}	ultimate compressive strength

σ_{uts}	ultimate tensile strength
σ_{vm}	Von Mises stress
σ_y	yield strength
τ_{xy}	shear stress on x face, y direction

1 Introduction

1.1 Background

Fluid flow encompasses our daily lives in various mechanics from aerodynamics, ocean currents, the circulatory system, HVAC systems, and pollutant dispersion. The impact of these flow dynamics is essential as they provide motivation for taking field measurements, performing experiments, and developing models. However, this is easier said than done: a majority of fluid flow is turbulent, complex, and large-scaled, making it difficult to determine theoretical models without oversimplification. Field measurements provide the most realistic data of flow interactions, but often contain various flow factors (topography, surface roughness, shear effects, advection, and heat transfer) that cannot be delineated for analysis. These measurements can also be costly, time consuming, and even impossible to perform depending on the site location. Computational fluid dynamics (CFD) is a useful tool to approximate and analyze flow simulations, but at times can be computationally expensive and may not always accurately represent realistic flow. Laboratory fluid configurations and measuring techniques help bridge the gap between these methods. Flow visualization and controlled measurements are essential to isolate various factors and provide test repeatability. By correlating these methods together, a proper analysis of fluid flow can be achieved.

From an academic viewpoint, experimentation and flow visualization reinforce and enhance fluid dynamic coursework for university students, provide new opportunities for researchers, and motivate the youth to pursue STEM related fields (Ekwueme *et al.*, 2015). Hands-on laboratory experiences have shown that students develop a stronger foundation

of fluid dynamic theories and greater personal satisfaction with the material (Cranston & Lock, 2012). This evidence further supports the benefits of employing laboratory set-ups.

Figure 1.1: Previous water channel located on the second floor of Bourns Hall B-wing.[1]

The center piece of the Laboratory for Environmental Flow Modeling (LEFM) at the University of California, Riverside was a circulating water channel, which was used for numerous research studies and educational purposes in external flow dynamics (Figure 1.1). However, there was a need to move the whole laboratory and the tank consequently had to be dismantled. This led to a new proposal for a redesign and build of the new circulating water channel. Although several flow and geometric features of the new water channel remained identical to the previous one, the addition of a transparent tank was designed for added research purposes involving organism hydrodynamics.

[1] Laboratory for Environmental Flow Modeling, Bourns College of Engineering, UCR. https://www.engr.ucr.edu/~marko/laboratory.htm

1.2 Project Overview and Requirements

The redesigned water channel consists of four main sections: the transparent tank, test channel, end tank, and pumping system, shown in Figures 1.2 and 1.3 on the next page. The transparent tank inner dimensions are 58.5 inches long, 46.25 inches wide, and 77.25 inches tall, with a recommended maximum working depth no larger than 66 inches. It was designed to hold a maximum of 773 gallons of water. Since Particle Image Velocimetry (PIV) measurements will be implemented for analyzing vertical fluid behavior, the tank walls were required to be transparent. Tempered glass panels ¾-inch thick were selected as the material for three of the walls, with a machined 1 inch thick acrylic sheet making up the final wall and connection to the test channel. A sloped PVC sheet was fabricated as the base of the tank for supporting the glass panels and easy draining. To reduce flexion and residual stresses in the glass, a steel frame was designed to support every edge interface of the tank. A crossmember was added to the frame design roughly three-quarters down the tank for additional flexion support. Bolts and gussets connect the individual beams together. Multiple layers of silicone sealant were added at all edges to ensure a watertight seal. Experiments in this tank will primarily focus on PIV measurements involving vertical fluid dynamics. A mechanism to separate the tank from the test section is currently undergoing design.

Figure 1.2: Redesigned water channel at Bourns Hall, located in B140.

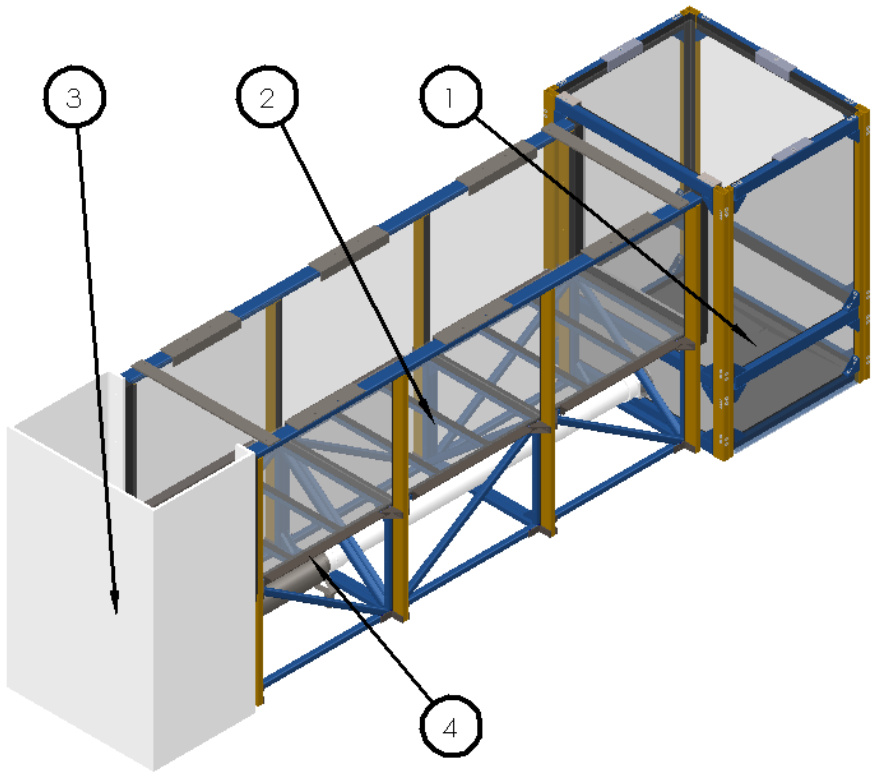

Figure 1.3: SolidWorks CAD model of water channel consisting of 1) transparent tank, 2) test channel, 3) end tank, 4) pumping system.

The dimensions of the test channel were required to be 157.5 inches long with a cross section of 40 inches wide by 43 inches deep. These dimensions were selected to closely match integer values of 4 meter length and 1 meter width for mathematical simplifications. Local vendors that were contacted could not provide dimensions in metric units, and those that could did not provide delivery. The length requirement was also influenced by the limited laboratory space and the pumping system. A 36 inch maximum depth limit determined the recommended sizing of the ¾-inch horizontal annealed glass panes and ½ inch vertical tempered side glass panes. The same 15 HP, 1500 GPM, 3 phase axial pump and several PVC connections from the previous channel were used. Flow rates are user defined and depend on the channel depth and a variable frequency drive (VFD) that controls flow velocity with fine resolution. Because of this, the pumping system was not deemed a significant section, but some information on flow circulation is available in Appendix F. A ball valve was installed between pipe sections to divide the transparent tank from the rest of the channel for experimentation purposes. The supporting frame and truss design were implemented to support 981 gallons of water and any additional dynamic loads and accommodate the pumping system underneath. The transparent tank and a polypropylene end tank that can hold 540 gallons of water enclose the test channel. A vast array of studies can be done in the test section which include boundary layer growth, urban dispersion, dye visualization, submerged body behavior, and similitude scaling. Measurements can be taken utilizing optical techniques such as PIV or Planar Laser Induced Fluorescence (PLIF) techniques.

The entire assembly and their components are meant to function as one rigid structure. However, due to the size of the project, it was decided to best optimize the design by individually analyzing sections. Undergraduate students were given the opportunity to assist in this build as part of their capstone project. Communication and teamwork became a key factor between teams since each section relied on the other. Adjustments made on one section had to be accommodated for in all other sections.

The significant components of the water channel were designed using Computer Aided Design (CAD) and analyzed for stresses using Finite Element Analysis (FEA) from SolidWorks. Meshes for every component were refined and optimized to validate simulation results. Curvature based meshes took favor over standard meshes due to their increased accuracy with complex geometries, albeit at the expense of computational time. Several iterations of increasing mesh density were tested to ensure mesh independent result. Finer meshes tend to introduce stress singularities where convergence fails, which are generally insignificant but were carefully accounted for in the simulation results.

Once the design was complete and simulations were verified, the majority of purchasing, fabrication, and manufacturing were done with local vendors. Assembly was carefully done in house, with the project timeframe fully dependent on the availability of components and unforeseen delivery and production problems that arose. A standard operating procedure was drafted to indicate general maintenance, cleaning, and precautions to take in case of accidents.

2 Transparent Tank

The primary focus for the transparent tank was ensuring that individual components did not fail and ensuring a watertight assembly. Section 2.1 lists the design requirements of the tank. Section 2.2 explains the glass and acrylic selection and dimensioning. Section 2.3 describes the PVC base and support structure for the tank. Section 2.4 reviews the bolted connection and stress calculations for the structure. For clarity, the schematic of the whole tank and its main parts in CAD are shown in Figure 2.1 and tabulated in Table 2.1 on the next page. Details regarding components' dimensions and machining are located in Appendix A. Information on the setup for creating density gradient profiles and taking measurements are given in Appendix E.

2.1 Design Requirements

The design requirements for the transparent tank include:

- transparent and observable walls to enable PIV measurements
- saltwater corrosion resistant surfaces
- prevention of organisms from entering pump
- connection with test section
- proper component/material selection, dimensioning, and machining
- failure prevention with factor of safety calculations for significant components
- creation of density gradient profiles
- method to isolate tank for experiments (this was outside the scope of the project, but the tank is designed to accommodate this feature in the future)

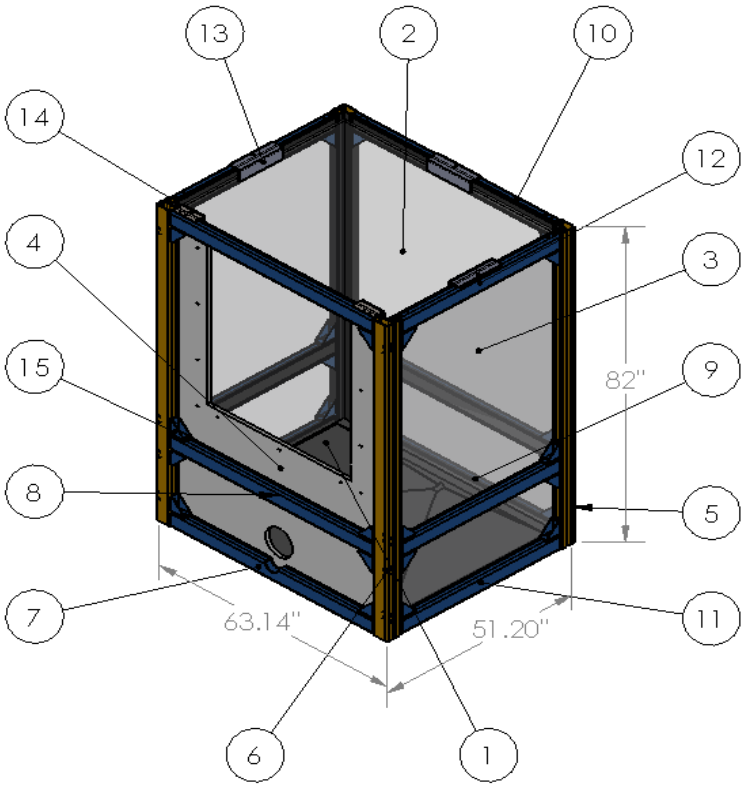

Figure 2.1: Schematic of transparent tank components. See Table 2.1 for components.

Table 2.1: Transparent tank main components.

Item No.	Component	Quantity
1	PVC Base	1
2	Rear Glass Pane	1
3	Side Glass Pane	2
4	Front Panel	1
5	Corner Beam Weld LF RB	2
6	Corner Beam Weld RF LB	2
7	Front Beam, Bottom	1
8	Front Beam, Middle and Top / Rear Beam, Middle	3
9	Rear Beam, Bottom	1
10	Rear Beam, Top	1
11	Side Beam, Bottom and Middle	4
12	Side Beam, Top	2
13	Angle Beams for Tempered Glass	3
14	Angle Beams for Plexiglass	2
15	Gussets	32

2.2 Glass and Acrylic

Glass or acrylic were the two options for the tank walls to fulfill the transparency requirement. It was decided that tempered glass be selected as the three experimental walls since 1) acrylic panels are easy to scratch and fog up over time, 2) it is 5+ times stronger than annealed glass, and 3) safety regulations and state codes require large glass panels less than 18" off the ground to be tempered. The recommended thickness for the panels was based off of the maximum stresses the glass and acrylic panels would undergo. For the principal stresses and failure criterion, a factor of safety of 3.8 is commonly used as a baseline for aquarium builds (Alho *et al.*, 2010) to account for low quality glass. The factor of safety can be calculated by two common failure theories for brittle materials: Brittle Coulomb-Mohr (BCM) and Modified Mohr. Since BCM is more conservative, it was selected for analysis. Table 2.2, directly taken from *Shigley's Mechanical Engineering Design*, gives the derived principal stress equations of the BCM criterion per quadrant of Mohr's failure lines. These equations are derived from Equation 2.4 on page 13.

Table 2.2: Brittle Coulomb-Mohr design equations.

Quadrant	Equation
$\sigma_1 \geq \sigma_3 \geq 0$	$\sigma_1 = \frac{S_{ut}}{n_{bcm}}$ (2.1)
$\sigma_1 \geq 0 \geq \sigma_3$	$\frac{\sigma_1}{S_{ut}} - \frac{\sigma_3}{S_{uc}} = \frac{1}{n_{bcm}}$ (2.2)
$0 \geq \sigma_1 \geq \sigma_3$	$\sigma_3 = -\frac{S_{uc}}{n_{bcm}}$ (2.3)

The rear glass pane was a component of interest since it is 11.5 inches wider than the side glass panels and would therefore exhibit the largest stresses and deflections. An analysis was first done without any beam supports as a worst-case scenario. Fixed end boundary conditions were placed on three glass edges. The hydrostatic pressure was simulated by applying a nonuniform, linear pressure distribution of 63.9 lbf/ft^3 was added at the top of the glass and extends to the bottom to simulate the hydrostatic pressure of a fully filled tank. The BCM factor of safety n_{bcm} and maximum deflection of the glass are shown in Figure 2.2a below and on Figure 2.2b on the next page.

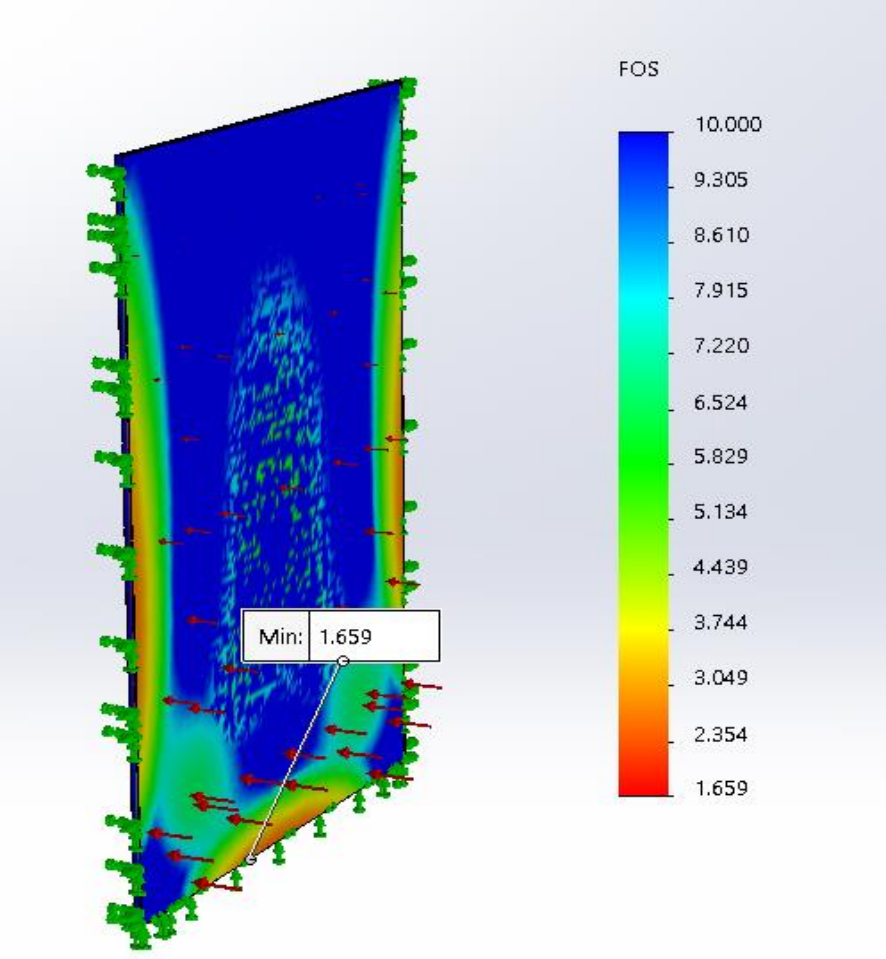

Figure 2.2a: Brittle Coulomb-Mohr factor of safety for rear glass.

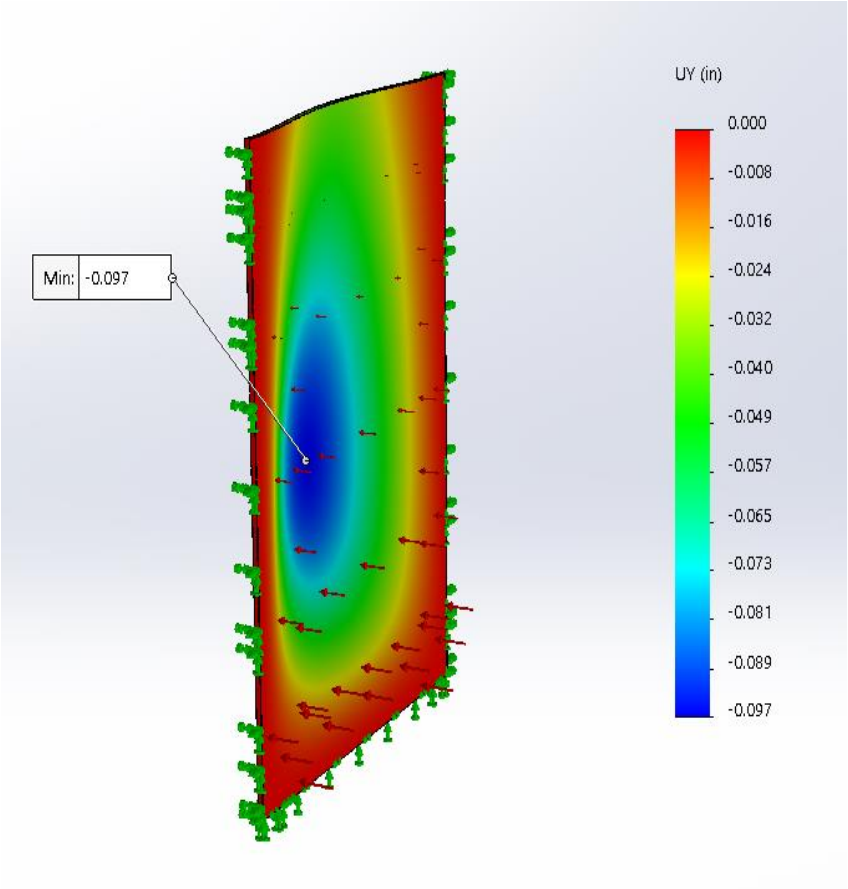

Figure 2.2b: Maximum deflection of rear glass.

With a minimum factor safety of 1.66, this worst-case model is under the desired factor of safety of 3.8. The maximum deflection of the glass was calculated to be about 0.1". In the ensuing sections, this will be revisited for an analysis with a support frame in place.

Along with the factor of safety, there are many other variables that need to be accounted for regarding the strength of glass. These include stress concentrations, fatigue loading, relative humidity, creep mechanisms, corrosion effects, individual glass surface flaw distribution, thermal shock, and deep scratches (Bansal and Doremus, 1986). There are solutions to some of these concerns. Point loads and stress concentrations can be

reduced by applying a soft material such as rubber between rough surfaces that glass would be in contact with. Scratches are often times found to be superficial but must be accounted for and occasionally checked for crack growth. Glass almost always fails in tension before compression, which occurs once tensile stresses overcome the compressive stress layer of the tempered glass surface. The compressive stress thickness of a typical tempered glass piece of thickness t is roughly $0.21t$ inches per side. For t = ¾ inches, this corresponds to a scratch depth of 0.1575 inches. Tempered glass can also withstand temperature differences of up to 300°F, which will likely never occur in the transparent tank. The overall assumption is that the 3.8 factor of safety accounts for these conditions.

A 1 inch thick acrylic sheet was selected as the interface wall between the transparent tank and the test section to allow for cutting and drilling. These cuts and the structural members reinforcement of acrylic panel are shown in Figure 2.3 and Appendix A. Since the panel would be reinforced with a rubber gasket and tubing from the test channel (discussed in the next chapter but shown in Figure 2.3b), the acrylic panel was not a significant area of interest for stress analysis.

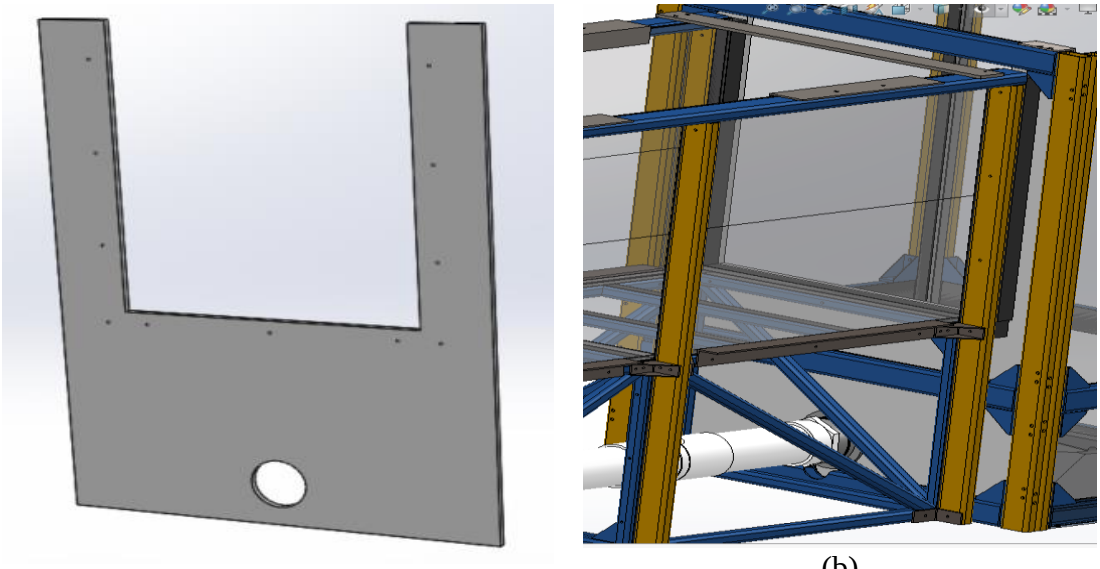

(a) (b)

Figure 2.3: (a) Plexiglass with machined and drilled sections. (b) Vertical support attachments shown will aid in compressing gasket, creating a rigid frame.

2.3 PVC Base and Support Structure

The CAD of the PVC base and support frame for the glass and acrylic panels are shown in Figure 2.4a and Figure 2.5, respectively. Both components were evaluated for stresses and factor of safeties. The base was analyzed with the von Mises criterion (Equations 2.4-2.6) for static failure, which relates the principal stresses $\sigma_1, \sigma_2, \sigma_3$ to the von Mises stress σ_{vm}. Principal stresses are calculated from axial, bending moment induced loading, an/or shear loading. An accurate estimation of the static safety factor n_{vm} relates the von Mises stress to the yield strength of the material. The support structure was analyzed for three failure conditions: 1) a revisited glass factor of safety n_{bcm}, 2) the maximum deflection of the glass, and 3) the von Mises stress on the structural members.

$$\sigma_1, \sigma_2 = \frac{\sigma_x + \sigma_y}{2} \pm \sqrt{\left(\frac{\sigma_x - \sigma_y}{2}\right)^2 + \tau_{xy}^2} \tag{2.4}$$

$$\sigma_{vm} = \left[\frac{(\sigma_1 - \sigma_2)^2 + (\sigma_2 - \sigma_3)^2 + (\sigma_3 - \sigma_1)^2}{2} \right]^{1/2} \quad (2.5)$$

$$n_{vm} = \frac{\sigma_{yield}}{\sigma_{vm}} \quad (2.6)$$

A PVC base was machined with grooves on the outer edge to act as a stand for the glass panels. The base was machined with a downward slope to assist with fluid and organism drainage. Manufacturing testing specified that the base is resistant to absorbing water, showing 0% absorption after a 24 hour submersion period. A simple simulation with the weight of water on the base was implemented to ensure the draining hole was not a stress concentration factor. Simulation results (Figure 2.4b) indicated a minimum von Mises factor of safety of 303 for the base.

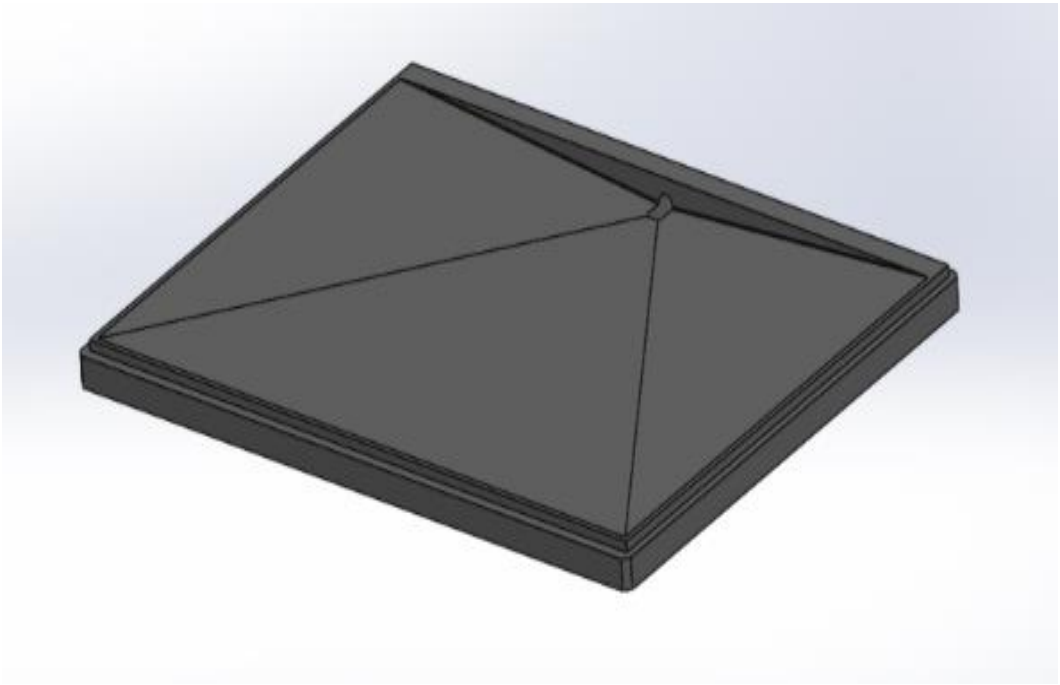

Figure 2.4a: CAD of PVC Base.

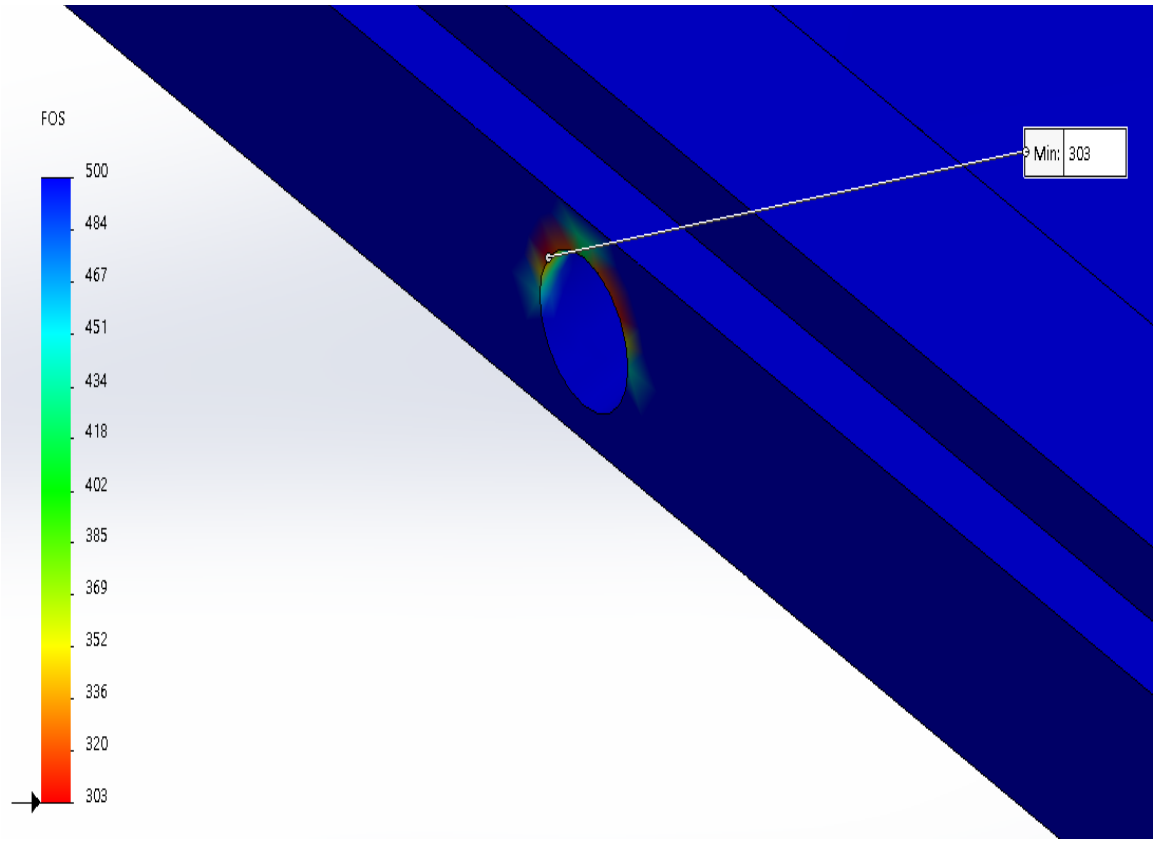

Figure 2.4b: Factor of safety for PVC base.

For the support structure, since standalone glass (solely held together by silicone) is not an acceptable design solution, a carbon steel support frame, primarily made up of ASTM A500 Grade B, needed to be added around all edges and interfaces, shown in Figure 2.5. Carbon steel was selected due to its high yield strength, relatively light weight, machinability, and availability. Since the glass and transparent tank as a whole were deemed the most significant part of the design, any costs and weight variables were neglected in designing the structure; an overdesigned approach was preferred. Due to the large principal stresses, deflections, and bending moments experienced by the standalone glass simulation from Figure 2.2, a cross beam 16 inches above the bottom beam was added to potentially reduce stresses and deflections. Although it would have been preferred that

the entire frame and components be simulated, this proved to be too computationally expensive due to the size of the mesh assembly and the complex contact sets between components. Instead, a simplified model focusing on the rear glass again was used (Figure 2.6). Fixtures were placed at bolt holes to resemble a bolted connection, which resulted in stress concentrations but were deemed insignificant. Boundary conditions were added to condition the glass component as fixed along all four edges. The simplified model was also given a global bonded contact set, meaning all components act as if they are welded. In reality, all components are held together by bolts.

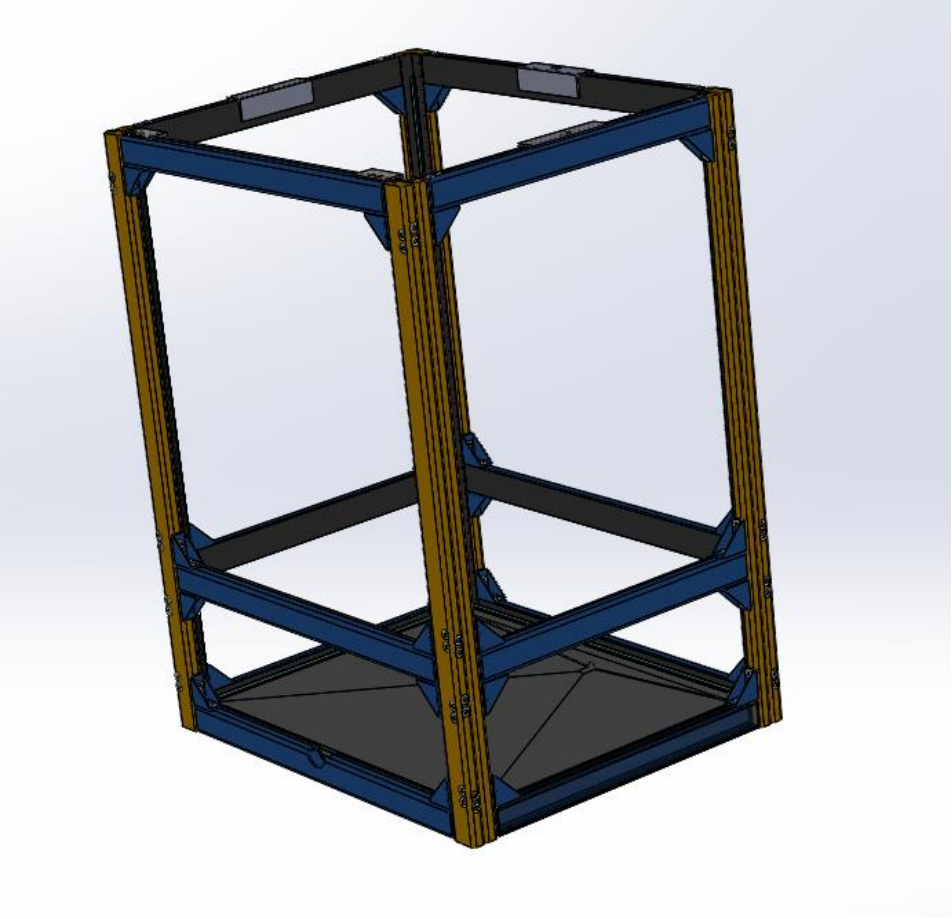

Figure 2.5: CAD of support frame for transparent tank.

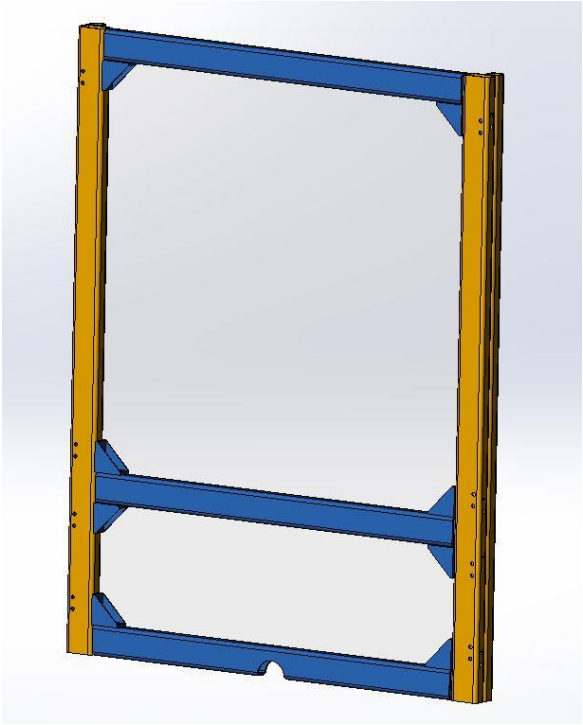

Figure 2.6: Rear glass support frame for simplified FEA analysis.

Figures 2.7-2.9 on the next two pages indicate results regarding the revisited glass factor of safety, maximum deflection, and the von Mises stresses on the structural members. Simulation results for the added support frame indicated a minimum glass factor of safety of about 4.36, maximum deflection of 0.045 inches, and a maximum von Mises stress of about 10,500 psi located at the “welded” gussets, which when compared to their yield strength of 36,000 psi gives a von Mises factor of safety of about 3.43. All values were deemed suitable enough to approve of the support frame design.

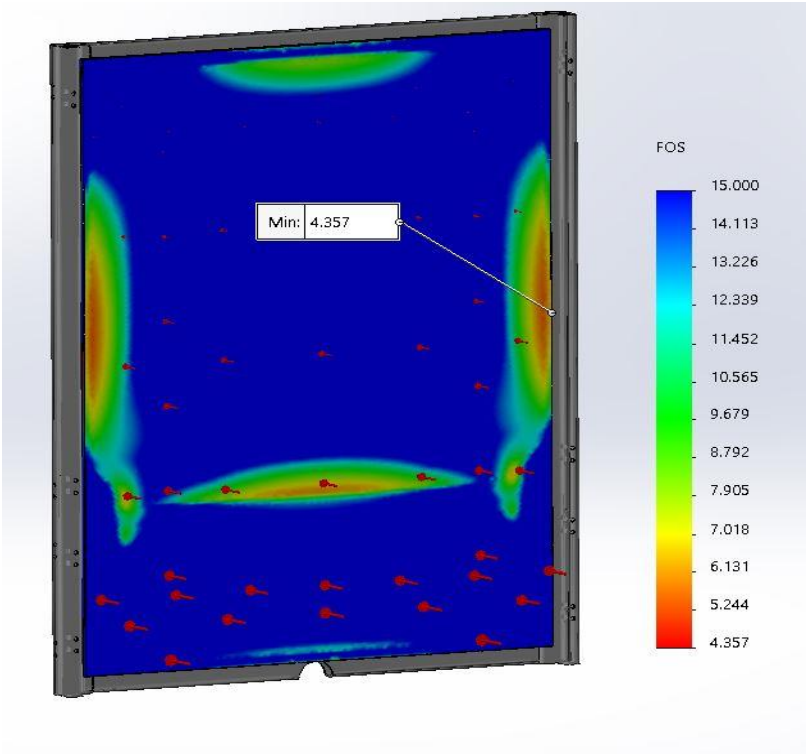

Figure 2.7: Brittle Coulomb-Mohr factor of safety for rear glass with support frame.

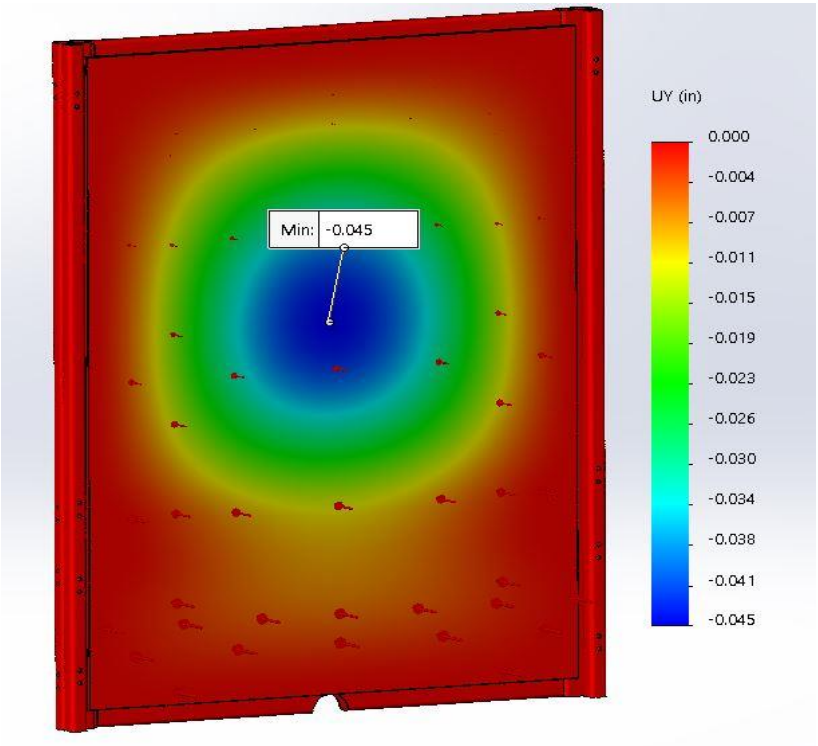

Figure 2.8: Maximum deflection of rear glass with support frame.

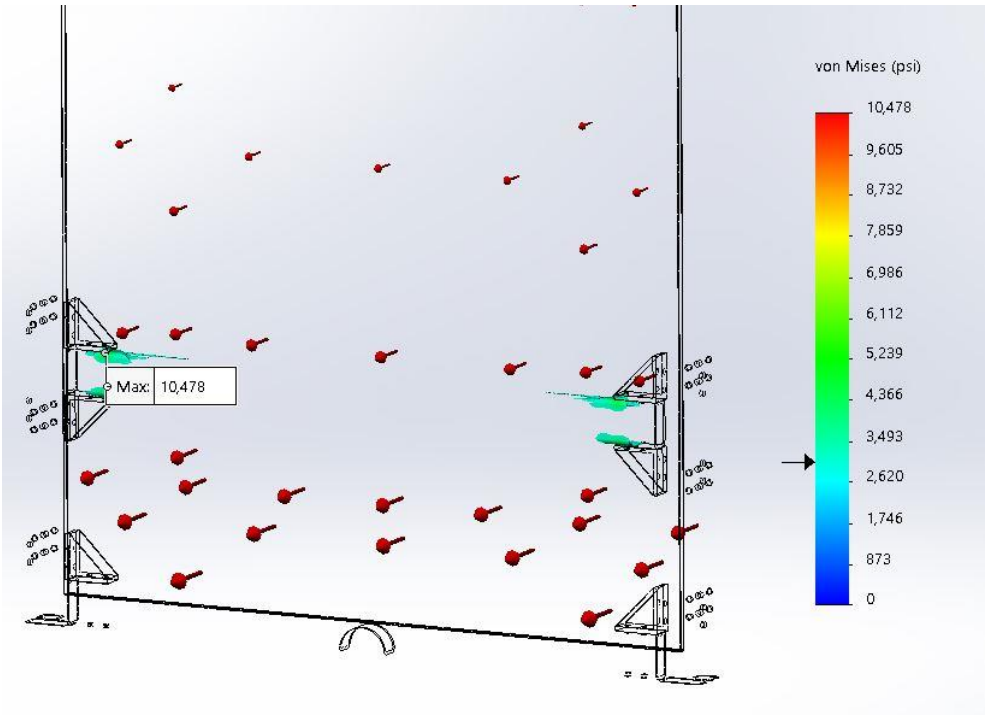

Figure 2.9: Von Mises stress distribution of support frame.

2.4 Bolted Joints

Since the support structure could not be welded together, it was decided to bolt together all support members. By doing so, it would ensure that the glass and support structure were in contact with one another; without contact, the support structure would serve no purpose. The members are connected together via corner gussets that share a similar bolt pattern to the support frame, which is shown in Figure 2.10 on page 23 and 24. With the bolts, the design goal was to ensure that 1) all internal and external forces on a bolt do not exceed its yield strength, 2) no shear forces besides the preload torsion are imposed on a bolt, and 3) bolts were not excessively tightened to the point that they would cause significant deformation in the members.

For bolt yielding, it was suggested that two bolts be added per gusset-beam connection to distribute the loads that each bolt would receive. The bolt patterns were

carefully positioned to avoid overlap and give room for tightening the nuts without any interference. Due to the high computational demands, a full scale analysis was not possible with 115 bolts and nuts and 230 washers to analyze. 18-8 stainless steel bolts were selected as the material due to availability at the time. Recommendations for bolt tightening come from *Shigley's Mechanical Engineering Design*, who recommend the preload F_i on a bolt be dictated by its tensile stress area A_t, proof strength σ_{proof} and whether the connection is permanent or temporary. These relationships are given below.

$$\sigma_{proof} = 0.85\sigma_{yield} \tag{2.7}$$

$$F_p = A_t\sigma_{proof} \tag{2.8}$$

$$F_i = \begin{cases} 0.75F_p & \text{for nonpermanent connection} \\ 0.90F_p & \text{for permanent connection} \end{cases} \tag{2.9}$$

A torque-preload relationship helps estimate the torque needed for a given preload,

$$T = KF_id \tag{2.10}$$

where d is the nominal diameter of the bolt and K is the torque coefficient nut factor that depends on factors such as lubrication and manufacturing processes. A nominal K value of 0.2 is recommended to be used if not specified or tested, which was used in this case.

Because the structural members being compressed are hollow tubes, preload values might be sufficient enough to cause the tubes to collapse, compromising the structural integrity. At the same time, not applying enough pretension in the bolt may lead to joint separation and place 100% of the hydrostatic load on the bolt. However, conservative

measures were taken for the bolts. They were assumed to take 100% of the load regardless of joint separation, implying a joint stiffness constant C of 1.

$$C = \frac{k_b}{k_b + k_m} \tag{2.11}$$

The total tensile stress on a bolt is the sum of the preload tension and any external axial loads on the bolt, P_{ext}. It is assumed that N_b bolts evenly distribute the load.

$$\sigma_b = \frac{F_b}{A_t} = \frac{C\left(\frac{P_{ext}}{N_b}\right) + F_i}{A_t} \tag{2.12}$$

A static factor of safety is then calculated to ensure the bolts does not exceed their proof strength.

$$n_p = \frac{\sigma_{proof}}{\sigma_b} \tag{2.13}$$

The second criterion that must be accounted for is prevention of shear loading. Joint separation indicates a loss of the frictional grip force between members, potentially putting the bolts in shear. The shear force capacity V_s to prevent this grip loss is given by:

$$V_s = F_i \mu_f n_e K_h \tag{2.14}$$

where μ_f is the friction coefficient between interfaces, n_e is the number of slip resistant interfaces, and K_h is a bolt hole coefficient dependent on the hole shape. Based off the steel-steel connection interface, μ_f was approximated to be 0.5. The hole coefficient varies on whether a hole is a clearance hole or slotted. Since all holes are clearance holes, the coefficient was approximated as 1. It should also be noted that the term $F_i \mu_f$ is the normal

force created due to the compression between members. With a bolt preload, external loads would be resisted by the frictional resistance between contact members. A slip resistance factor of 1.25 is recommended to account for variability in constants.

$$n_{vs} = \frac{V_s}{1.25P_{ext}} \tag{2.15}$$

It should be noted that when determining this joint separation factor of safety of the shear force against the frictional grip, the out of plane bolts (pointing into the page) that induce a frictional grip in the members in Figure 2.10a are resisting the shear due to the force on the side glass, not the rear glass. The side glass has a maximum force of about 5,200 lbf, which should be used as P_{ext} for only Equation 2.15. This force is also assumed to be evenly distributed between the 12 bolts.

It was important to ensure both yielding and shearing bolt modes of failure are not reached. Any of the three glass sides will have the same restrictions. The rear glass support is the most significant since it has the largest force on it. Figures 2.10a and 2.10b displays the bolt pattern and how the bolts are predicted to be loaded.

For the rear glass configuration in Figure 2.10a, the external load P_{ext} is the hydrostatic force on the rear glass, roughly 6,500 lbf. It is assumed that the top four out of plane bolts do not carry any of the load. The external force per bolt (12 total, referred to as N_b) is assumed to be evenly distributed: $P_{ext}/N_b = 542\ lbf$. The ½ inch diameter stainless steel bolts have a tensile area of 0.1419 in^2 and a yield strength of 40,000 psi. A nonpermanent connection was selected, giving a recommended preload of F_i = 3,619 lbf, which requires a 30 ft·lb torque. The number of interfaces n_e for joint slippage prevention

on one of the side glass panels is shown by the three left gussets in Figure 2.10b. It should be noted that the vertical bolts connecting the gusset-beam-gusset interface were also assumed to each have a slip interface, implying that each gusset contains two slip interfaces. Since each side is symmetrical, a total of six gussets and thus twelve interfaces are present if we neglect the top two gussets.

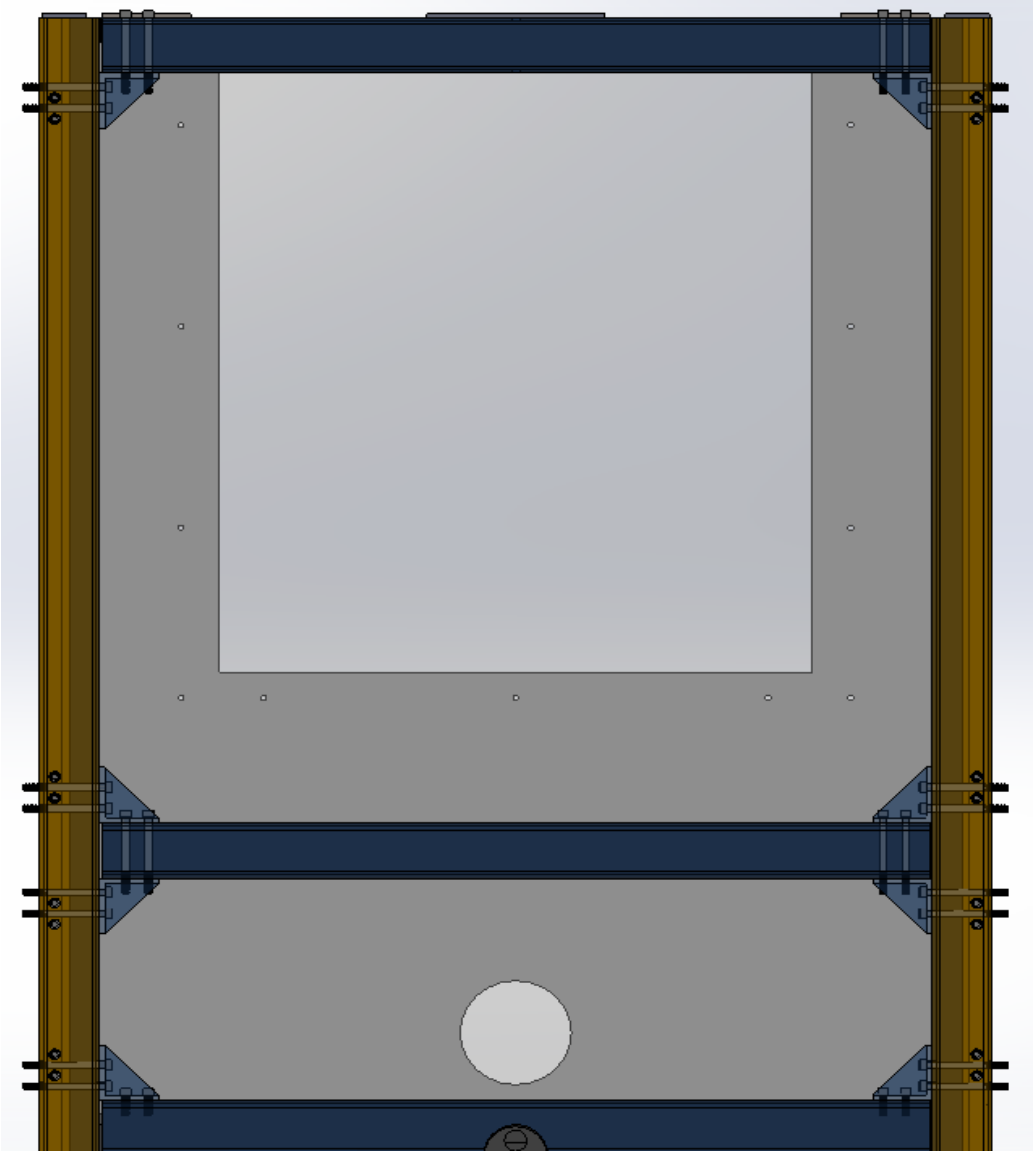

Figure 2.10a: Bolt configuration for rear glass side wall. For analysis purposes, the bottom 12 out of plane bolts (into the page) are assumed to carry the entire load evenly. Washers and nuts are not shown.

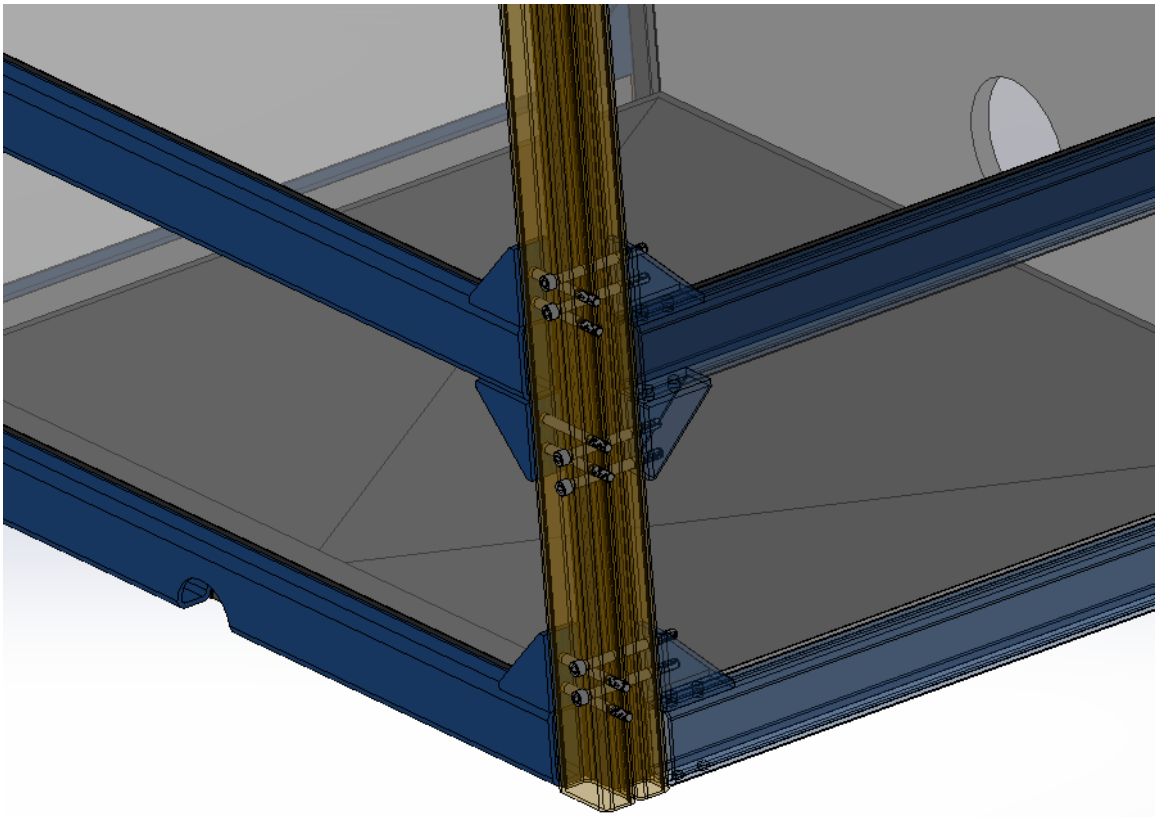

Figure 2.10b: Six axially loaded bolts relative to side glass. The frictional force due to the preload is induced between gussets and vertical beam. Six bolts located on the opposite side add to a total of 12 bolts that assist members to carry shear force V_s.

The third criterion was to check the hollow members would not yield at high preload values. This was analyzed in FEA to determine the effect of the preload on the compressed members by calculating the von Mises factor of safety n_{vm}. The inward buckling of the hollow members and gusset was determined by setting up a compressive load equal to the preload F_i on both sides (Figure 2.11). A washer was added to distribute stress. Figures 2.11a, 2.11b, and 2.11c indicate the structural member's factor of safety for three different preloads applied. Any significant washer stress or deformation can be neglected since they are meant to distribute the load on the members.

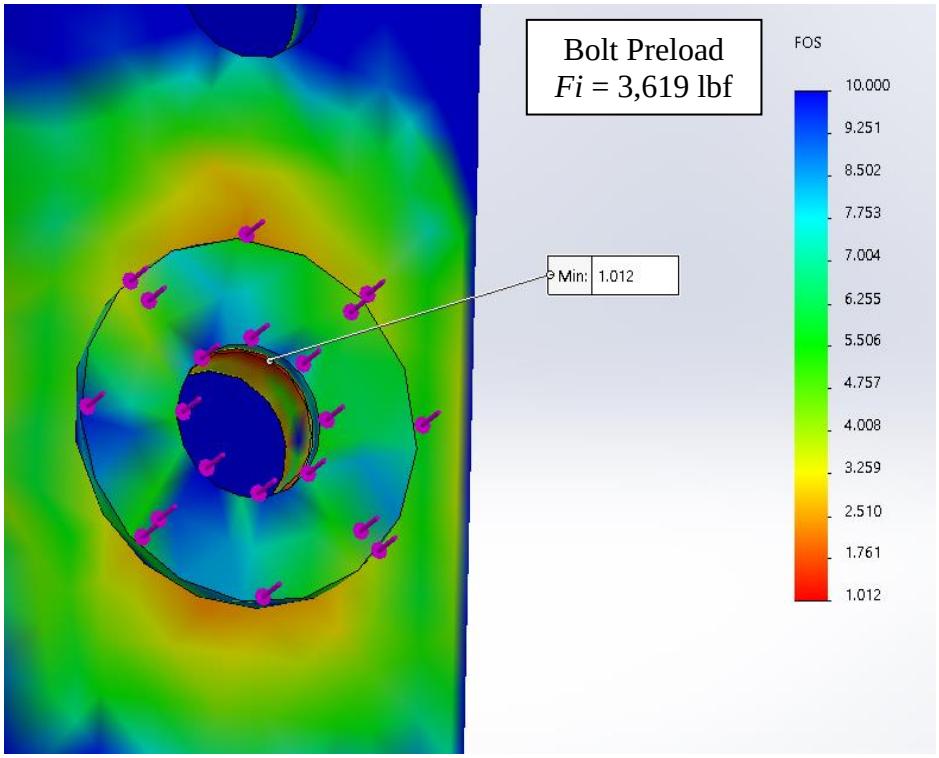

Figures 2.11a: Yield check of inward buckling beams with F_i = 3,619 lbf.

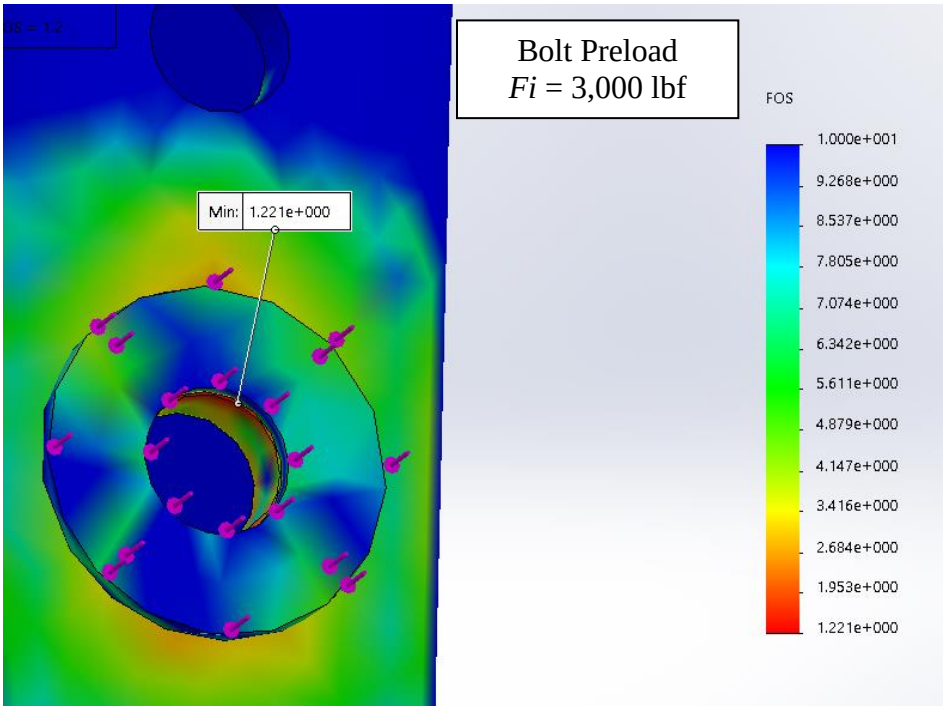

Figure 2.11b: Yield check of inward buckling beams with F_i = 3,000 lbf.

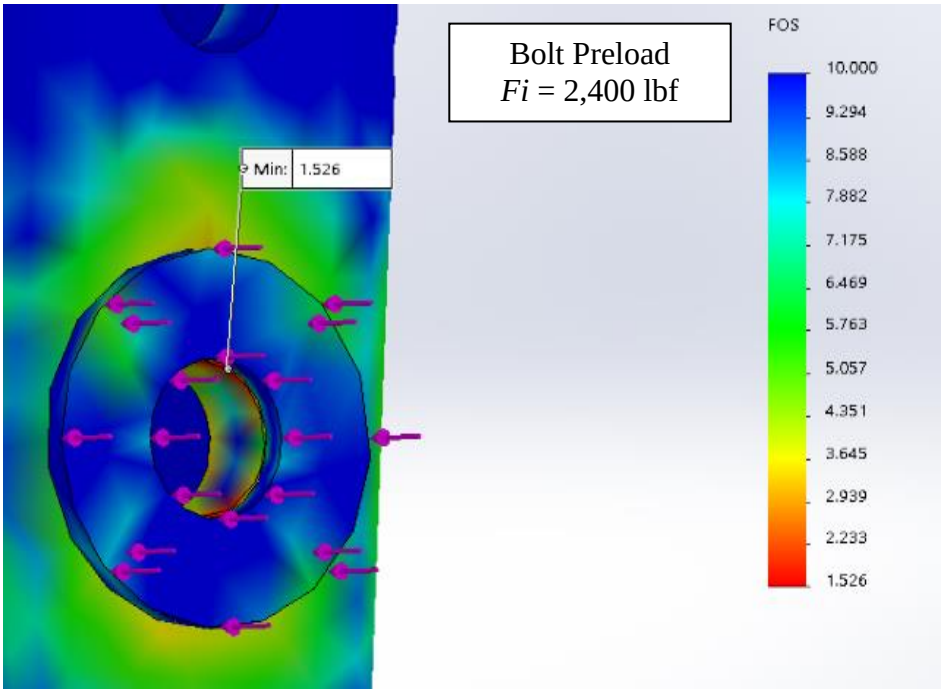

Figure 2.11c: Yield check of inward buckling beam with F_i = 2,400 lbf.

The proof strength safety factor (2.13), von Mises safety factor (2.6) for the structural support beam with regards to joint deformation, shear slippage safety factor (2.15), and the bolt von Mises safety factor (2.6) were determined for the three given preloads used for the joint deformation analysis above. This data is shown in Table 2.3. It should be noted that by definition, the bolt proof strength safety factor will always be greater than the bolt von Mises safety factor since the latter considers induced shear by torsion from the preload tightening. Based off of the preload values, it was decided that a torque between 17.5-20 ft·lb would be used when tightening with a dial wrench to account for the beam deformation and shear factor of safety. The bolt stresses were mostly neglected since they are meant to be pretensioned near their yield strength.

Table 2.3: Failure mode check for out of plane bolts with respect to the rear glass. P_{ext} = 542 lbf per bolt. P_{ext} for the shear safety factory is 5200 lbf.

F_i (lbf)	Torque (ft·lb)	Proof strength safety factor, n_p	Beam von Mises safety factor, n_{vm}	Shear safety factor, n_{vs}	Bolt von Mises safety factor n_{vm}
3,619	30	1.15	1.012	4	1.03
3,000	25	1.36	1.22	3.32	1.22
2,400	20	1.64	1.53	2.66	1.49

There are several factors that one should be aware of. One is understanding the difficulty of getting the exact desired torque and preload. Reusing nuts affects the nut factor and measurement tools must be correctly calibrated to be used. All calculations are thus approximations that are meant to consider for a worst case scenario.

The second is that bolts will also experience axial stresses due to the induced bending moment, which was neglected for mathematical simplification. If one wanted to analyze this effect, each bolt configuration's centroid would first need to be found. The moment arm distance between the force's centroid and the bolt pattern centroid acts as an extra load known as an offset or eccentric load. The axial stresses are thus proportionally related to the resultant moment and its moment arm, but inversely related to the polar moment of inertia of the bolt pattern. Hence, bolts further away from the centroid experience larger axial stresses, but the more bolts present, the larger the polar moment of inertia and the smaller the bending stress.

The third factor is that of the in-plane vertical bolts. The bottom six gussets in Figure 2.10a contain a total of eight pretensioned bolts. These bolts were assumed to not feel any stresses due to axial or bending, and only serve to add slip resistance to the beam.

Finally, the combined stresses due to the hydrostatic pressure and preloaded bolts on the members was not accounted for. This would essentially be a combination of Figures 2.9 and 2.11. Further analysis is recommended for all these variables.

3 Test Channel

Similar to the transparent tank, the test channel was partitioned into several sections for failure prevention analysis. The design requirements for the glass selection, support structure, and bolted joint configuration are all explained in detail. The CAD for the test channel is shown in Figure 3.1, with a description of the significant components tabulated in Table 3.1. Details regarding component dimensioning , cutting, and machining are given in Appendix B. Information regarding the flow characteristics of the channel is presented in Appendix F.

3.1 Design Requirements

The primary design requirements for the test channel include:

- failure prevention with factor of safety calculations for significant components
- connection with transparent tank and end tank
- clearance below the channel for housing the pump and pipe fittings
- controlled flow with observable test section

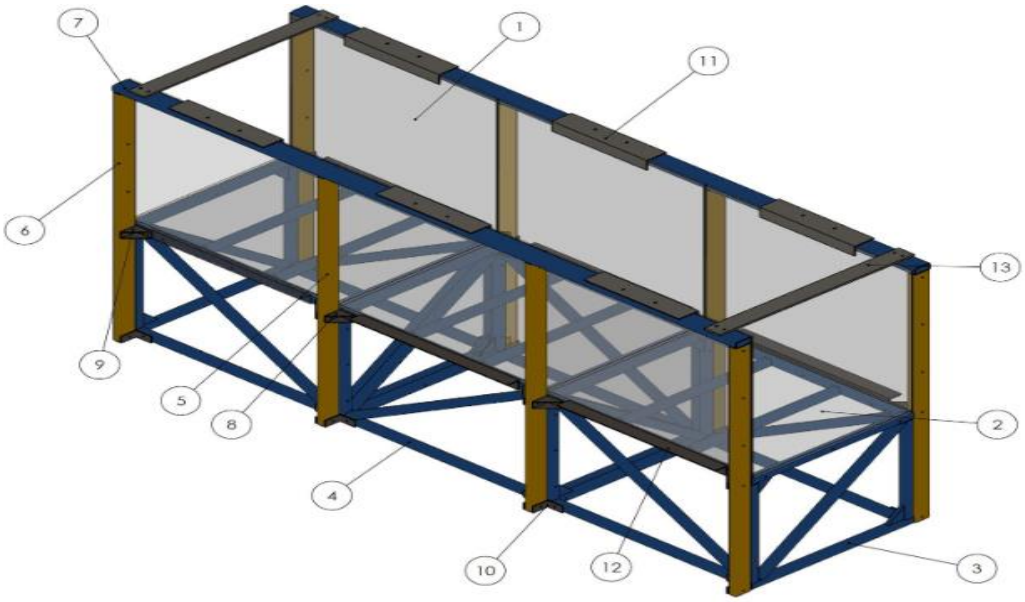

Figure 3.1: CAD of test channel section. See Table 3.1 for components.

Table 3.1: Test channel main components.

Item No.	Component	Quantity
1	Tempered Glass	6
2	Annealed Glass	3
3	Chassis Module 1	2
4	Chassis Module 2	1
5	Middle Vertical Members	4
6	End Vertical Members	4
7	Horizontal Members	2
8	Middle Corner Gussets	8
9	End Corner Gussets	4
10	Corner Angle Irons	12
11	Top Angle Beams	6
12	Bottom Angle Beams	6
13	Flat Bars	2

3.2 Glass

A total of nine glass panes make up the test section. Simulation results for the BCM factor of safety and maximum deflection are shown in Figure 3.2. It was decided that ¾ inch thick annealed glass with dimensions 52.5 inches long x 40 wide was adequate as the horizontal component, the latter fulfilling the 1 meter width requirement. Since the horizontal glass is supported by a chassis support structure, minimal deflections will occur, prompting the decision to go with annealed glass. To account for the chassis module, the FEA simulation on the annealed glass was conducted together with the chassis, depicted in Figure 3.5. ½ inch tempered glass measuring 52.5 inches long x 43.5 inches tall was selected as the vertical panels to account for the lack of support and the larger deflection that they would undergo relative to the horizontal glass. A similar approach was taken with a worst case scenario of the channel entirely filled to determine n_{bcm} and the maximum deflection, which were found to be about 2 and 0.075 inches, respectively. Since the water depth is unlikely to reach above halfway of the channel, and the hydrostatic force is proportional to the square of the water depth, the glass factor of safety will be greater than 4, satisfying the 3.8 minimum requirement.

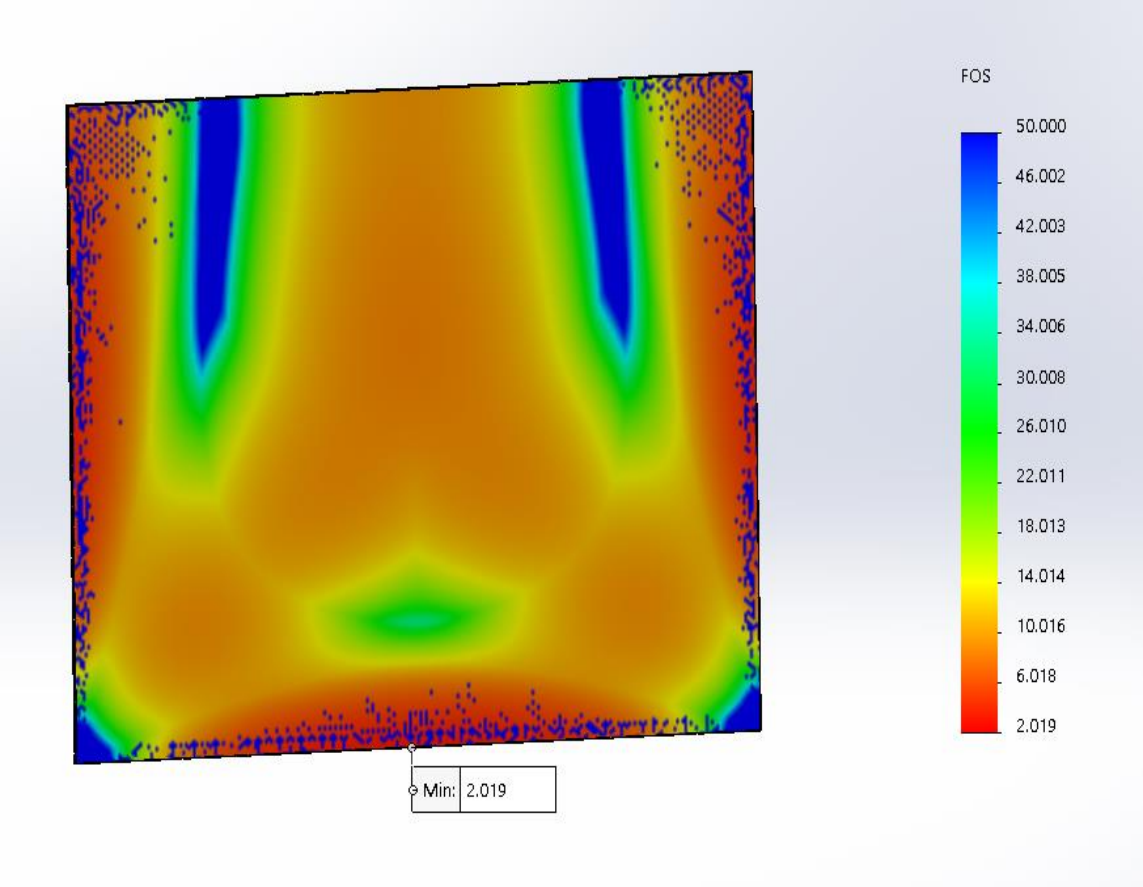

Figure 3.2a: Brittle Coulomb-Mohr factor of safety for test channel vertical glass.

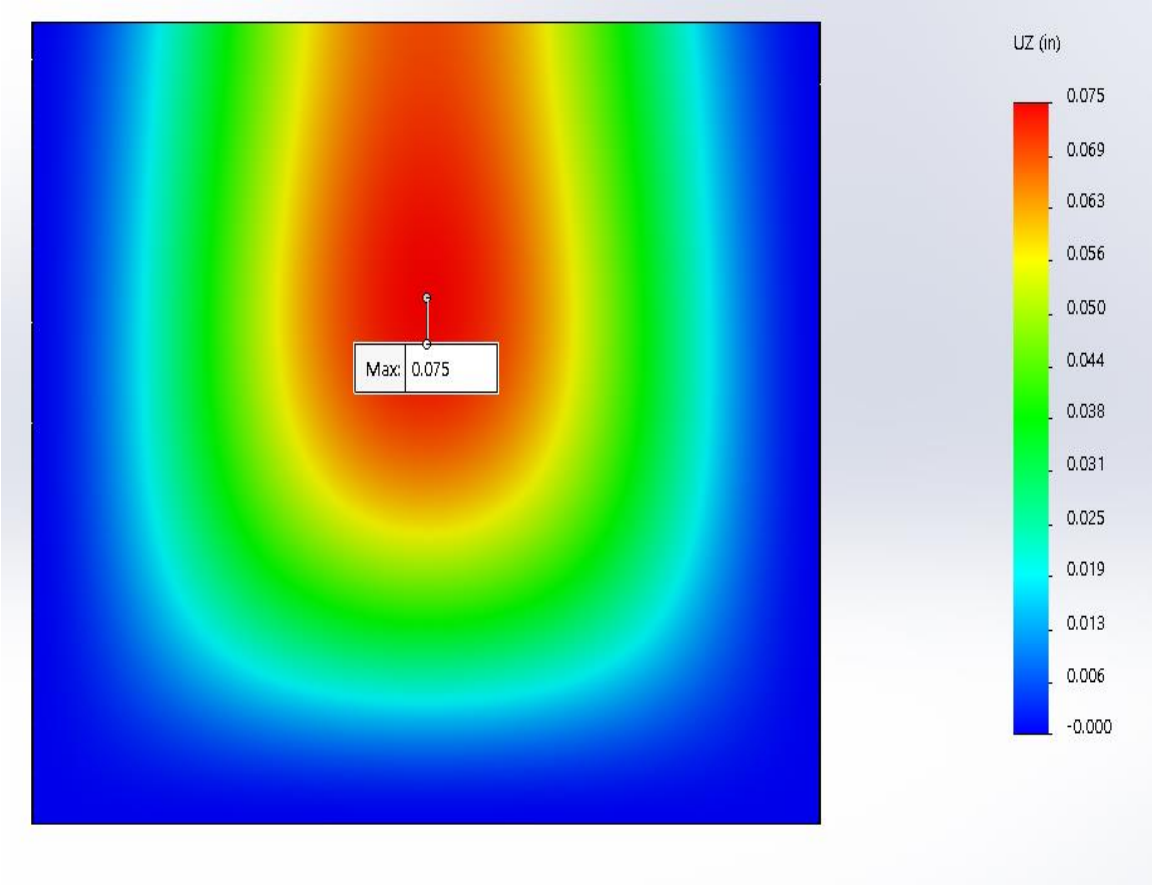

Figure 3.2b: Maximum deflection of test channel vertical glass.

3.3 Support Structure

The purpose of the support structure is to prevent any glass panels from detaching from the silicone, provide rigidity to the frame, and absorb/distribute the hydrostatic loads being exerted without yielding. As detailed in Figure 3.1, the support frame primarily consists of three chassis modules, eight vertical members, and two horizontal members to connect vertical members together, all of which are made of ASTM A500 Grade B carbon steel tubing. These pieces are connected together with corner gussets, corner angle irons, and bolts. Angle beams were added at the top and bottom of the vertical glass panels. The

gussets, angle irons, and angle beams consist of ASTM A36 carbon steel, while the bolts, nuts, and washers are made up of a combination of Grade 8 and Grade 9 steel.

The three chassis modules shown in Figure 3.3 are required to withstand an approximate weight of 10,000 lbf of water and an additional 1,050 lbf from the weight of the glass panels. Each module is therefore required to hold a total weight of about 3,683 lbf. Each chassis was required to be 52.5 inches long, 34 inches high, and 41 inches wide. Individual carbon steel tubes were welded together in a truss design. A close-up of one chassis is shown in Figure 3.4. To select the proper dimensions of the carbon steel tubing, several FEA simulations were run in order to select the proper sizing to minimize costs and weight. The general solution consisted of adding diagonal cross members to prevent torsion and reduce the forces endured by the vertical tubes. Corner gussets were also added opposite of diagonal beams to distribute stresses. After several iterations of altering tubing dimensions and finding a proper von Mises factor of safety it was decided that 2” x 2” x ¼” carbon steel welded tubing would sufficiently hold the total weight requirement. The chassis simulation, displayed in Figure 3.5, was concurrently analyzed with the annealed glass to simulate a realistic scenario.

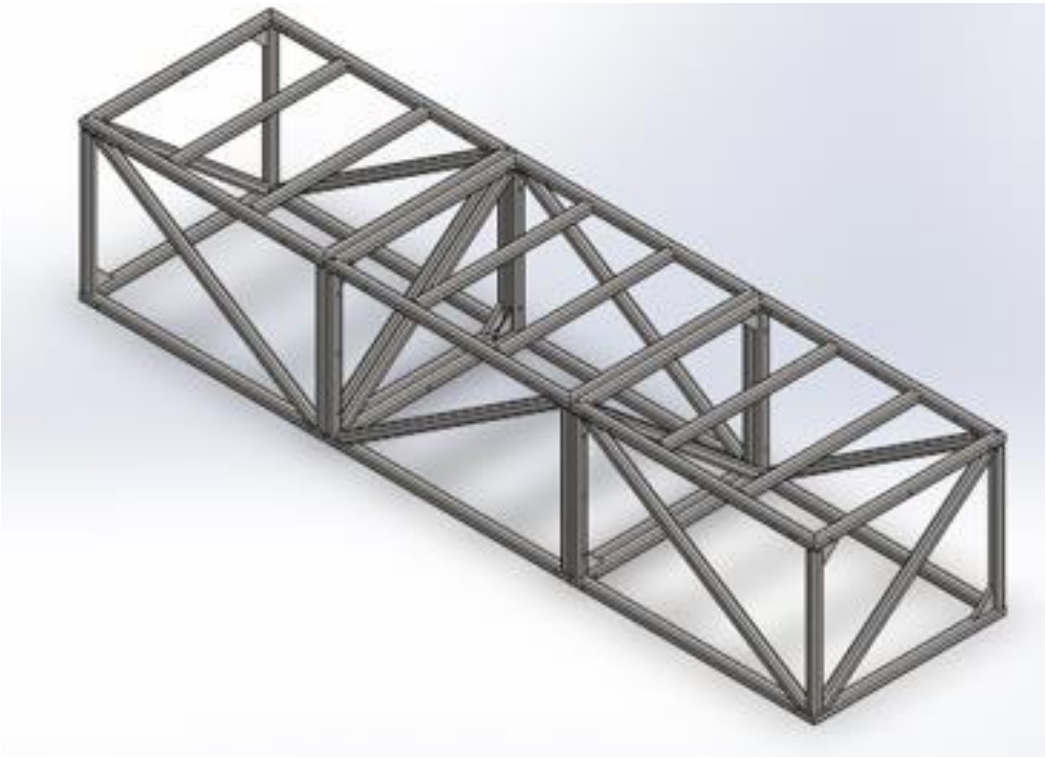

Figure 3.3: Chassis modules.

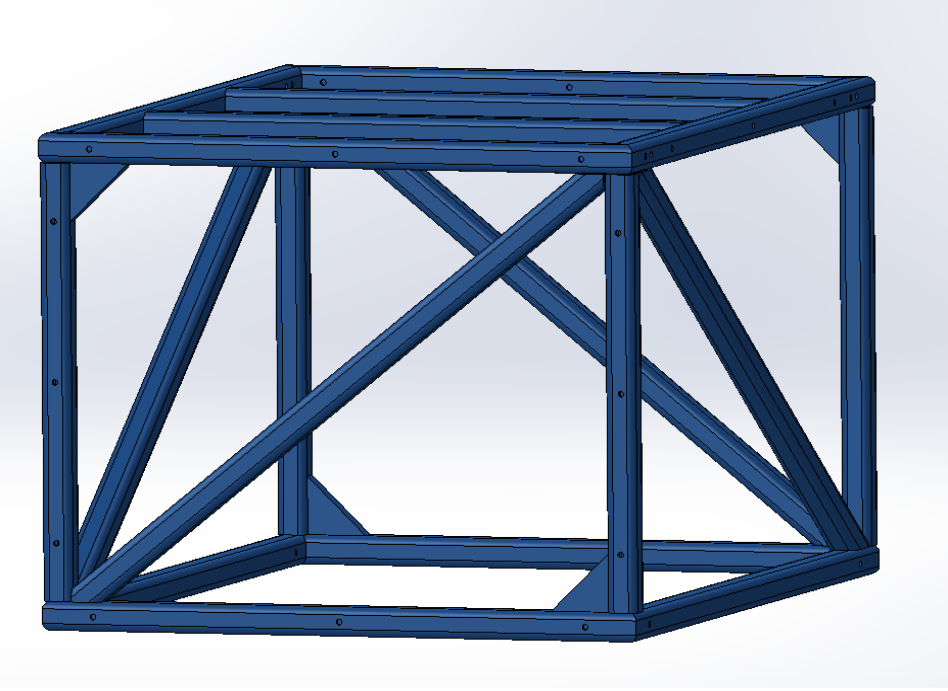

Figure 3.4: Close-up of truss design. Corner gussets shown are welded to aid in distributing stresses.

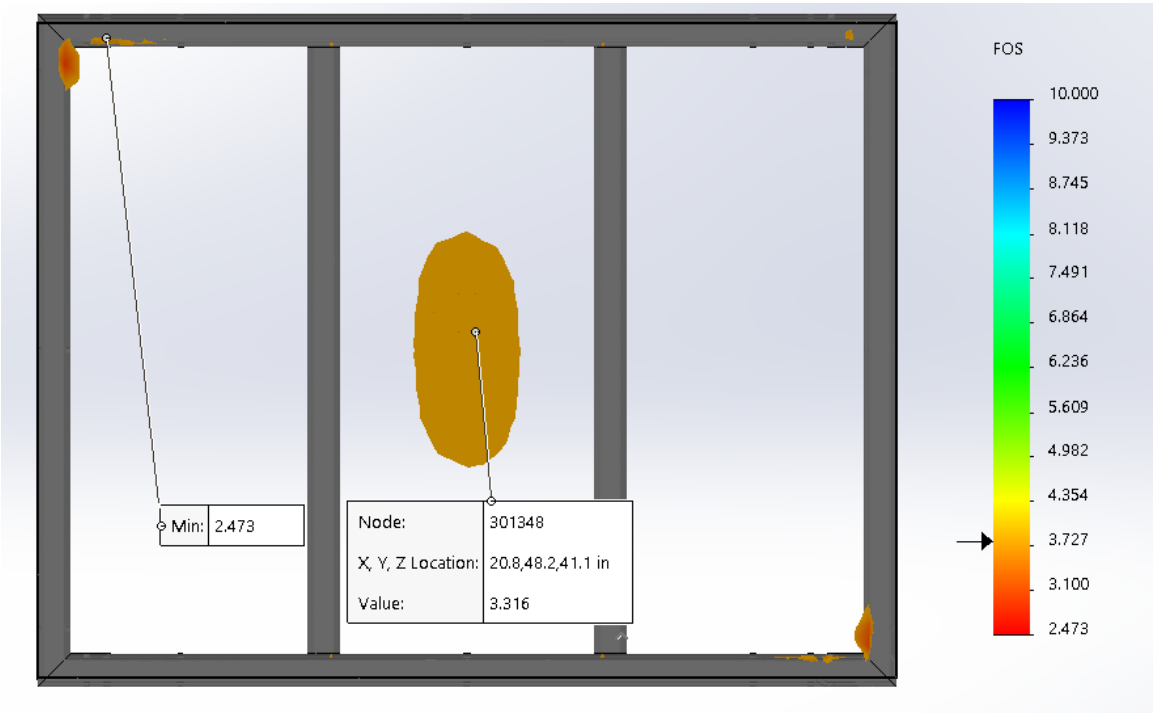

Figure 3.5a: Brittle Coulomb-Mohr factor of safety for annealed glass.

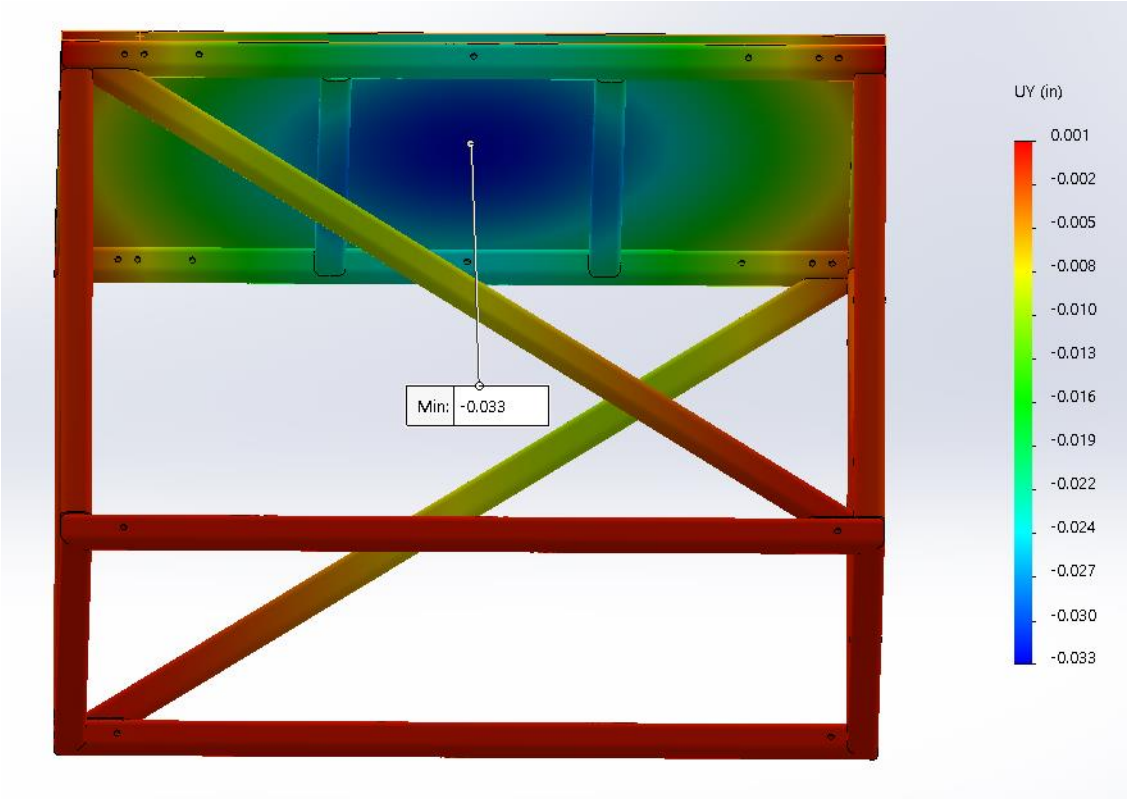

Figure 3.5b: Maximum deflection of annealed glass.

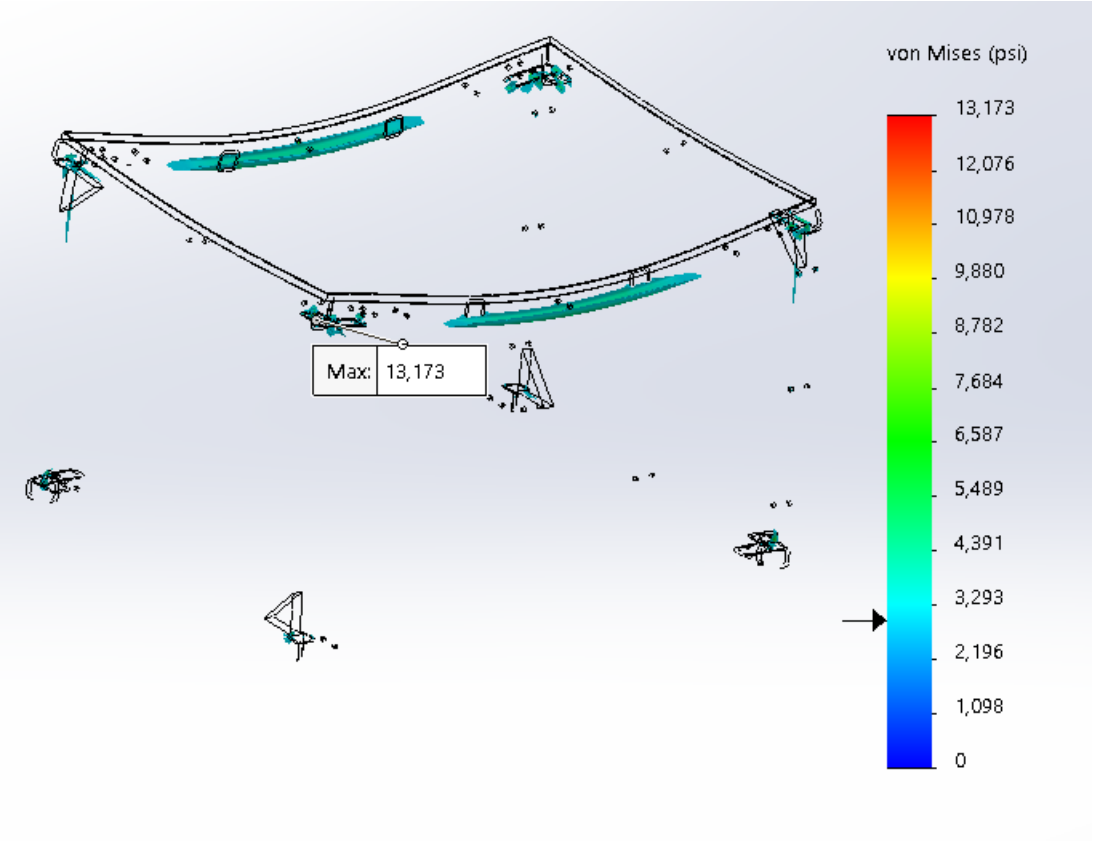

Figure 3.5c: Maximum von Mises stress of chassis module.

The worst case scenario of the channel filled entirely indicated a glass factor of safety of about 2.5 and a chassis von Mises factor of safety of about 3.5. Since the channel will almost never be filled more than halfway up, the factors of safety can be deemed 5 and 7, respectively, for the annealed glass and the chassis.

The eight vertical support members are bolted to the chassis modules with the use of corner gussets in the middle section and angle iron gussets at the bottom section, the latter not needing a gusset since they do not experience as much stress. The vertical members must withstand the bending moment about the joint where they are connected with the corner gussets. The two middle vertical members on each side will experience the largest stresses and deformations since they account for two hydrostatic forces, each

equaling half of the total hydrostatic force on a vertical glass panel. In contrast, the end vertical members only account for half of the hydrostatic force on a vertical glass pane. Simulations were run to check for any significant bending and deflection of the vertical members, assuming that the gussets are welded together with the vertical member and chassis.

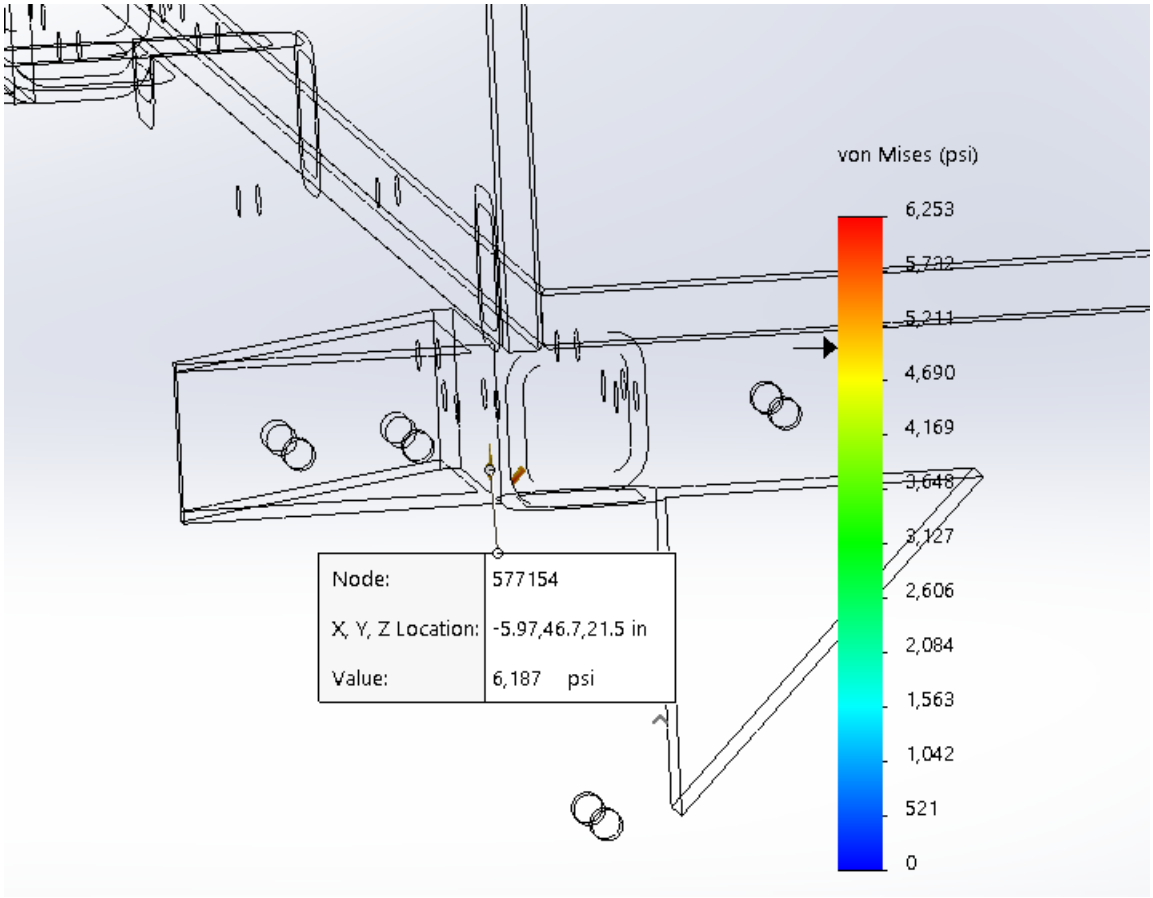

Figure 3.6: Maximum von Mises stress of vertical members.

One thing to note is the assumption that both middle vertical members experience two hydrostatic forces, half of the total from each glass. Therefore, it is assumed that the maximum von Mises stress is roughly half of that indicated in Figure 3.6. Another thing to note is the accuracy of the simulation results. This is due to the mesh quality being coarser

since the simulation has more components added to it. Creating a high quality, fine mesh for this large component was too computationally expensive. With a calculated von Mises stress of about 6,200 psi and accounting for symmetry due to the other glass panel, the von Mises factor of safety is approximately about 3.7, which was deemed appropriate for the component. Despite this, the assumption made was a bonded (welded) joint at the vertical member – chassis interface with the corner gusset, which is not the realistic case. It is necessary that the joint be rigid to prevent detachment of the vertical beam and glass. This involves a strength analysis of the bolt which would experience an axial stress due to the preload, the hydrostatic force attempting to push the glass out, and the bending moment induced by the centroid of the hydrostatic force. These are described in more detail in Section 3.4.

The two long horizontal members that span the length of the test channel have welded slots (not shown in CAD) that slide into the vertical support members from the top and are then bolted together. This provides a rigid support for preventing the vertical glass panels from toppling inwards as well as a platform for adding railings or instruments in the future.

The angle beams at the top and bottom edges of the vertical glass act to support the glass from falling inwards and to ensure a tight fit at the bottom by compressing the glass panels together. Both angle beams were not added to the previous simulation. It was assumed that the angle beams supporting the bottom edge of the glass would help prevent the glass from pushing outwards and breaking the silicone bond apart, thus raising the factor of safety for the glass and reducing the deflection of the glass.

3.4 Bolted Joints

There are five significant bolt configurations that occur within the test channel. These include the following: 1) chassis to chassis modules, 2) gussets and angle irons to chassis and vertical members, 3) angle beams to chassis and horizontal members, 4) horizontal members to vertical members, and 5) end tanks to test channel. A total of 140 bolts and nuts and 280 washers make up the test channel connections. Steel alloy bolts with similar grade washers and nuts were selected due to their high tensile strength. 316 stainless steel bolts with PVC plastic sealing washers were used to ensure compression against the tank faces for a watertight seal. Joint member thicknesses for each section were measured to ensure bolts were of adequate length.

1) Chassis to chassis modules

To ensure proper alignment and add rigidity, each chassis module was bolted together with 12 socket head black-oxide steel alloy bolts. As one can see in Figure 3.7, the bolt pattern was intricately placed to ensure proper alignment and ease of assembly. These bolts are not meant to sustain any loads other than a preload force and induced shear due to tightening. Similar to the transparent tank, it was important that these bolts connecting chassis members together not be excessively tightened. Otherwise, unnecessary stresses would be induced at the hole, possibly causing yielding, collapsing, and permanent deformation in the chassis when combined with water weight. Because of this, the bolts were not tightened to more than 10 ft·lbs.

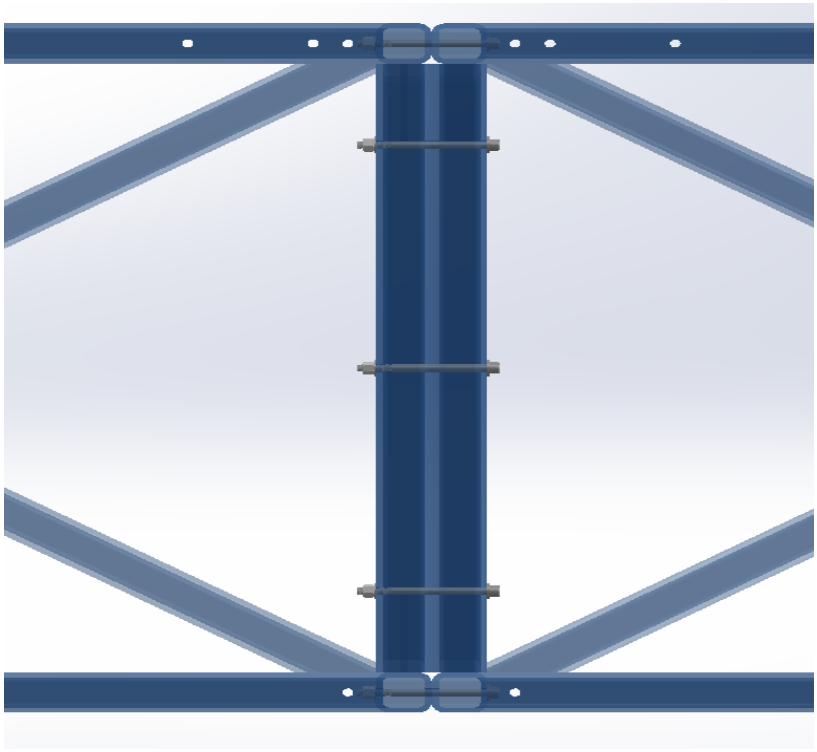

Figure 3.7a: Side view of chassis to chassis modules bolt connection.

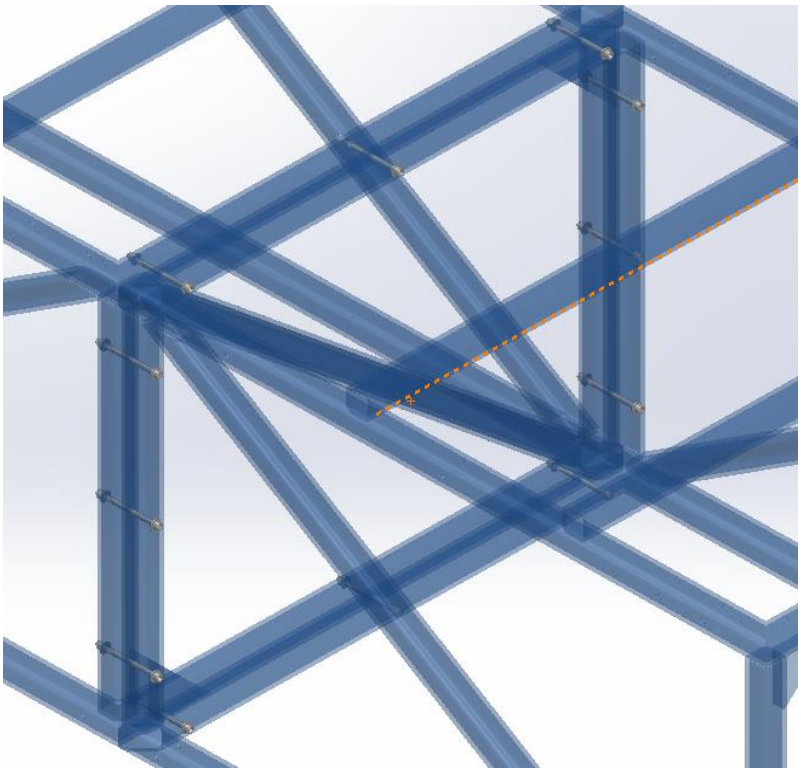

Figure 3.7b: All 12 bolts shown connection chassis modules together.

2) Gussets and angle irons to chassis and vertical members

The corner gussets and angle iron connect the chassis and vertical members together. The gussets are located at the midsection of the structure, shown in Figure 3.8a. These consists of two bolts to each gusset-chassis interface and two bolts total to the gusset-vertical member interface. The angle irons are located at the bottom of the structure shown in Figure 3.8b and only consist of one bolt for each interface. A bolt pattern analysis was performed on the bolts and nuts holding together the corner gusset components. Bending stress were once again neglected. The connectors are both made of a high grade steel alloy ($\sigma_{yield} \approx 140,000$ psi, dictated by the lower grade nut, but roughly three and a half times greater than that of the transparent tank bolts). With a maximum hydrostatic force on the glass being approximately 1825 lbf and a sample preload of F_i = 1,500 lbf, the minimum factor of safety was calculated to be 5.5.

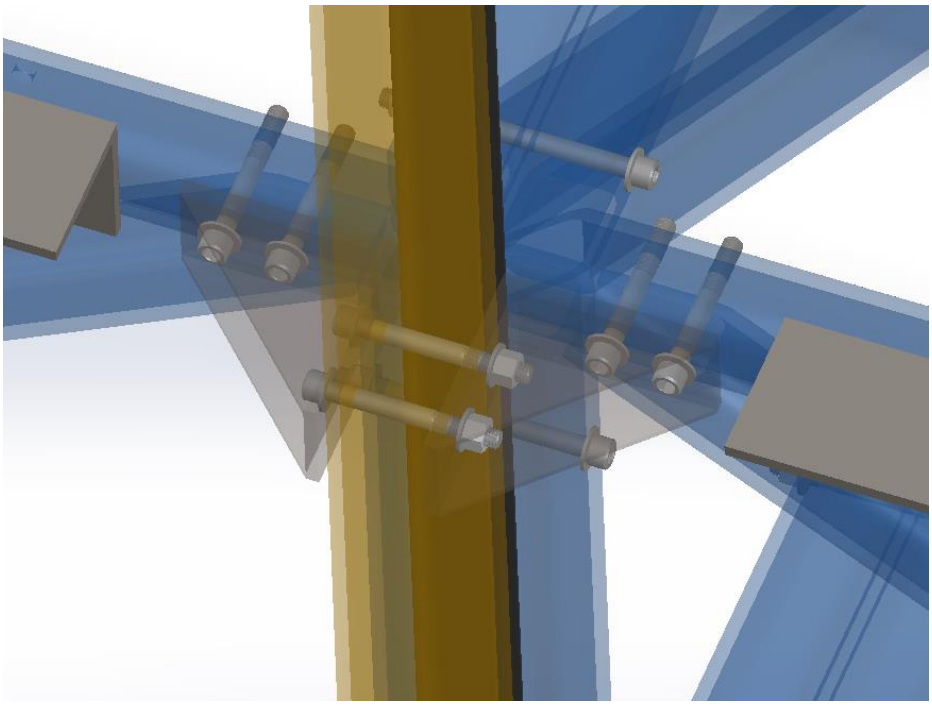

Figure 3.8a: Gussets to chassis and vertical members bolt connection.

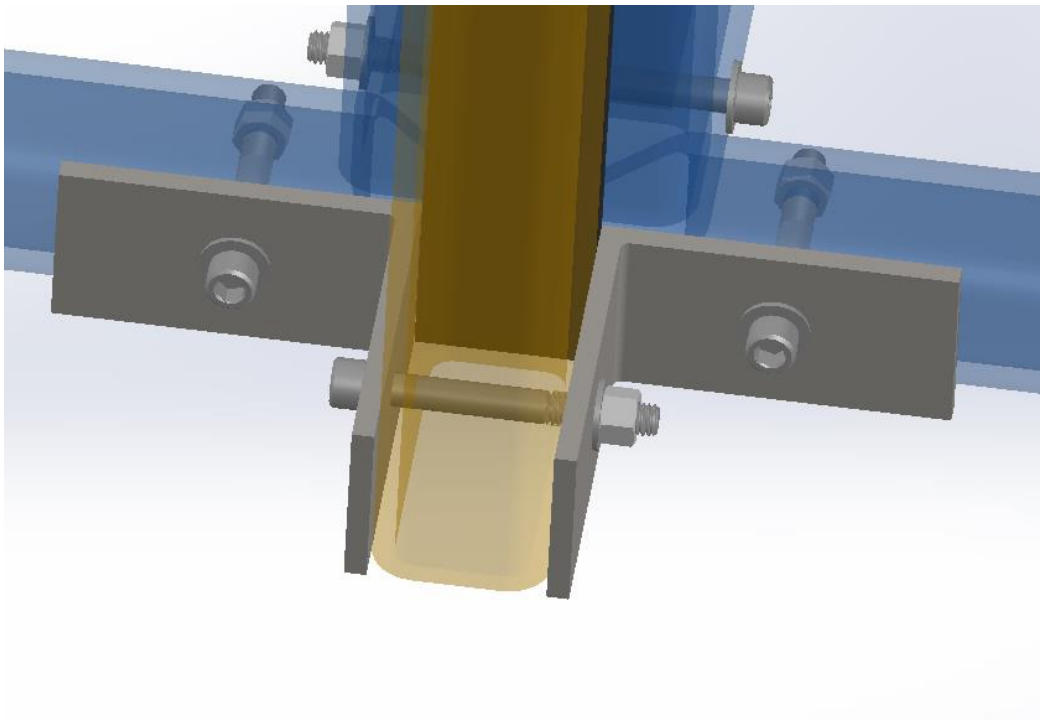

Figure 3.8b: Angle irons to chassis and vertical members bolt connection.

3) Angle beams to chassis and horizontal members

The angle beams located at both the bottom and the top of the glass play an important role by adding rigidity to the structure (see Figure 3.9a and b). The angle beam at the mid-section located at the lower vertical glass edge aids in glass deflection and reducing the maximum principal stresses on the glass. Another important parameter of them is that they help compress the silicone and glass inward during installation, ensuring a watertight joint. the maximum stress is located connection to the chassis is shown in Figure 3.9a. The upper angle beams serve to help keep the top pane in place.

4) Horizontal Members to vertical members

As mentioned in Chapter 3, the horizontal members have welded slots (not shown in the CAD or this paper) that slide into the top of the vertical members. Holes were drilled to accommodate bolts, adding rigidity to the top level of the structure which is susceptible to bending loads.

Figure 3.9a: Angle beam to chassis module bolt connection.

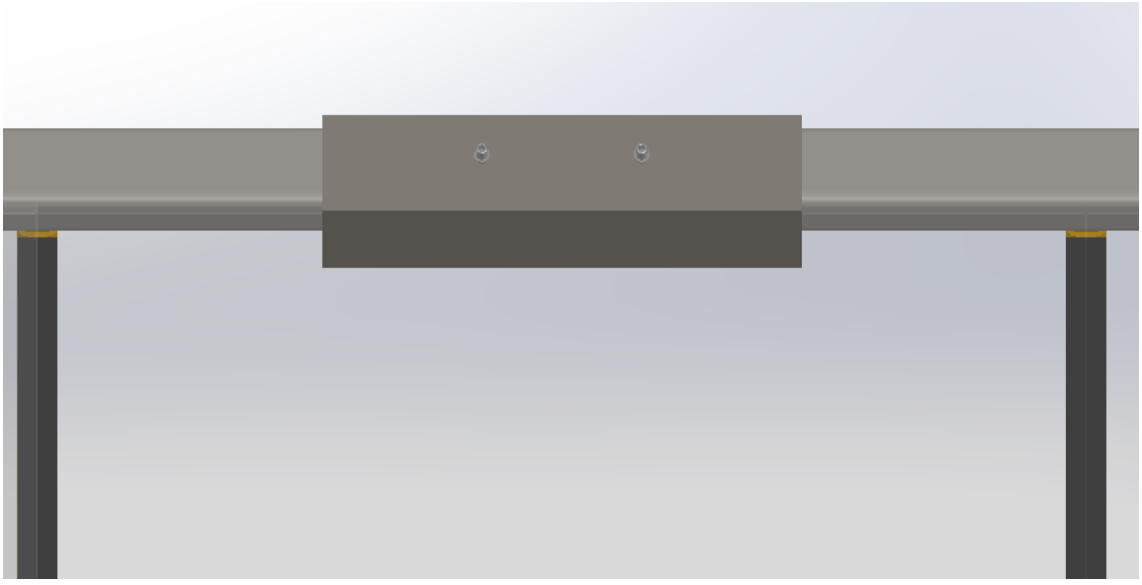

Figure 3.9b: Angle beam to horizontal member bolt connection.

5) End tanks to test channel

The connection between the tanks and test channel is the most significant bolt configuration for the entire water channel. To ensure a leakproof seal, there must be a sufficient and permanent compressive force between the vertical members and the tanks. This is achieved with a rubber gasket profile placed in between these sections. To account for CAD schematics of these connections are given in Figures 3.10. Since the primary goal was to ensure a tight seal, bolts were not configured for a specific preload and were thus not analyzed for stresses.

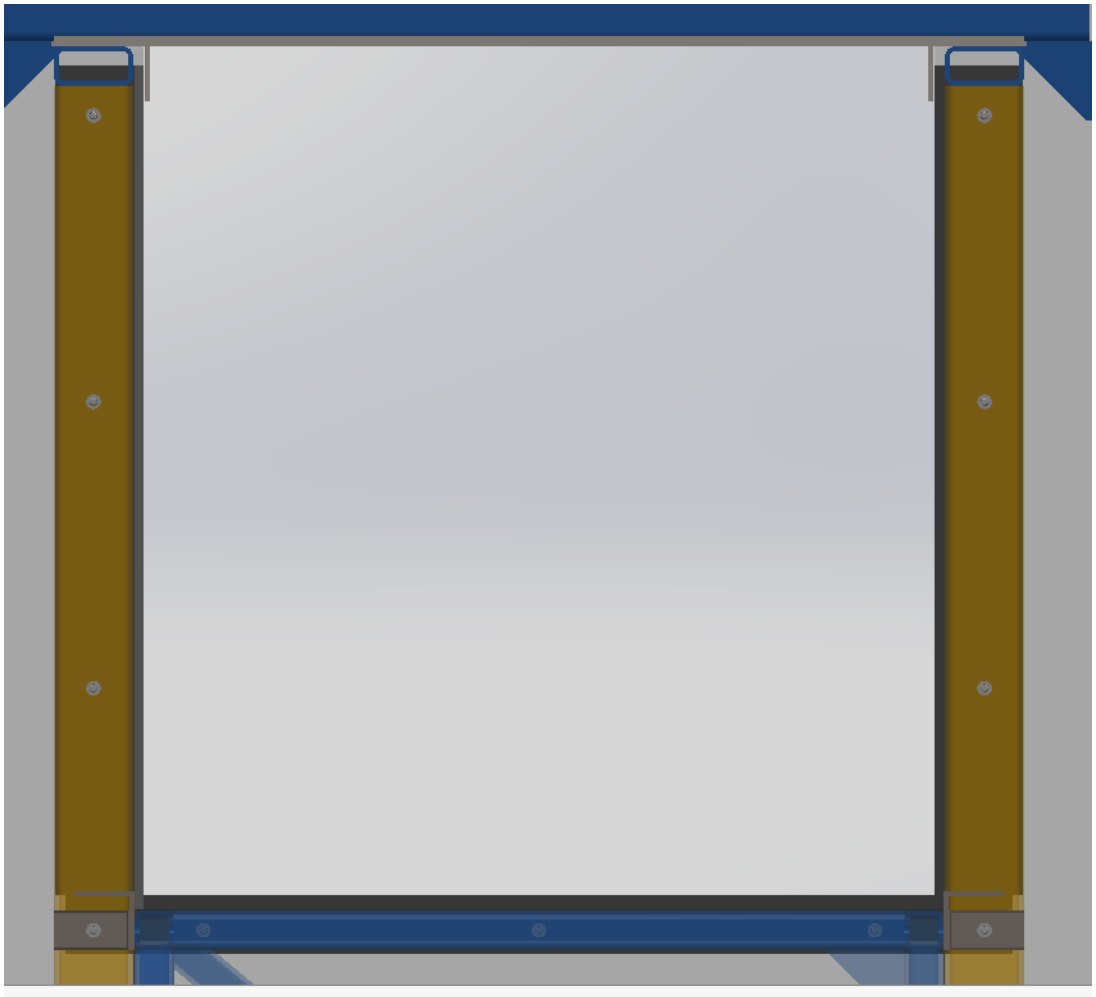

Figure 3.10a: Front view of test channel – end tank connection.

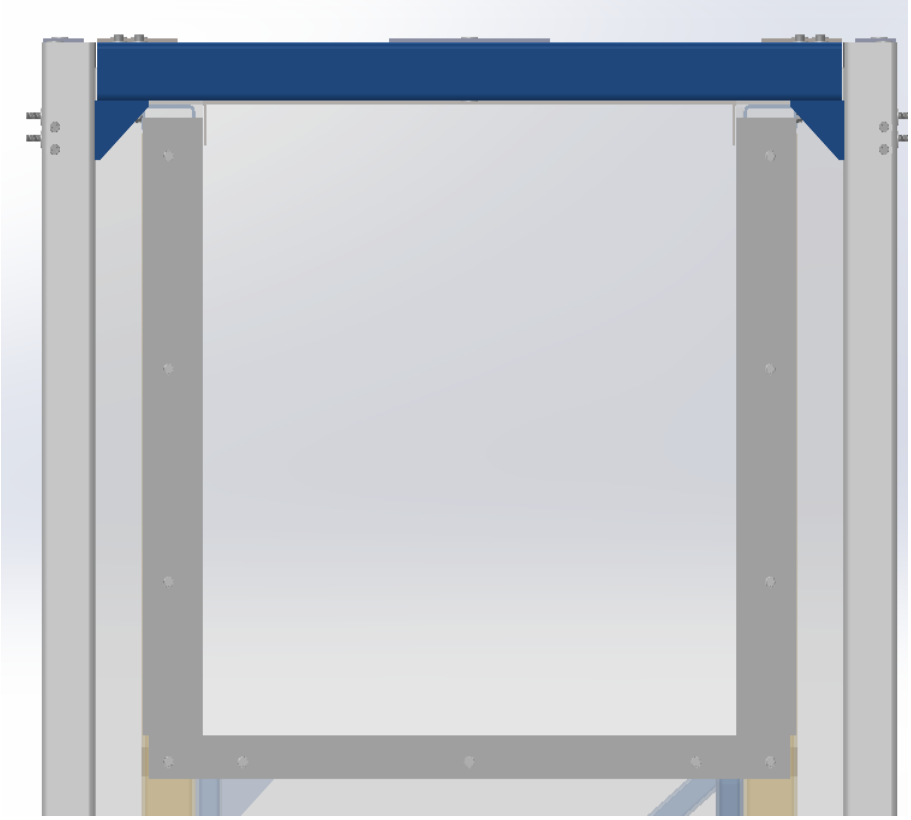

Figure 3.10b: Rear view of test channel – end tank connection.

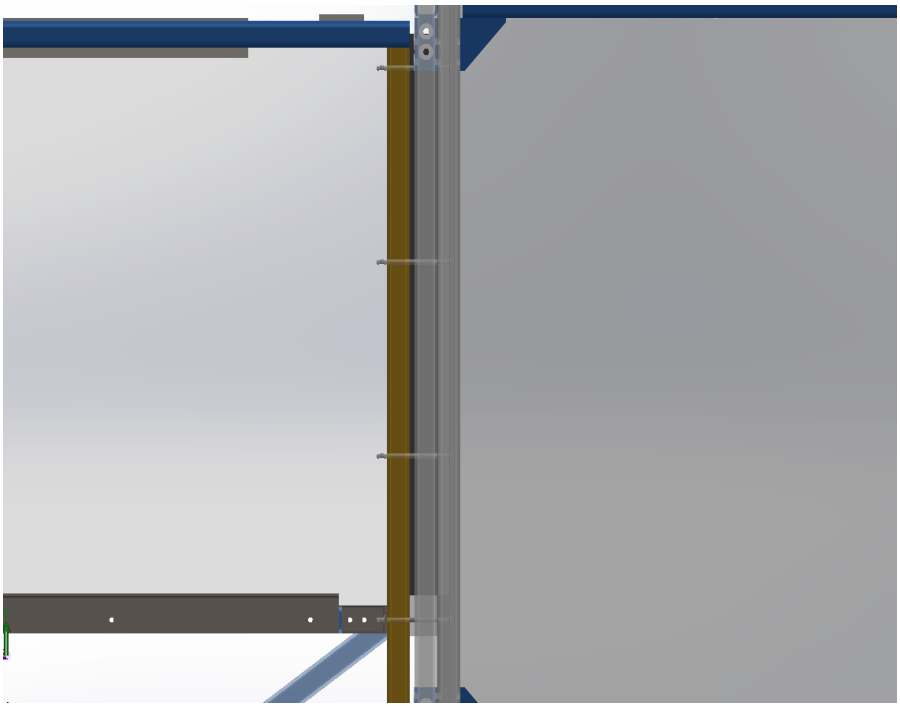

Figure 3.10c: Side view of test channel – end tank connection.

4 End Tank

The sole purpose of the end tank is to enable recirculation of water back through the pump. The important parameters of this tank were determining its strength and deflection due to the static pressure of water, assuming the tank was completely filled. A CAD schematic is shown in Figure 4.1. The tank was assumed to be fully welded along all inner edges, which serves as a good approximation to the real-life scenario. The tank dimensions were selected large enough to eliminate backflow. Further testing by utilization both CFD and experimentation is recommended to validate flow parameters and pump characteristics.

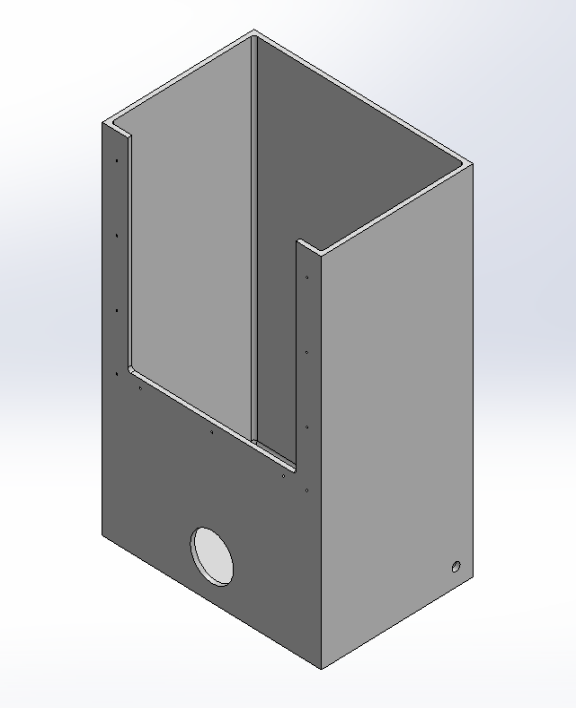

Figure 4.1: CAD schematic of end tank.

For the stress distribution shown in Figure 4.2, a maximum von Mises stress of about 1,562 psi is shown to be located at the fillets where the tank opening is, giving a 2.18 factor of safety. This is due to the nature of fillets being a location of stress concentration,

and the added pressure from the side walls raises the stress at this location. This high stress peak should be accounted for if the water level in the tank is raised relatively high to its maximum depth. If this is the case, it is recommended that a steel frame be welded around the entire tank for added rigidity.

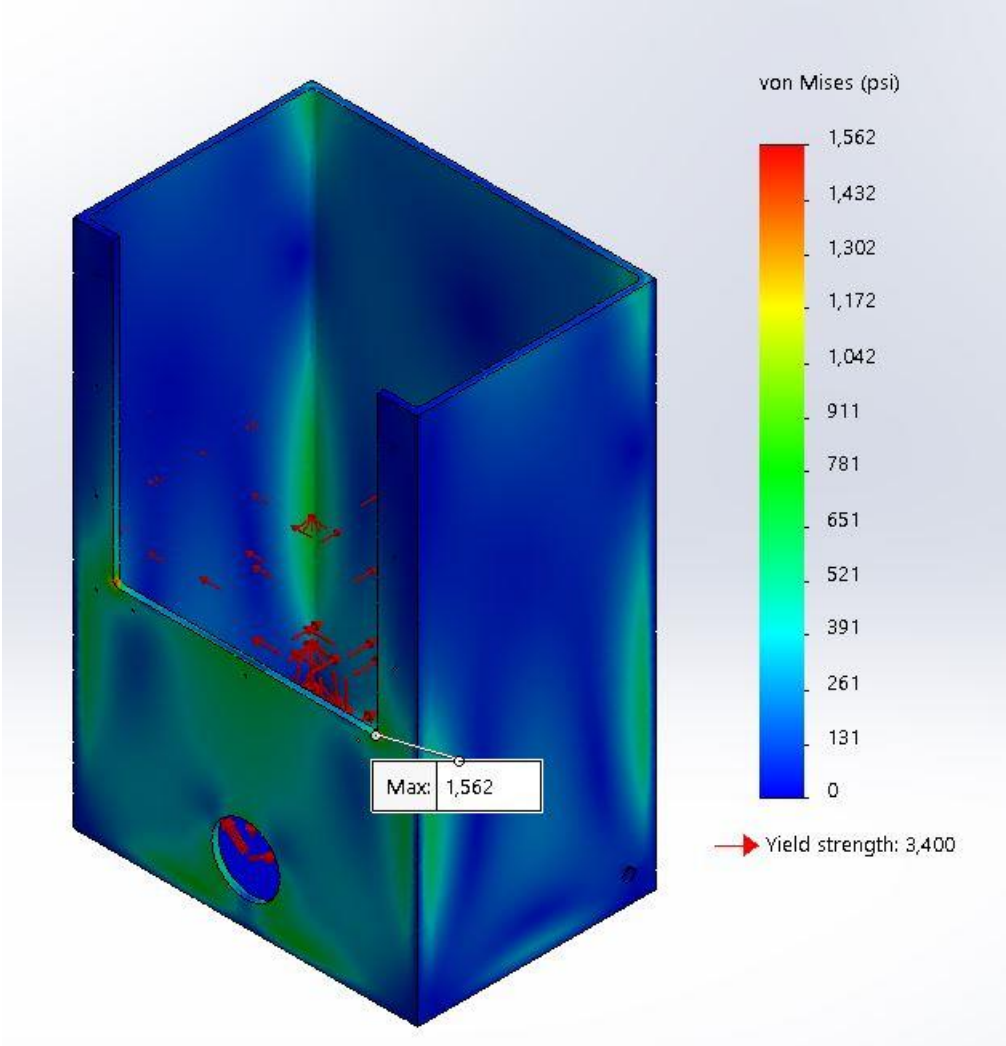

Figure 4.2: Von Mises stress on end tank.

The deflection of each wall is shown in Figure 4.3 on the next page. Neglecting the maximum displacement due to the opening of the front wall being supported by the rubber gasket, the maximum displacement is found to be approximately 1.47 inches. It serves as a good reminder that this case of a fully filled tank will likely never occur and that any noticeable deformation can be resolved by welding a steel reinforcement frame around the tank.

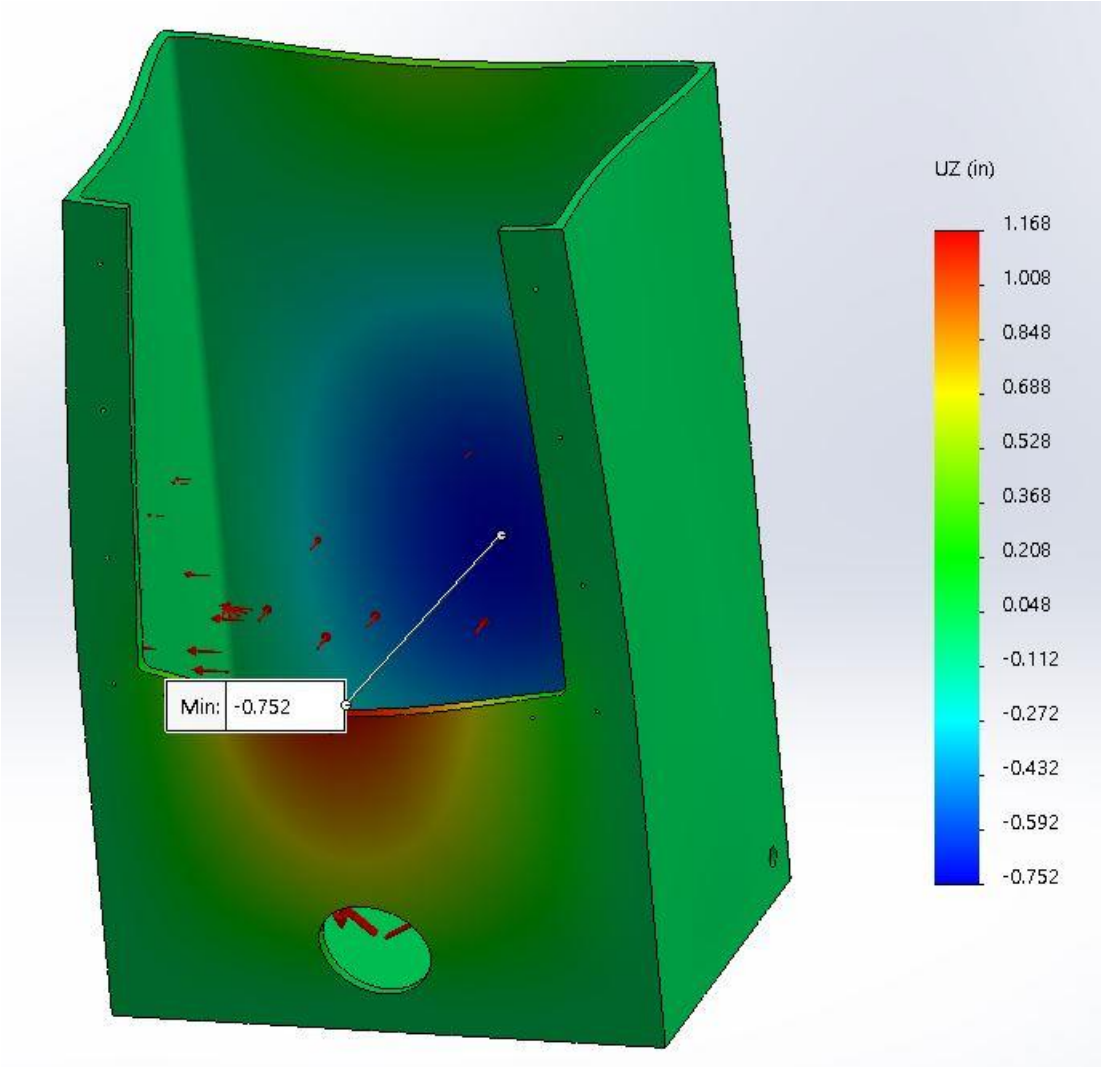

Figure 4.3: Maximum deflection of end tank.

Material selection for the tank was based off the calculated von Mises stress and availability/pricing of vendors, the latter playing a much greater significant role. Considering manufacturing, delivery time, cost, and material, cast polypropylene was selected as the tank material. The tank consists of several polypropylene sheets welded together. With a yield strength of 3,400 psi, a factor of safety of 2.43 was calculated for the von Mises stress (ignoring the fillet stress concentration).

5 Water Channel Assembling

With the design complete, purchasing and assembling was ready to begin. The assembling was done in three phases. To account for floor space and the difficulty that would arise if the test channel was put together first, the first phase was to assemble the transparent tank and test it for any leaks. The next phase was to connect the test channel with the transparent tank and then add each of the three chassis sections one by one. The last phase was to bond the necessary pipe connections and pump beneath the chassis modules, then bolt and bond the plastic end tank to the vertical support members and the pipe connections, respectively. For this part, all components were tested for leaks. As one can imagine, a perfect design and assembling scenario is impossible to achieve in real life; many problems with installation arose, which caused a chain reaction that affected several components. These are discussed relative to their respective section.

5.1 Transparent Tank

Metal tubing and raw metal beams were purchased from KH Metals & Supply, a local metal supplier and then directly sent to a machine shop for welding and drilling. The PVC base was purchased from Boedecker Plastics Inc., located in Texas. Fred's Glass in Riverside provided the glass for the transparent tank. Once cleaned of rust and painted, the support frame was first bolted together and placed upright around the PVC base to check for any irregularities. This was installed on the floor due to the weight of the entire structure. The bolt pattern required that the bottom front and rear beams be installed and tightened first. Once the frame was set up around the base, it came to immediate attention that the rear and right side of the support structure were not aligned properly with the PVC base. This may have been due to several things, which include floor unevenness and/or any dimensioning errors of the base or support structure, but this meant that parts of the support structure would not be in contact with parts of the glass. If not addressed, the water pressure may have ripped the silicone off of the glass and caused a leak. Unfortunately, photos of the initial support frame setup and the misalignment issue were not taken, but this issue was deemed "fixable" simply by filling the gaps with silicone and letting it dry once the glass panels were installed. In doing this, the assumption was that the dried silicone would act as a layer of rubber that contacts the glass and metal frame. Figure 5.2 is as a visualization of the frame setup without any other components in the way.

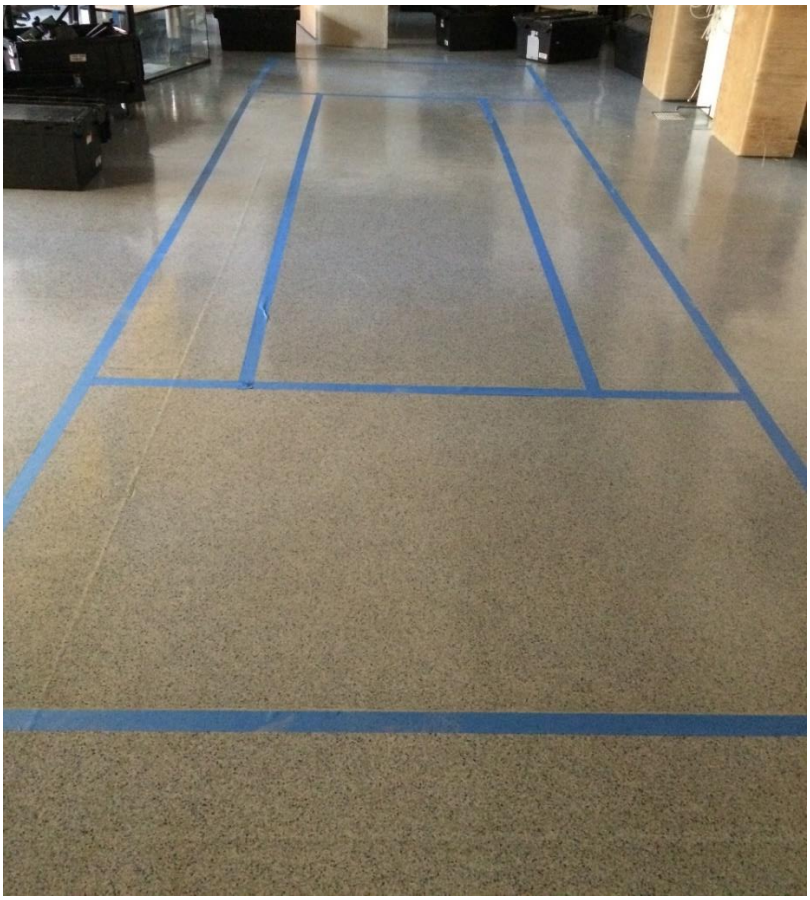

Figure 5.1: Marked tape indicating the 76.25 ft^2 space taken up by the water channel, located in Bourns Hall B140.

Figure 5.2: Support frame holding together the three tempered glass panels.

Once the support frame was setup, rubber sheets were placed on all interfaces that the steel would contact glass to reduce any stress concentrations, and the three tempered glass panels were then installed. This was done by removing the right side beams of the support frame to accommodate room to move the glass inside. Silicone was added all over the PVC base groove that the three glass panels would stand on. Because of this, the installation process had to be done relatively quickly before the silicone dried. This led to all three panels not being centered about the PVC base and the left side glass panel being further away from the front section than the right side, which would create another large gap. Once all the panels were fixed in place with the angle beams, the entire frame was reconnected to hold the glass together until the front panel was ready to be installed.

The acrylic front panel, made of Plexiglass, was purchased from Ridout Plastics, located in San Diego, who also cut it to size to match the opening to the channel. Once delivered, the machine shop at Bourns College of Engineering here at UCR drilled the appropriate holes for the bolts and the fitting. The panel (shown in Figure 5.3) was then put in place with silicone and the entire frame was bolted together. The large gap where the front panel and left side glass panel edges connect was soaked with silicone.

Figure 5.3: Machined Plexiglass front panel.

However, once the entire frame was reconnected, two new issues arose. First, a gap formed between the vertical beams of the front panel and the gussets of the side beams. To combat this, rubber profiles the same shape as the gussets were added to close the gap and

form contact between all members (Figure 5.4). Although this effectively reduces the joint member stiffness, the design assumption was that the bolts feel 100% of the external loading; the joint member stiffness is zero. The second problem was that when looking from the top, the front panel appeared to be at a substantial angle from the bottom edge to the top edge. If left unfixed, this would have misaligned the inside bolts with the channel-tank rubber gaskets and the channel vertical members.

(a) (b)

Figure 5.4: (a) Rubber profiles added in between the gussets and vertical beam to allow for joint contact. (b) Closeup of rubber profiles.

Because of this, it was decided to reinstall the front panel, which is shown in Figure 5.2. Once the silicone was removed, the front panel was ready to move. However, the sharp corners that remained from the initial channel cut were not accounted for when lifting the

panel up, causing one side to experience too much bending, resulting in one section cleanly snapping off (Figure 5.5). To fix this, the pieces were bonded together with acrylic weld-on, but the bond took several attempts before ensuring it was adequate enough. Once complete, the entire panel was reinstalled with an emphasis on preventing it from angling. Silicone was added around the crack for added measure.

(a) (b)

Figure 5.5: (a) Plexiglass snap due to the stress concentration at the sharp corner of the opening. (b) Close-up of the snap.

Once the front panel was reinstalled, a quick inspection showed that several interfaces between the glass-rubber-metal beams were not in contact with one another. This was resolved by adding an adequate layer of rubber in between the interface and forcibly

compressing it against the glass to ensure contact. After this, the pipe components were added with the front panel and base for leak testing.

5.2 Test Channel

For the test channel, all tubing and metal was purchased from Industrial Metal Supply in Riverside. Fred's Glass again provided the tempered and annealed glass panels. All machining was done at Riverside Machine Works. The machinists ensured that their method of welding provides a flat reference for both the top and bottom of the chassis. With the transparent tank complete, it was decided to first compress the rubber gasket between the vertical members and the front panel, shown in Figure 5.6. After cleaning off rust and painting, a large, handmade rubber gasket with matching bolt pattern was added between the acrylic panel and the vertical support beam. The gasket is composed of six layers of ½" 30A durometer rubber sheets pasted together in a U-shape with Scotch-Weld 1357 High Contact Neoprene Adhesive for added bonding strength. This same paste was used on both the acrylic panel and vertical beam for extra adhesion. Once added, 316 stainless steel bolts were inserted and tightened through the front panel – rubber gasket – vertical member and first chassis module. As mentioned in Chapter 4, the preload torque on these bolts was not considered since it was assumed that the gasket would first deform before any considerable bolt loading. The bolts were tightened in a specific pattern to ensure each section received a similar amount of compression. This was hard to quantify since some bolts had more difficulty getting through their respective hole than others. Once it appeared that the gasket was fully compressed, silicone was added around the bolts and the joint crack.

Figure 5.6a: Gasket appearance from inside of the transparent tank.

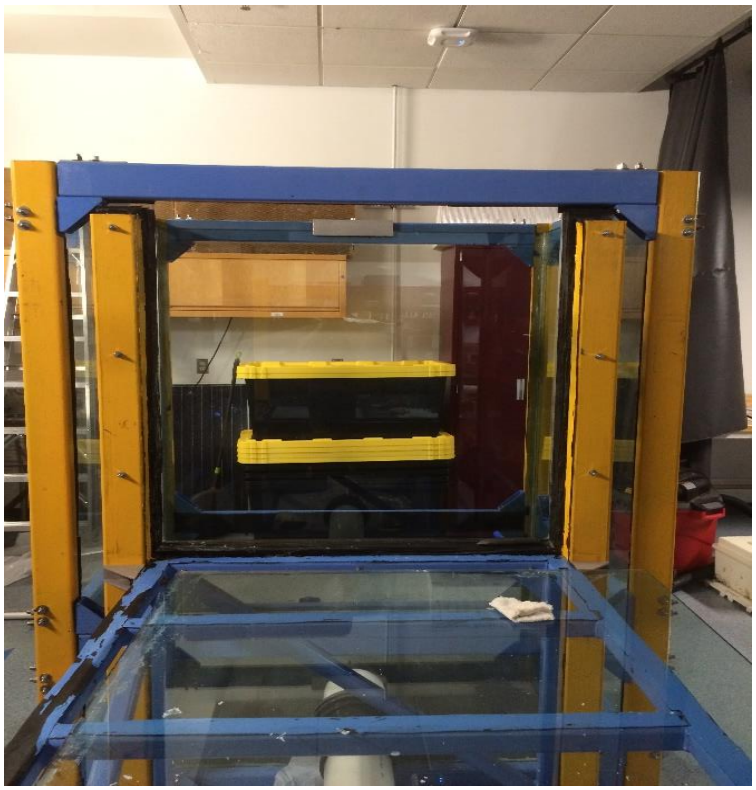

Figure 5.6b: Gasket appearance from outside the transparent tank.

However, when tightening the bolts to the cracked potion of the front panel, the weld between the two acrylic parts snapped. It was decided to leave the panel the way it was rather than remove everything to redo the weld. Silicone was added all around the crack to minimize water leakage. For future purposes, it is recommended that a welded acrylic plate be added on both the inside and outside of the cracked section to create a more permanent, watertight bond.

With the gasket compressed and the front panel temporarily fixed, the vertical members were then set up to guide the two other chassis modules into position (Figure 5.7a and b on the next page). These were connected together by the two slotted horizontal members. By adding the vertical members, clamps were able to be placed on top to help pinch the glass during silicone curing to prevent as much misalignment as possible. The test section was assembled one section at a time, beginning with the section closest to the transparent tank. Similar to the transparent tank, rubber was added along all glass-metal interfaces to reduce any stress concentrations that may potentially arise.

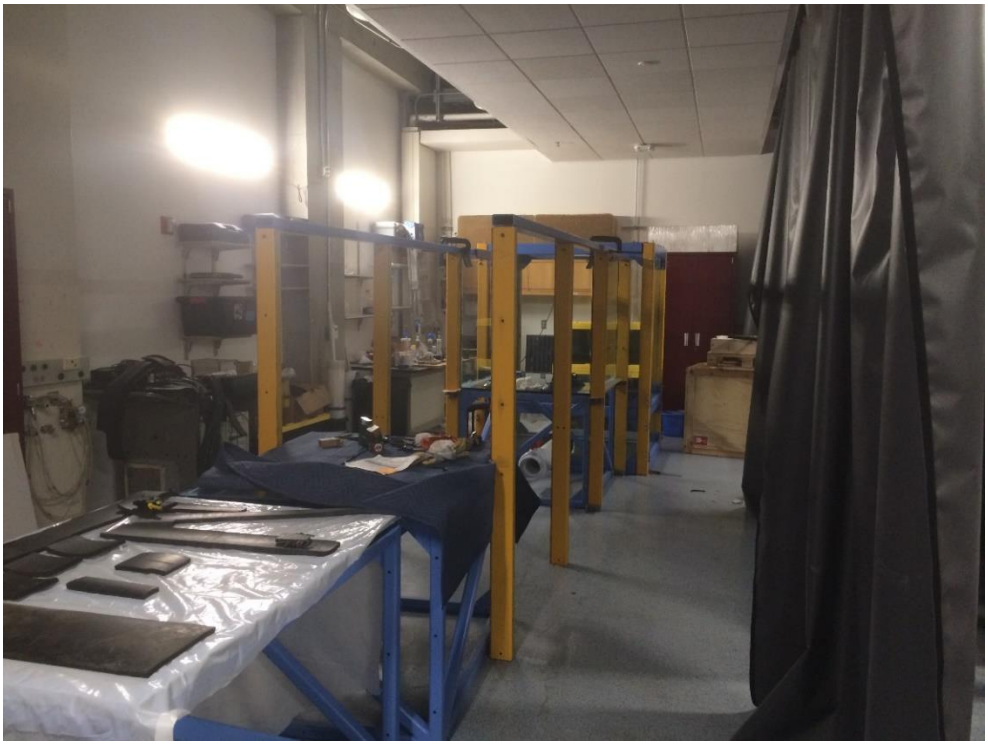

Figure 5.7a: Setup of the vertical members. This was done to guide the chassis modules and to aid in holding the vertical glass panels together once installed

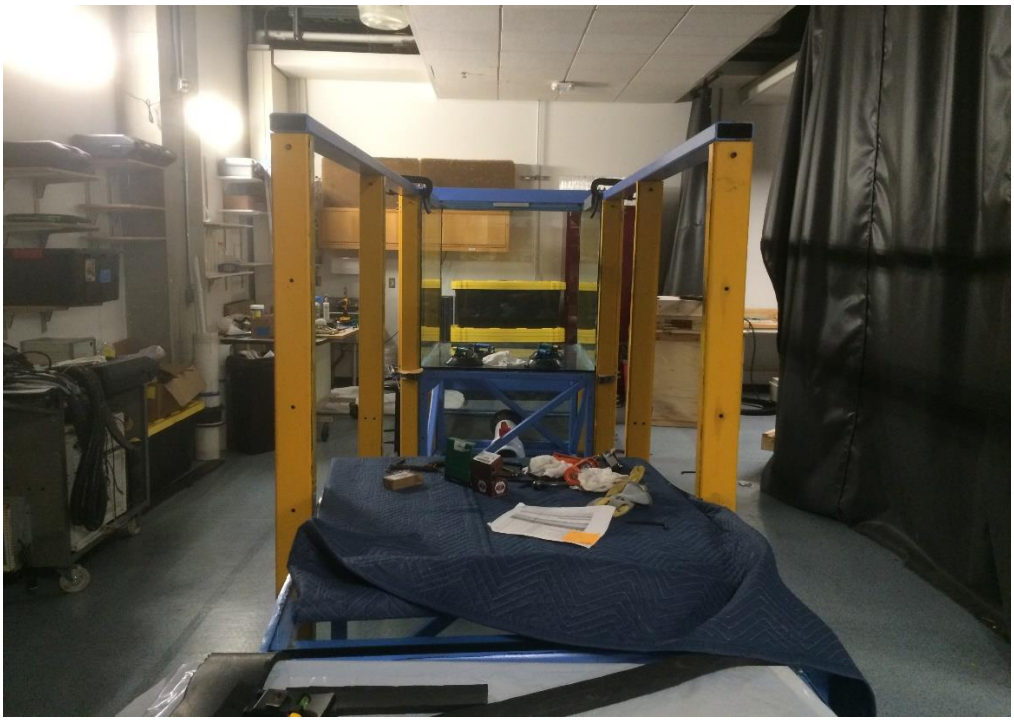

Figure 5.7b: Front view of the vertical/horizontal member setup.

The horizontal glass panels were placed inside first to serve as a base for the vertical glass panels. Silicone was then added all around the horizontal glass edges and up the vertical members. The vertical glass panels were added one side at a time; once in, the end/corner gussets and the bottom/top angle beams of the same side were tightened. Figures 5.8-5.12 show the setup of each section and a visual of the bolt misalignment between the second and third chassis module that is explained in the next paragraph.

Figure 5.8: First section completed.

Figure 5.9: Alternative view of the first section.

Figure 5.10: Second section completed.

Between the second and third chassis section, the floor unevenness became prominent enough that the chassis-chassis bolts did not align. Although the bolts were able to be forced through the member holes, part of the chassis ended up at an angle with its end in midair. To combat this, shims were added around significant areas until it appeared the chassis was flat relative to the floor. Once complete, the third section was installed (Figure 5.11). A second layer of silicone (Figure 5.13) was added along all the inner glass edges as well as over the rubber gasket for further waterproofing.

Figure 5.11: Bolt misalignment between second and third chassis module.

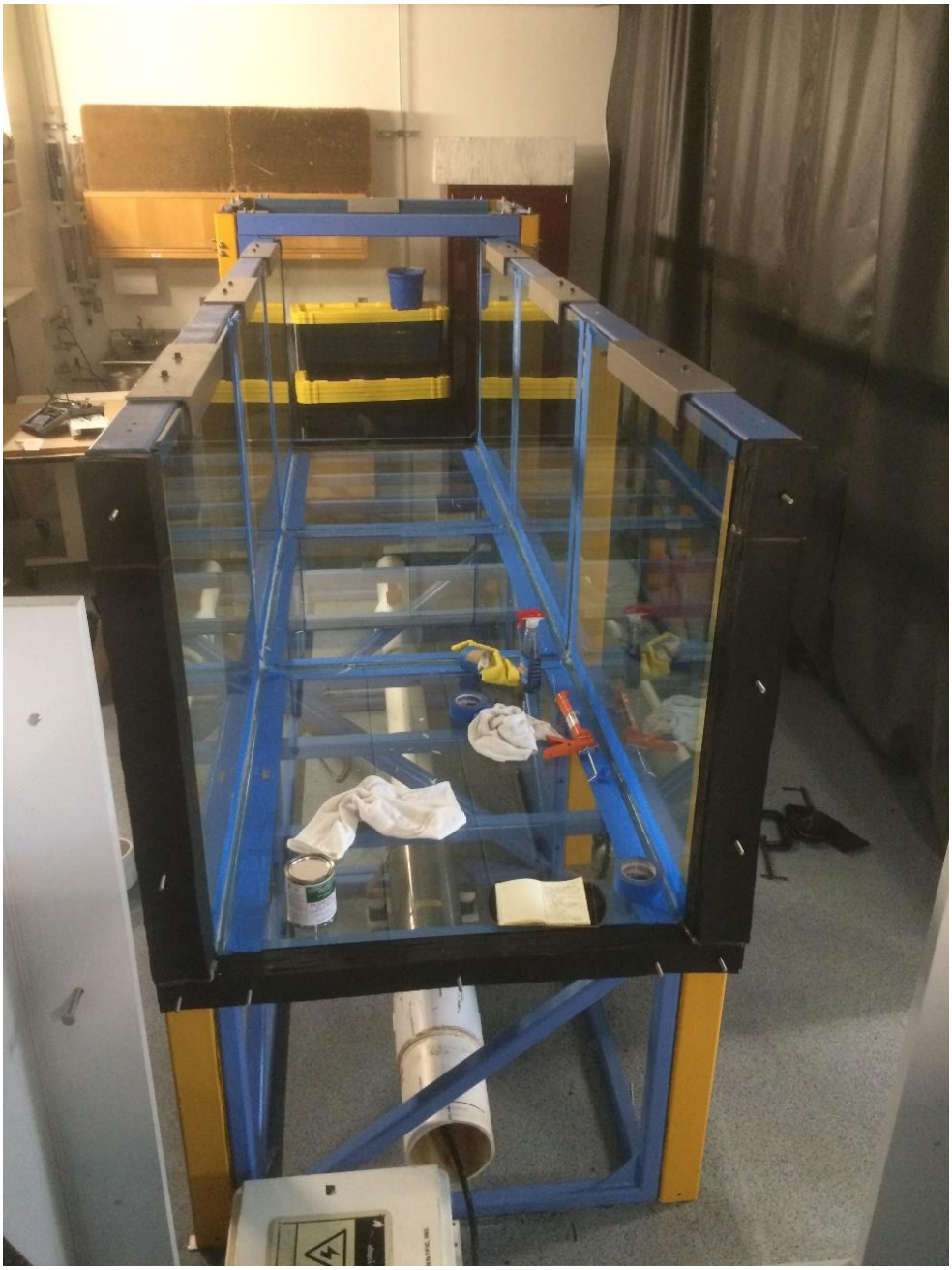

Figure 5.12: Third section completed.

Figure 5.13: Second layer of silicone added at all glass edge interfaces and all over the rubber gasket.

5.3 Pumping System and End Tank

During test channel installation, it was decided that the end tank should be purchased from a professional vendor instead of welding and constructing it in-house to avoid any irregularities that may have formed at the hands of inexperienced students. A vendor proved difficult to find, but eventually the end tank was purchased from Plastics Welding & Fabrication LTD., located in Buda, Texas, who make their tanks out of

copolymer polypropylene; the simulations from chapter 4 are directly derived from the approximated mechanical properties of this material.

Figure 5.14: Delivered end tank.

The installation of this final section proved to be the most difficult; several attempts at creating a watertight seal failed. The consistent issue was that of the 8” bulkhead fitting tightened to the end tank. When compressing the rubber gasket between the end tank and test channel vertical members, the front face of the tank would slightly deform, which may have led to the fitting becoming misaligned with the front face, decreasing the compression between the gasket and the tank. Along with this, leak testing the entire connection indicated several weak points in the threaded and socket connections of the piping. Trial

and error eventually led to every one of these components being resolved. The final assembly put together is shown below in Figure 5.15.

Figure 5.15a: Angled view of filled channel for leak testing.

Figure 5.15b: Closeup of channel.

6 Summary

After completion of several design iterations and numerical simulations of the structural integrity deemed appropriate, the water channel components were purchased, manufactured, and assembled together both as outsource work orders for local machine shops and in house projects handled by students. One important takeaway is that one should never expect CAD drafts and parts to match exactly that of real life, as indicated in the assembling section. The weight of the entire assembly was also underestimated, as moving components often presented a problem. Delays due to delivery, machining work, accidents, and leaking problems proved to be a huge issue, constantly setting back the time for completion. However, assembling the channel with as much precision as possible and fixing and problems took priority over any timeframe, the expectation being that the final product indicates so.

Possible future upgrades for the water channel include:

- Flow conditioning honeycombs and screens
- Railings for towing experiments
- Wave generation mechanism for wave propagation
- Gate between the transparent tank and test section
- PIV camera and laser holders
- Lightning and shading screens
- Stratification system
- Bolt replacement on the transparent tank to use steel alloy bolts

It is also recommended that ongoing maintenance and further testing be done on the tank to ensure proper procedures are taken in case of an accident. This includes:

- Constant monitoring of leaks and weak points/stress concentration raisers of component, some of which include the acrylic front panel crack, the compression of the rubber gasket, and the fillets of the plastic end tank.
- Acquiring an accurate representation of the stresses on components, which can be done with a strain gauge on areas of interest to measure the strain and thus the stress at a location, which can then be compared to numerical results.
- Considering creep loading on the glass is important. As mentioned before, relative humidity and constant loading reduces the strength of glass.
- One important parameter missing are the dynamic forces that occur due to turbulent mixing and vibrational response due to the pump. When the pump was run, it induced a large amount of turbulent mixing in the glass tank. The added stresses due to this should be accounted for in a static-fatigue analysis, accounting for the fluctuations of turbulent mixing and vibrations from the pump.
- Verification of test section flow quality.
- Modification of current Standard Operating Procedure (SOP) and any additional SOP's based off future modifications.

References

Alho, A. T. P., Farias, M. H., & Neto, J. L. S. (2010). On the Design of a Circulating Water Channel for the Brazilian National Institute of Metrology - Inmetro. *15th Flow Measurement Conference (FLOMEKO)*, 1–7.

Balaji, C. R., & Behera, B. (2014). Growth of Boundary Layer Thickness and Length of Fully Developed Flow in Open Channel. *Department of Civil Engineering, National Institute of Technology, Rourkela*.

Budynas, R. G., & Nisbett, J. K. (2011). *Shigley's Mechanical Engineering Design*.

Cranston, G., & Lock, G. (2012). Techniques to encourage interactive student learning in a laboratory setting. *Engineering Education*, *7*(1), 2–10.

Doyle, K. B., & Kahan, M. A. (2003). Design strength of optical glass. *Optomechanics*, *5176*, 14–25.

Economidou, M., & Hunt, G. R. (2009). Density stratified environments: the double-tank method. *Exp Fluids*, 453–466.

Fastenal Industrial & Construction Supplies Technical Reference Guide. (2005), *S7028*(9), 1,9-11,19-24,A1,A6.

Galvez, R., Hoo, J., Perez, O.R. (2017). Final Design Report. FLD-2: Terminal Side Tank and Recirculation Pump System. ME 175C Senior Design Project. *Department of Mechanical Engineering, University of California, Riverside*.

Guzman, F., Zuniga, A., Li, M. Davila, I. (2018). Final Design Report. EFM1: Laboratory Water Channel Re-design. ME 175C Senior Design Project. *Department of Mechanical Engineering, University of California, Riverside*.

Hennessey, T. V. (2005). The Design and Construction of an Open Channel Recirculating Water Tank for the Study of Biological Hydrodynamics.

Lee, J. H. W., & Chu, V. H. (2003). Density Stratification. *Turbulent Jets and Plumes: A Lagrangian Approach*. 135-145.

Loehrke, R. I., & Nagib, H. M. (1976). Control of Free-Stream Turbulence by Means of Honeycombs: A Balance Between Suppression and Generation. *Journal of Fluids Engineering*, *98*(3), 342-353.

Millero, F. J., & Huang, F. (2009). The density of seawater as a function of salinity and temperature. *Ocean Science Discussions*, *6*(1), 153–169.

Millero, F.J. and Poisson, A. (1981). International one-atmosphere equation of state for seawater. *Deep Sea Res.* Vol. 28A. 625-629.

Nedyalkov, I. (2012). Design of Contraction, Test Section, and Diffuser for a High-Speed Water Tunnel. *Chalmers University of Technology*.

O. Ekwueme, C., E. Ekon, E., & C. Ezenwa-Nebife, D. (2015). The Impact of Hands-On-Approach on Student Academic Performance in Basic Science and Mathematics. *Higher Education Studies*, *5*(6), 47.

Oster, G. (1965). Density Gradients. *1965 Scientific American, Inc.*

Panah, A. E., & Barakati, A. (2017). Design and Build a Water Channel for a Fluid Dynamics Lab. *American Society for Engineering Education*.

White, F. M. (2011). *Fluid Mechanics* (7th ed.). 701-741.

Wilhelmus, M. M., & Dabiri, J. O. (2014). Observations of large-scale fluid transport by laser-guided plankton aggregations. *Physics of Fluids 26, 101302*.

Cellini, F., Peterson, S. D., & Porfiri, M. (2017). Flow velocity and temperature sensing using thermosensitive fluorescent polymer seed particles in water. *International Journal of Smart and Nano Materials*, *8*(4), 232–252.

Roque, G., Meneghini, J. R., Aranha, J. A. P., & Coleto, W. G. P. (2005). Design, Assembling and Verification of a Circulating Water Channel Facility for Fluid Dynamics Experiments.

Loehrke, R. I., & Nagib, H. M. (2010). Control of Free-Stream Turbulence by Means of Honeycombs: A Balance Between Suppression and Generation. *Journal of Fluids Engineering*, *98*(3), 342.

Bansal, N. P., Doremus, R. H. (1981). Handbook of Glass Properties. *Materials Engineering Department. Rensselaer Polytechnic Institute.* 363-377.

Lalli, C. M., & Parsons, T. R. (2002). Biological Oceanography: An Introduction. *Journal of Experimental Marine Biology and Ecology*, *202*(2), 24.

Fernando, H. (2002). Turbulent Mixing In Stratified Fluids. *Annual Review of Fluid Mechanics*, *23*(1), 455–493.

Sutherland, B. R., Hughes, G. O., Dalziel, S. B., & Linden, P. F. (2000). Internal waves revisited, 209–232.

Steeve, B. E., & Wingate, R. J. (2012). Aerospace Threaded Fastener Strength in Combined Shear and Tension Loading. NASA/TM 217454.

Appendix A: Transparent Tank

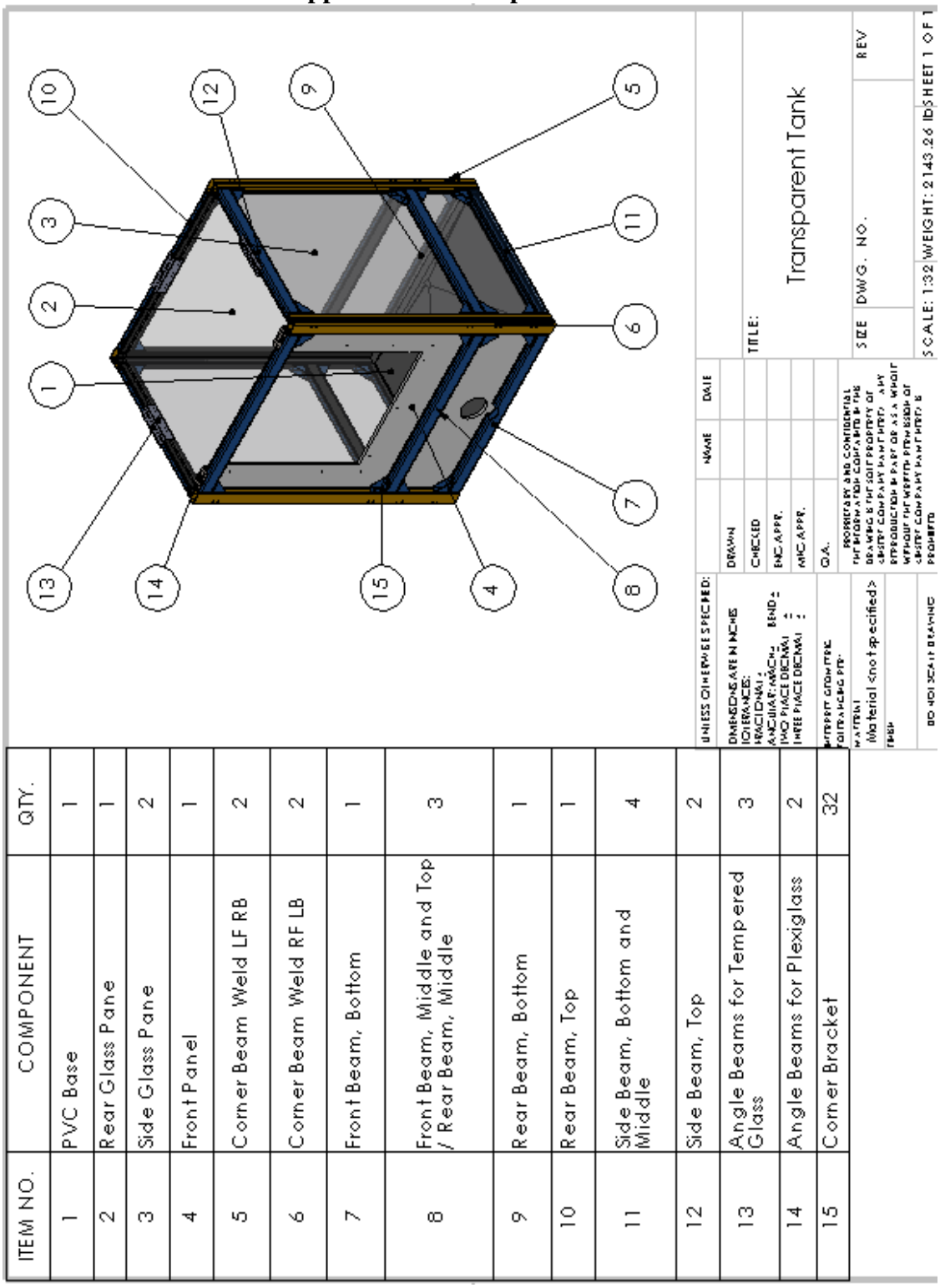

ITEM NO.	COMPONENT	QTY.
1	PVC Base	1
2	Rear Glass Pane	1
3	Side Glass Pane	2
4	Front Panel	1
5	Corner Beam Weld LF RB	2
6	Corner Beam Weld RF LB	2
7	Front Beam, Bottom	1
8	Front Beam, Middle and Top / Rear Beam, Middle	3
9	Rear Beam, Bottom	1
10	Rear Beam, Top	1
11	Side Beam, Bottom and Middle	4
12	Side Beam, Top	2
13	Angle Beams for Tempered Glass	3
14	Angle Beams for Plexiglass	2
15	Corner Bracket	32

Figure A1: Transparent Tank Components

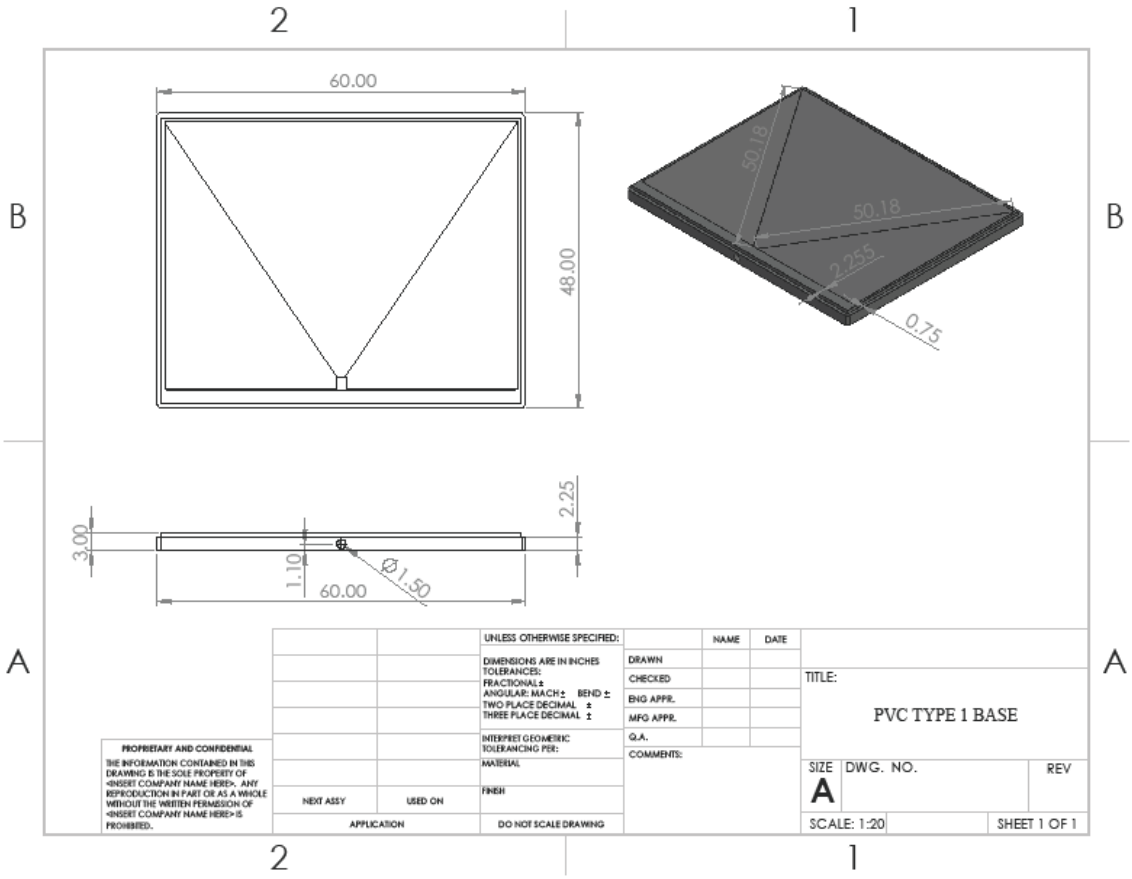

Figure A2: PVC Type 1 Base

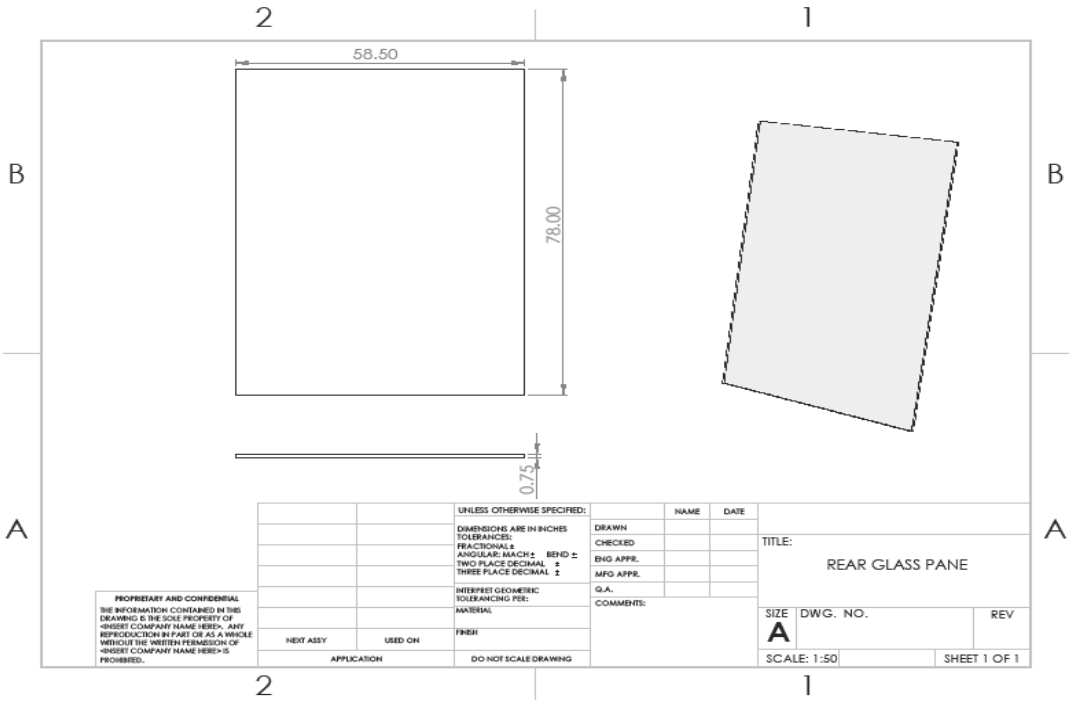

Figure A3: Rear Glass Pane

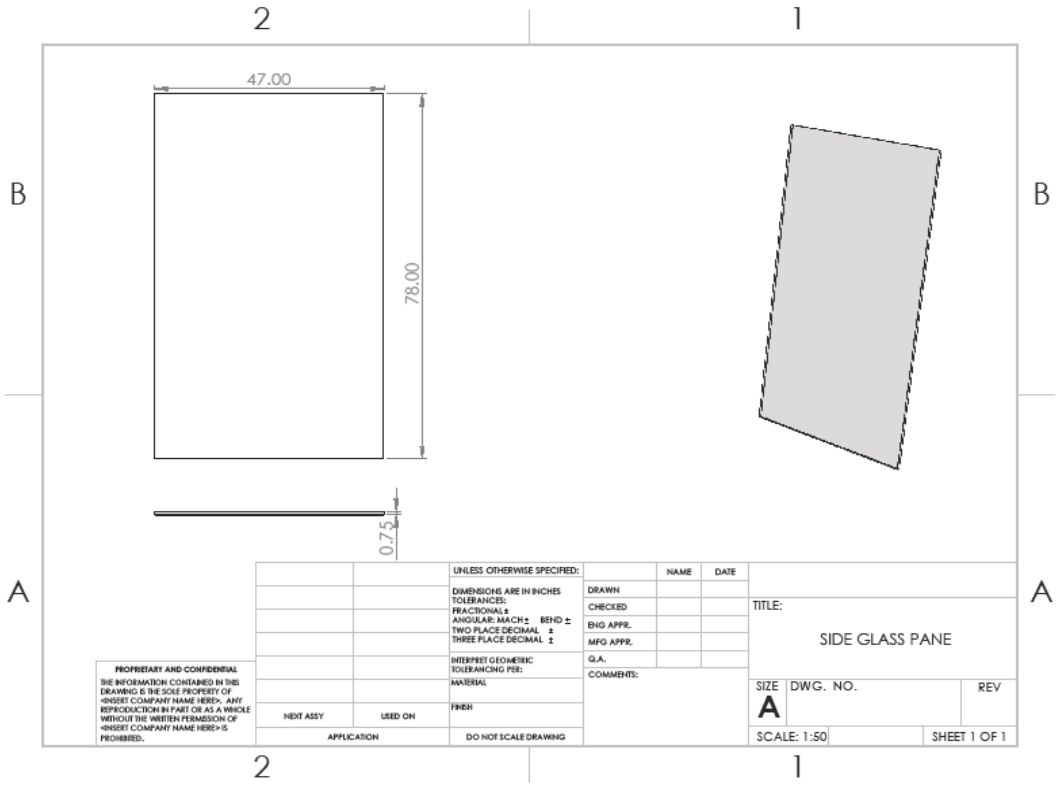

Figure A4: Side Glass Pane

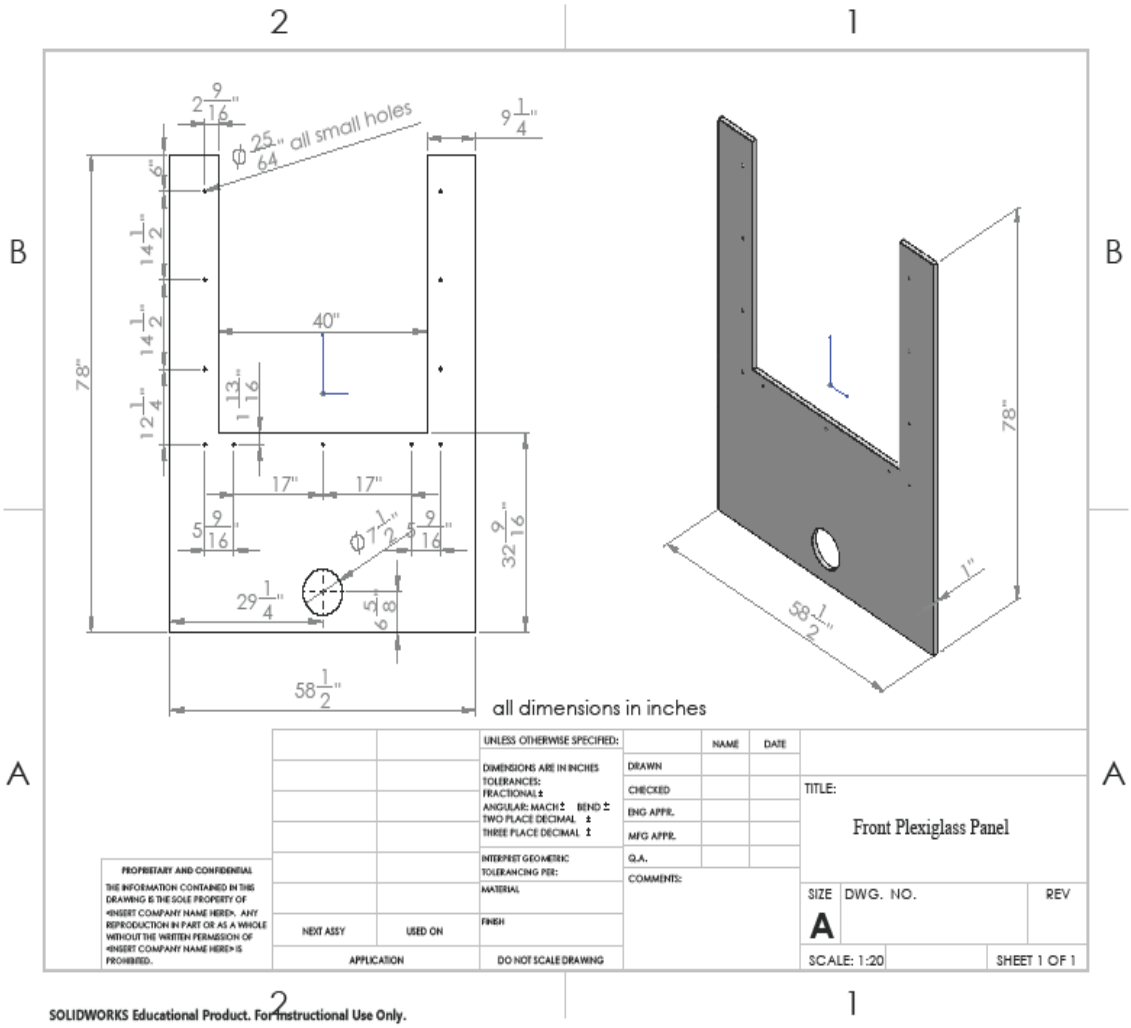

Figure A5: Front Panel

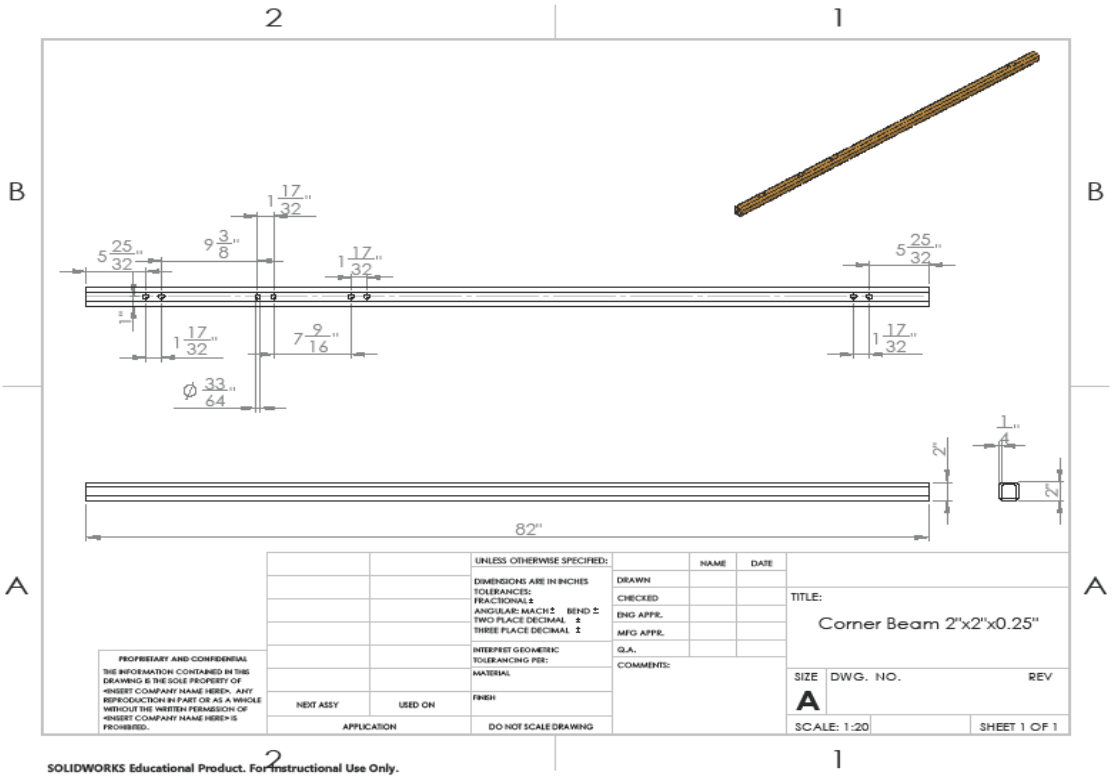

Figure A6: Corner Beam 2” x 2” x 0.25”

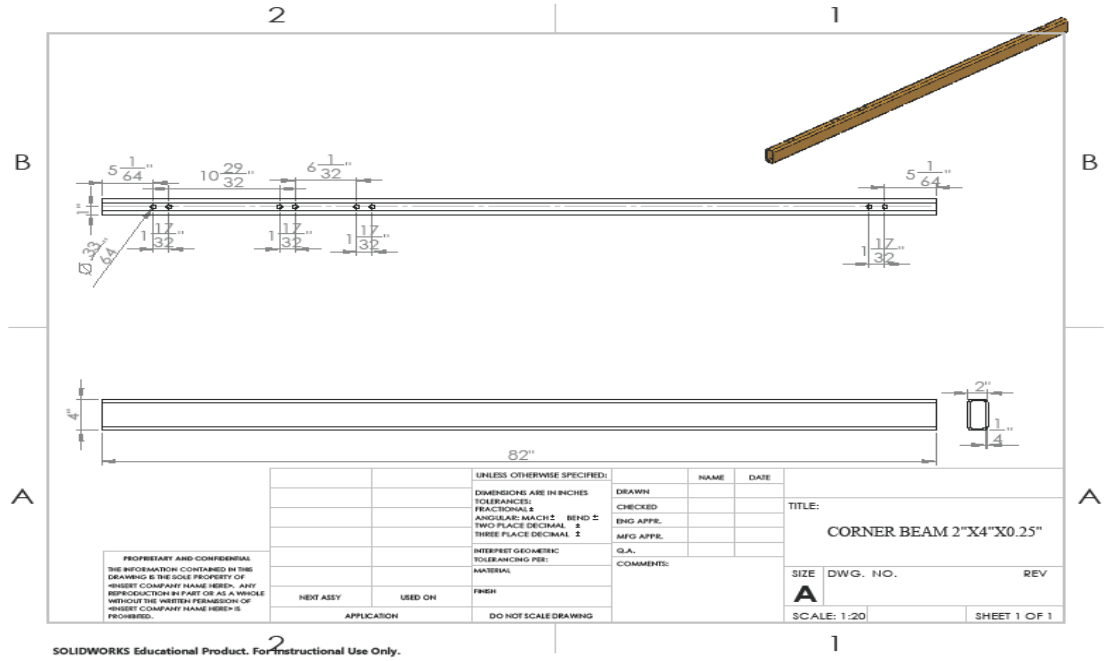

Figure A7: Corner Beam 2” x 4” x 0.25”

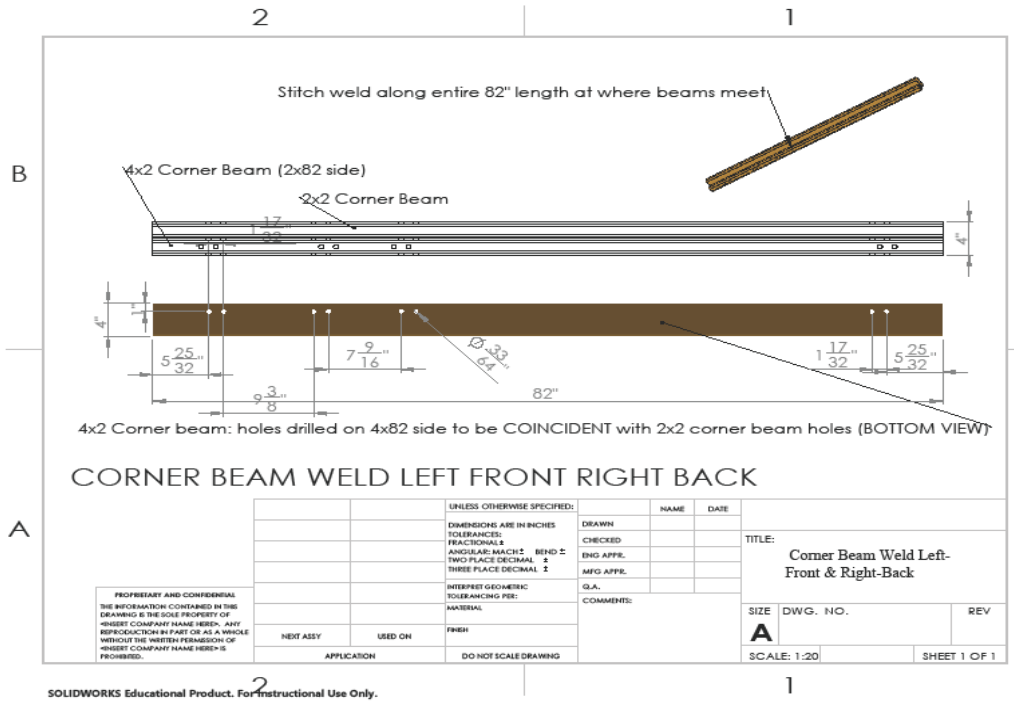

Figure A8: Corner Beam Weld Left-Front & Right-Back

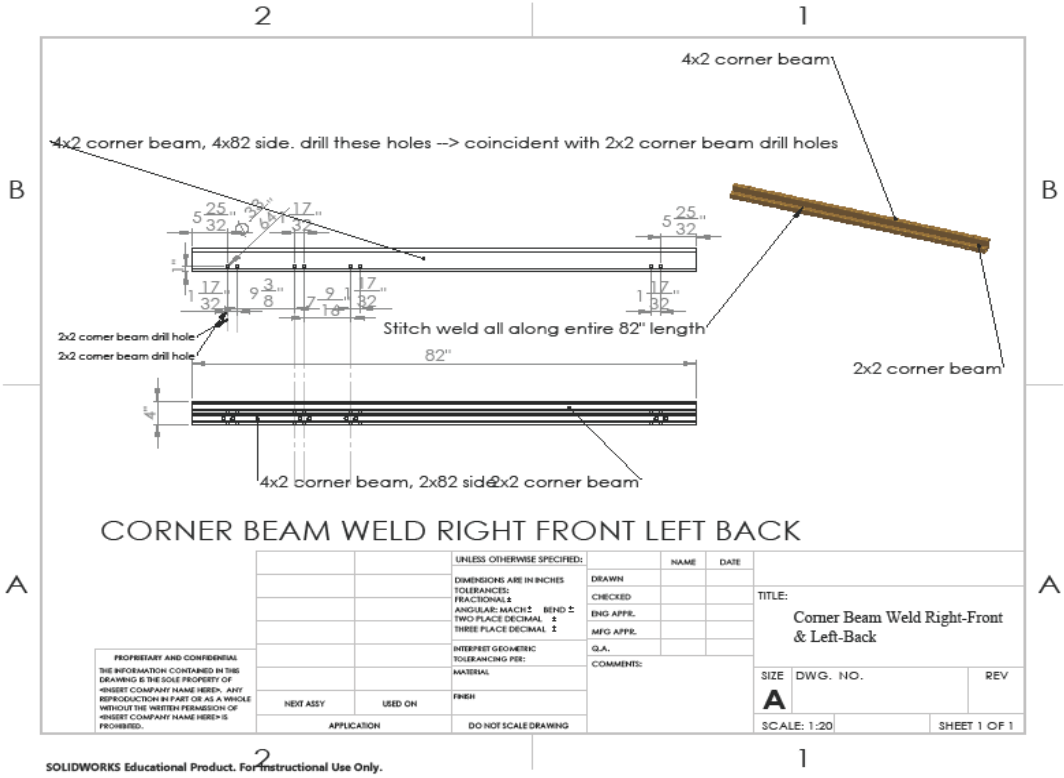

Figure A9: Corner Beam Weld Right-Front & Left-Back

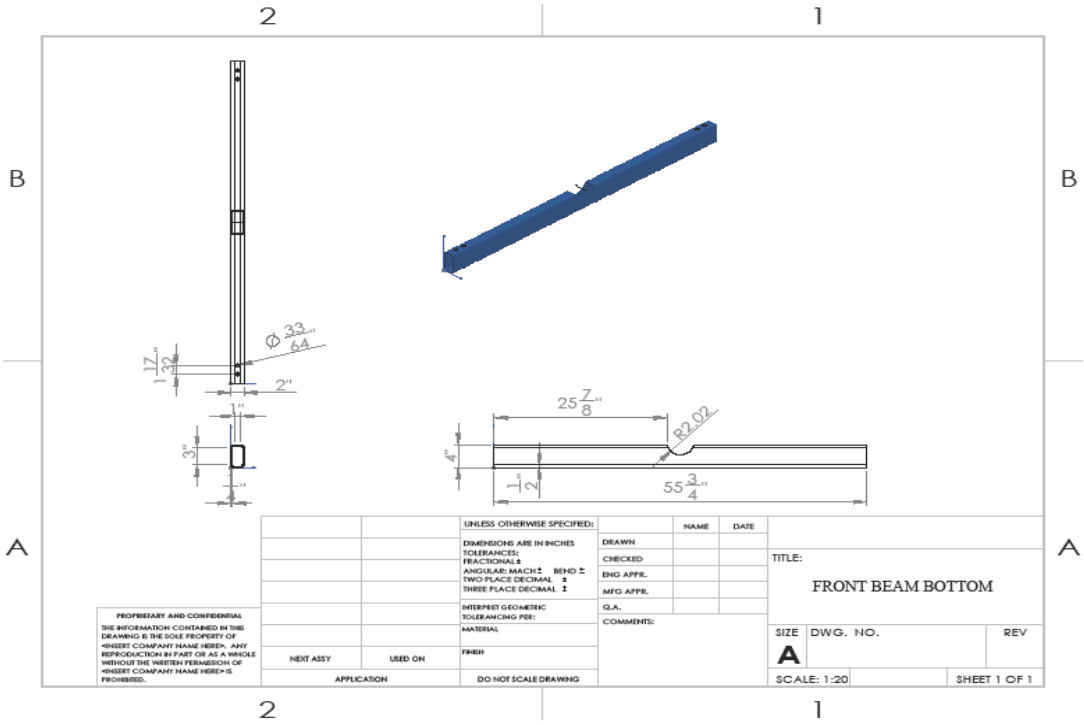

Figure A10: Front Beam, Bottom

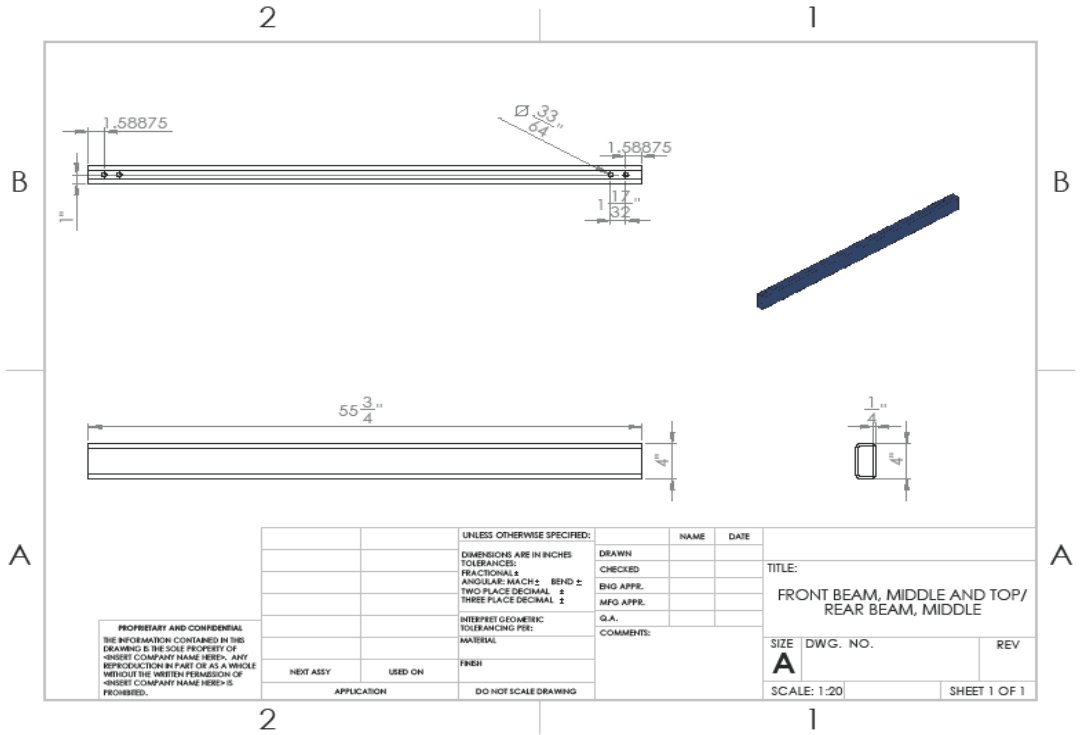

Figure A11: Front Beam, Middle and Top / Rear Beam, Middle

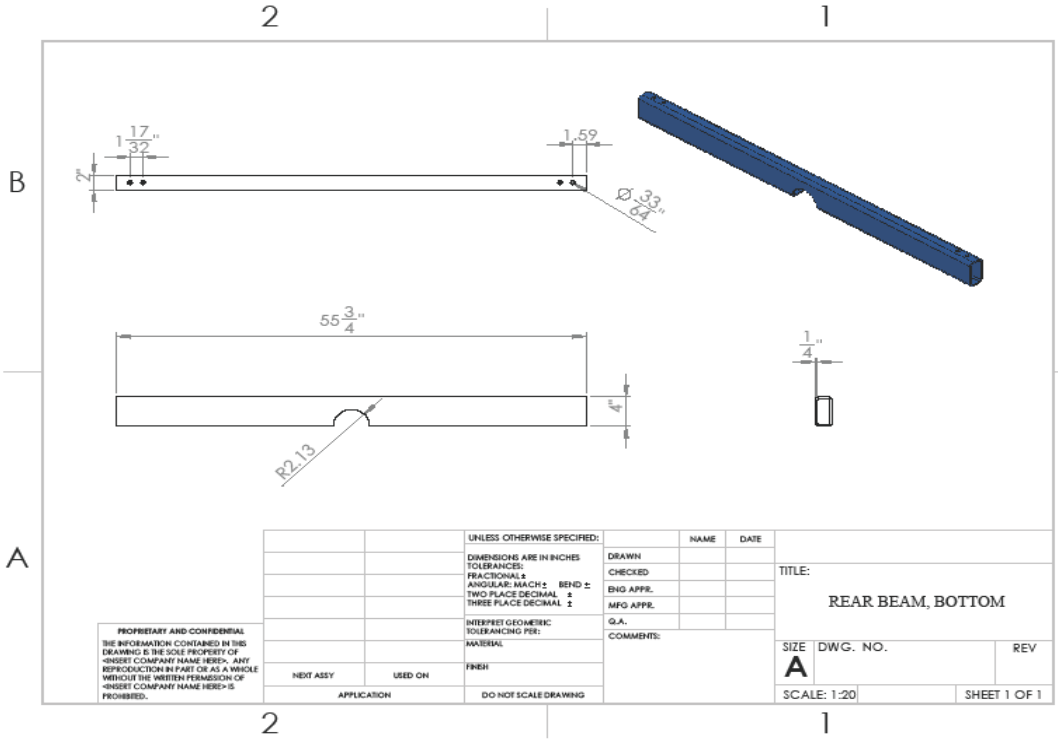

Figure A12: Rear Beam, Bottom

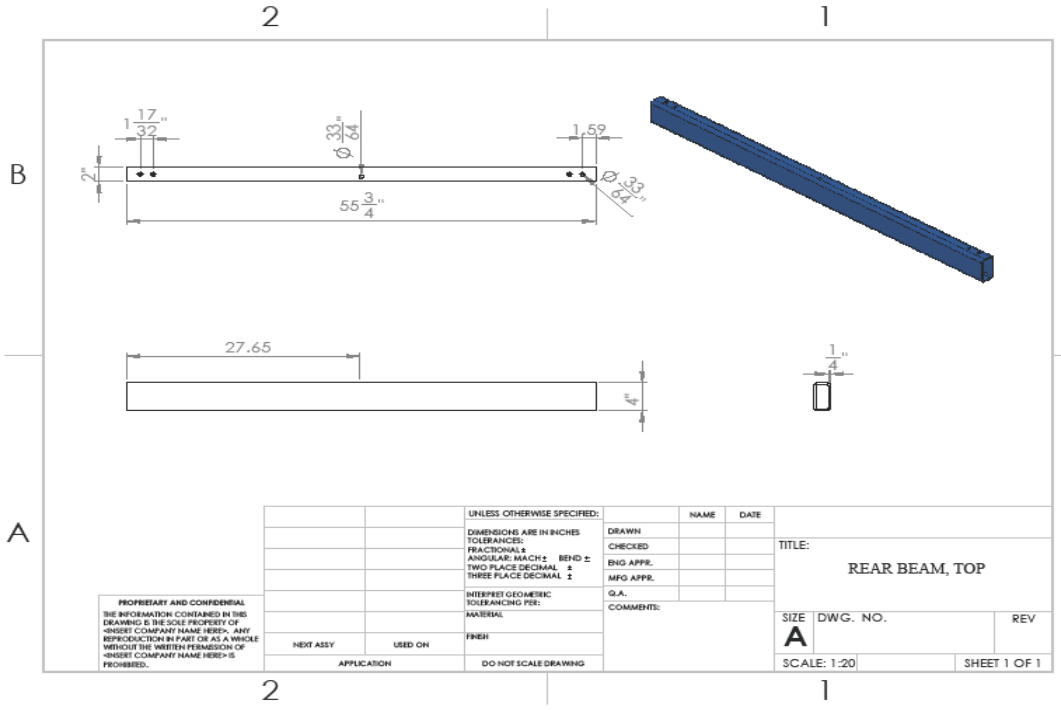

Figure A13: Rear Beam, Top

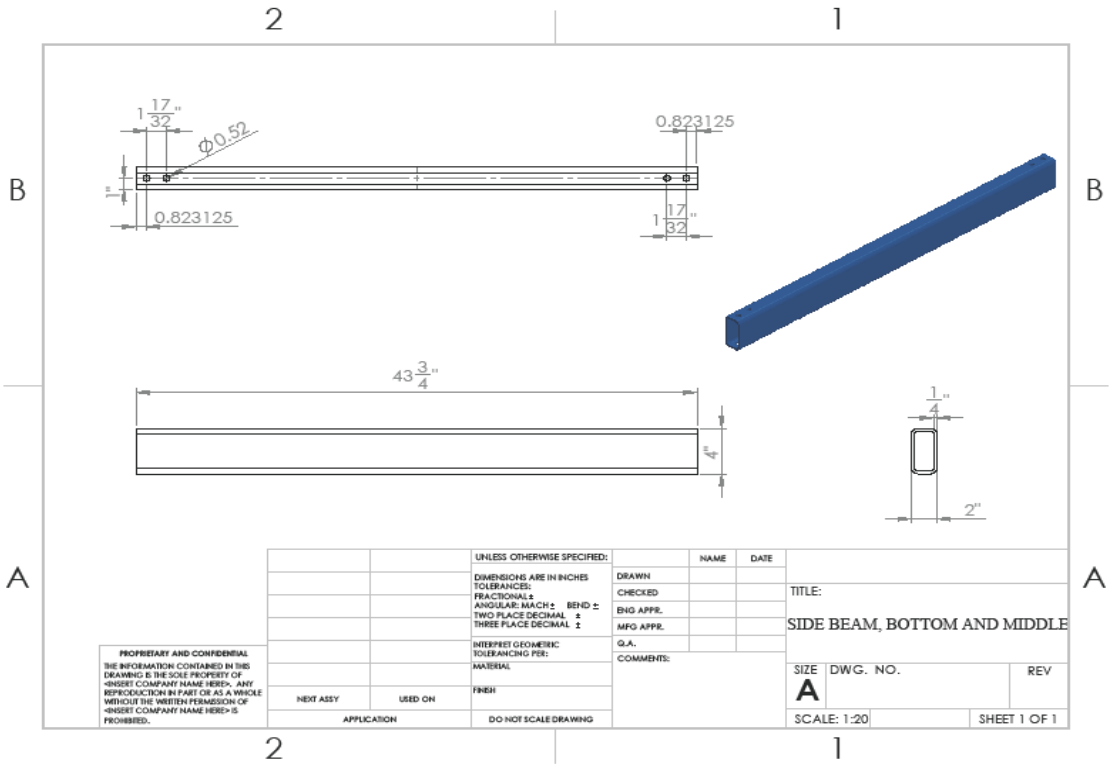

Figure A14: Side Beam, Bottom and Middle

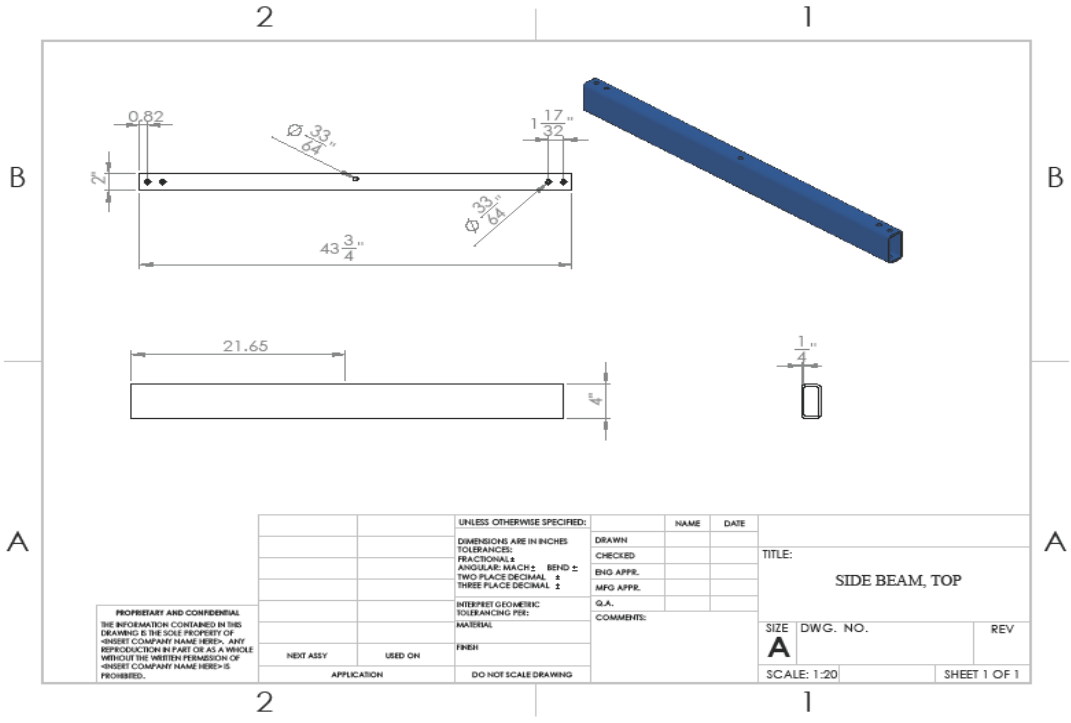

Figure A15: Side Beam, Top

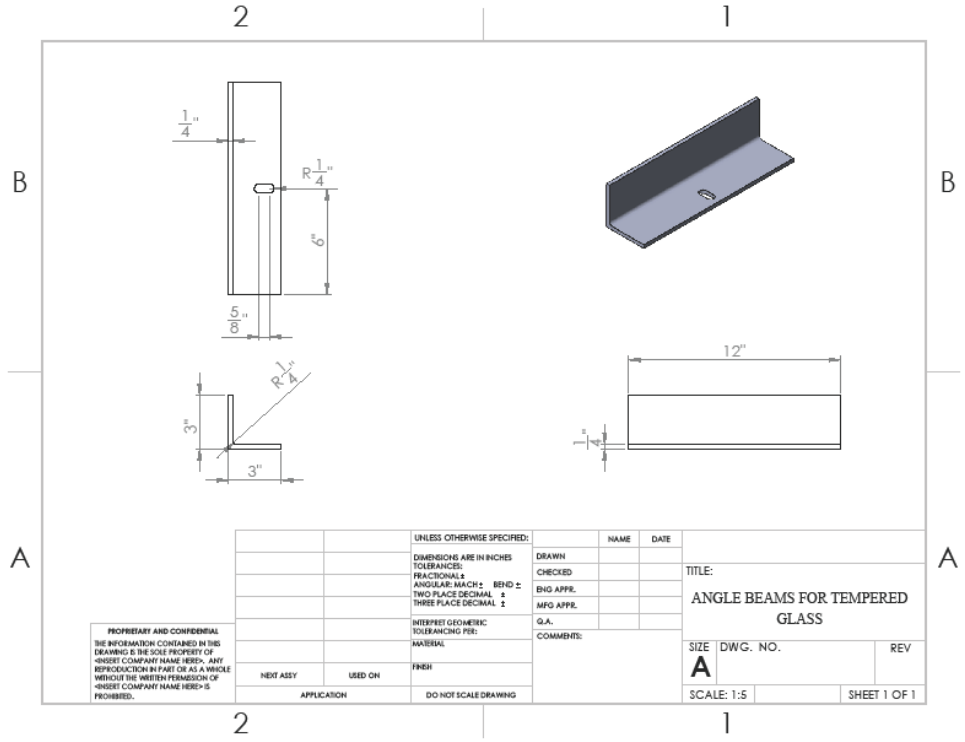

Figure A16: Angle Beams for Tempered Glass

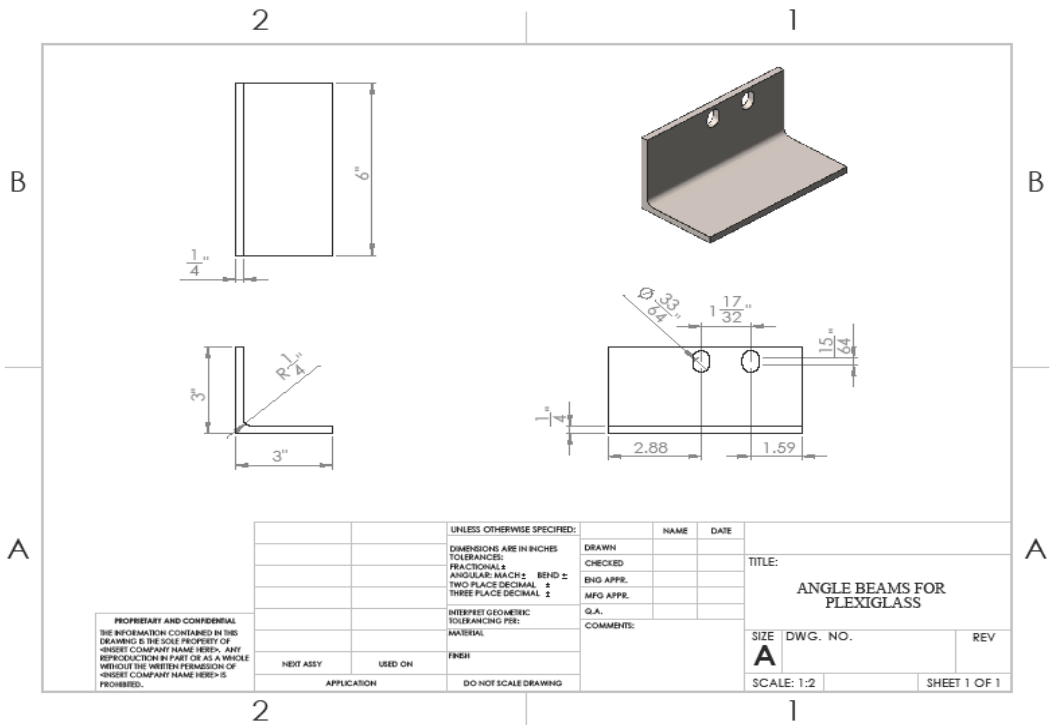

Figure A17: Angle Beams for Plexiglass (Front Panel)

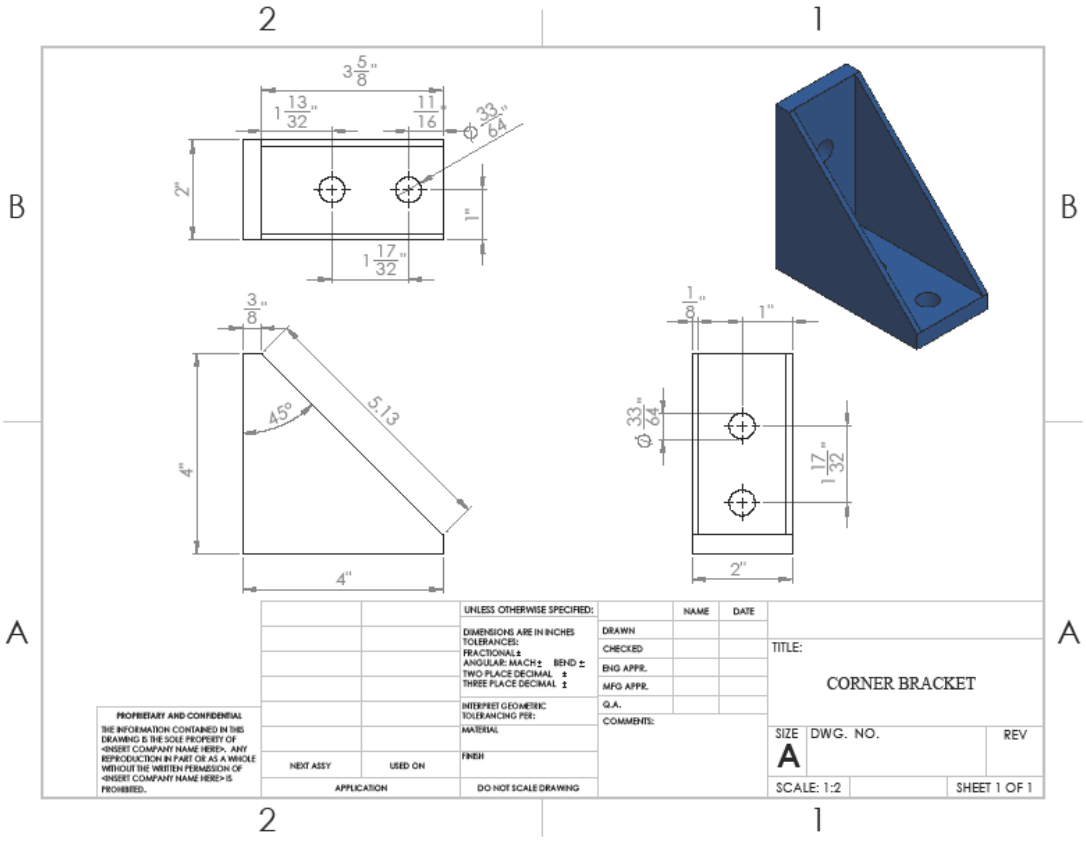

Figure A18: Corner Bracket

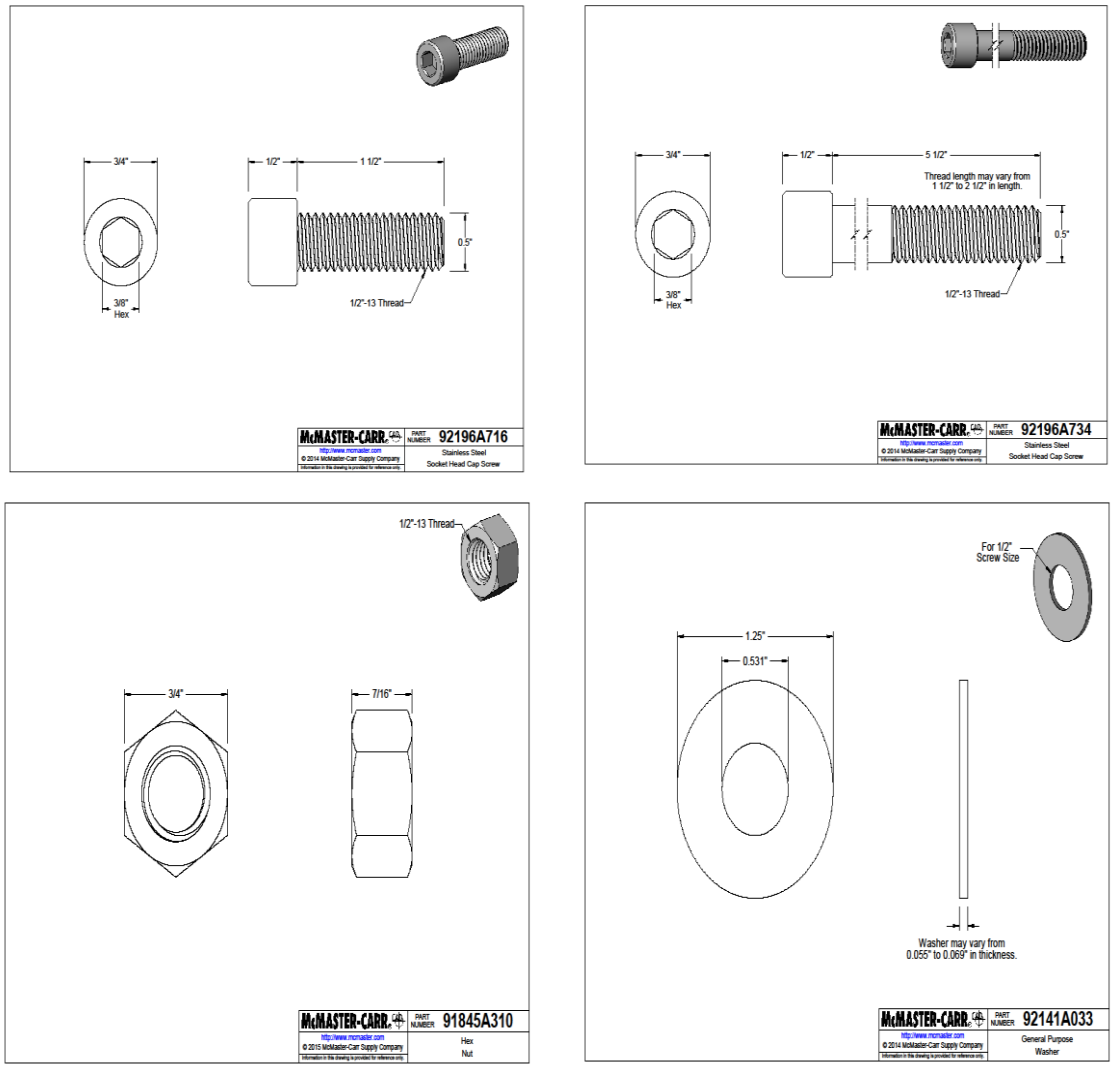

Figure A19: Bolts, Nuts, and Washers for Transparent Tank

Appendix B: Test Channel

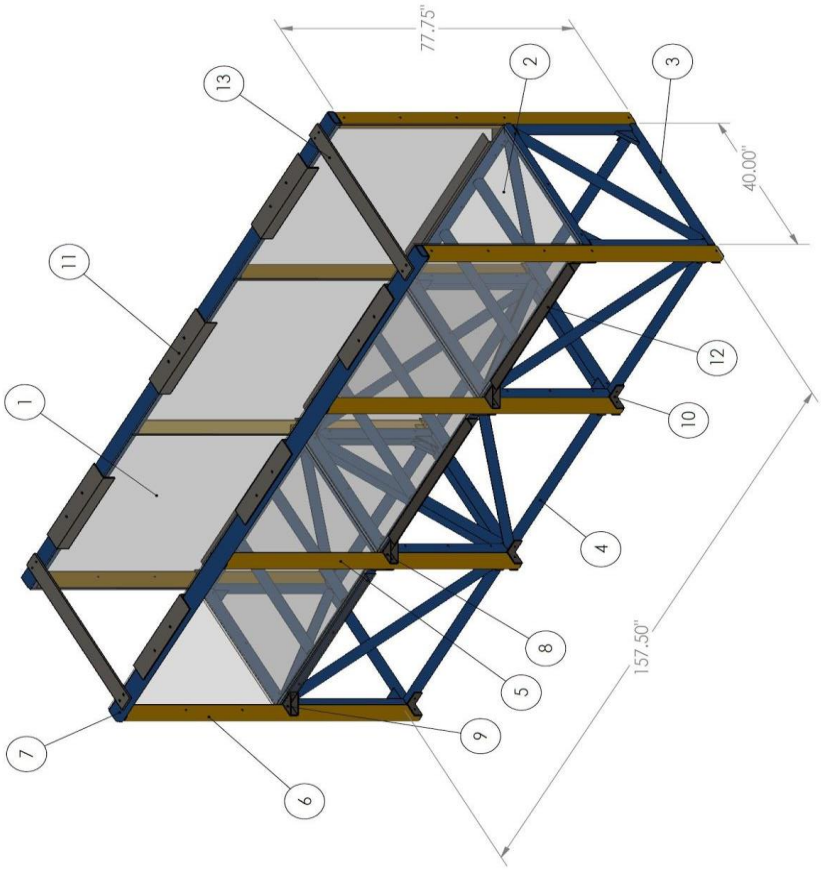

ITEM NO.	COMPONENT	QTY
1	Tempered Glass/	6
2	Annealed Glass	3
3	Chassis Module 1	2
4	Chassis Module 2	1
5	Middle Vertical Members	4
6	End Vertical Members	4
7	Horizontal Members	2
8	Middle Corner Gussets	8
9	End Corner Gussets	4
10	Corner Angle Irons	12
11	Top Angle Beams	6
12	Bottom Angle Beams	6
13	Flat Bars	2

Figure B1: Test Channel Components

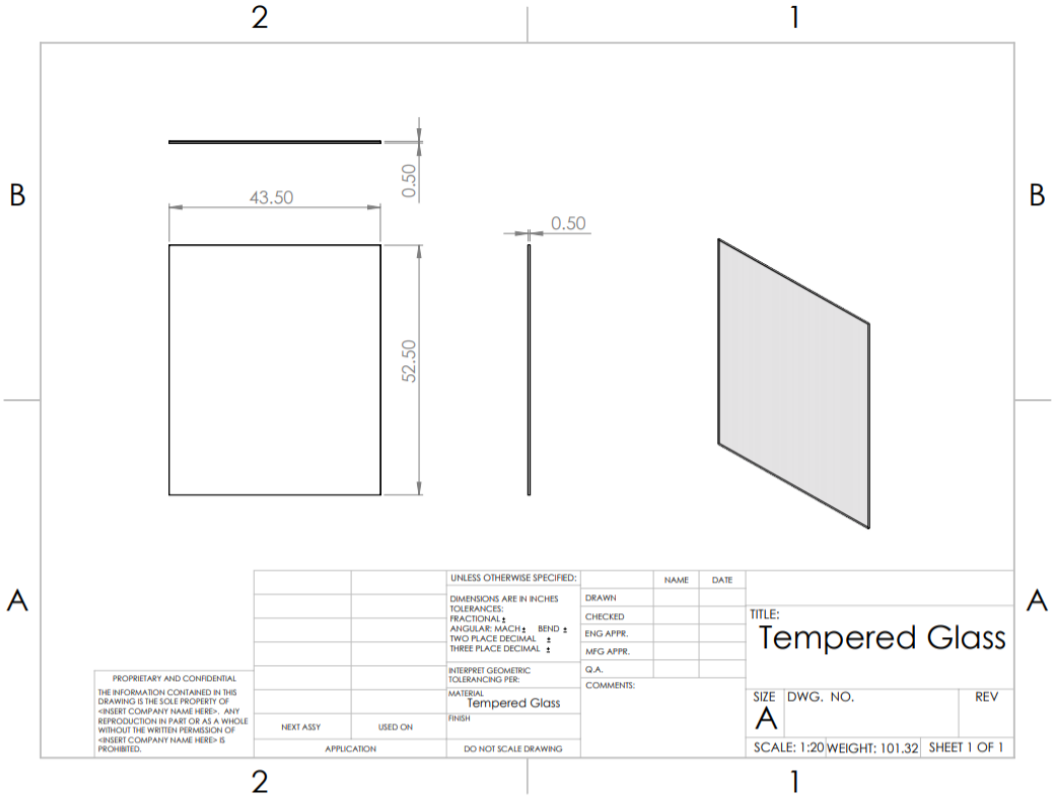

Figure B2: Tempered Glass

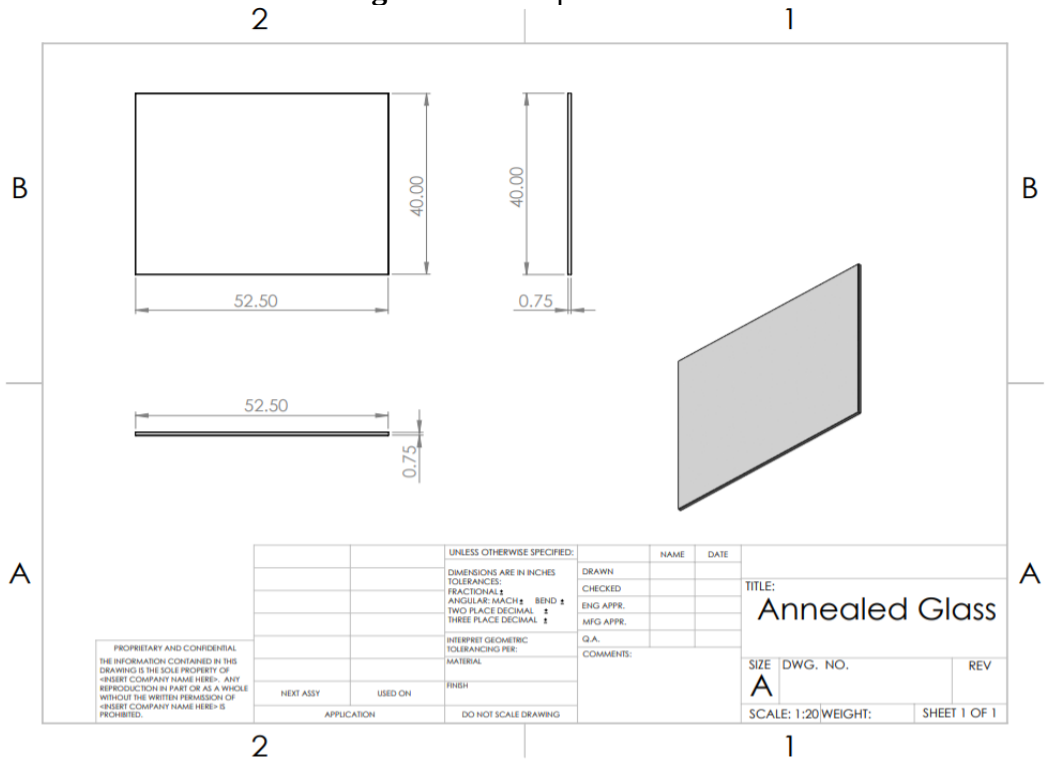

Figure B3: Annealed Glass

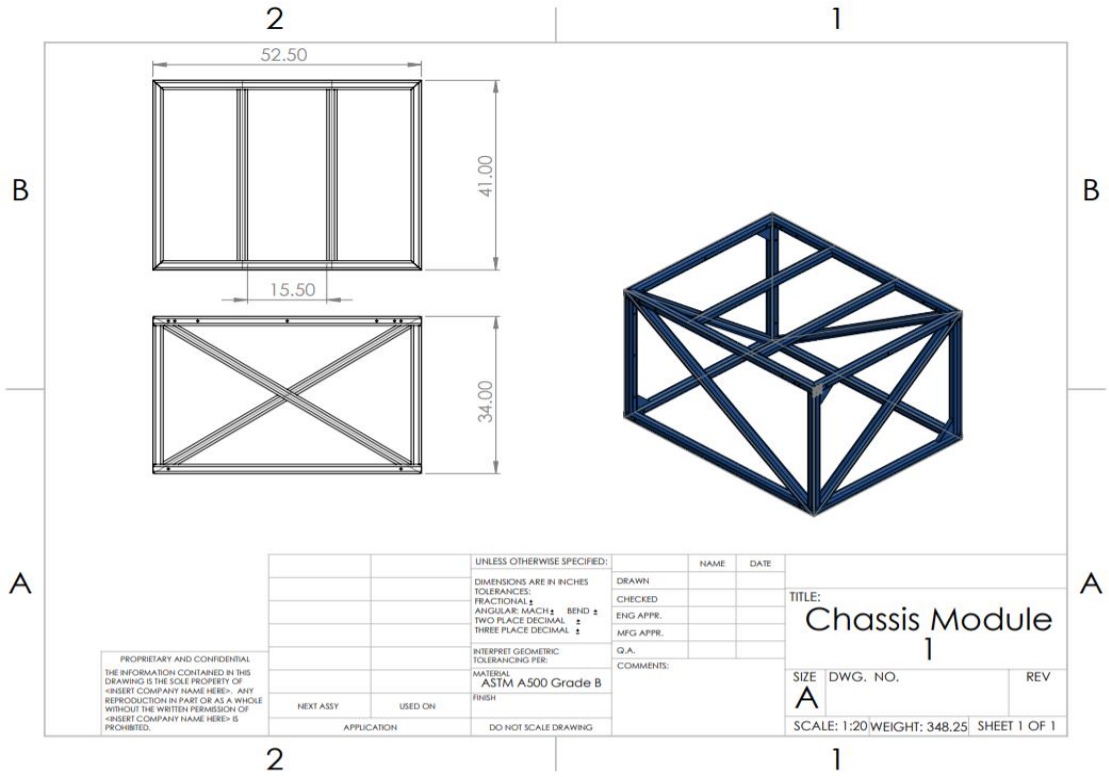

Figure B4: Chassis Module 1

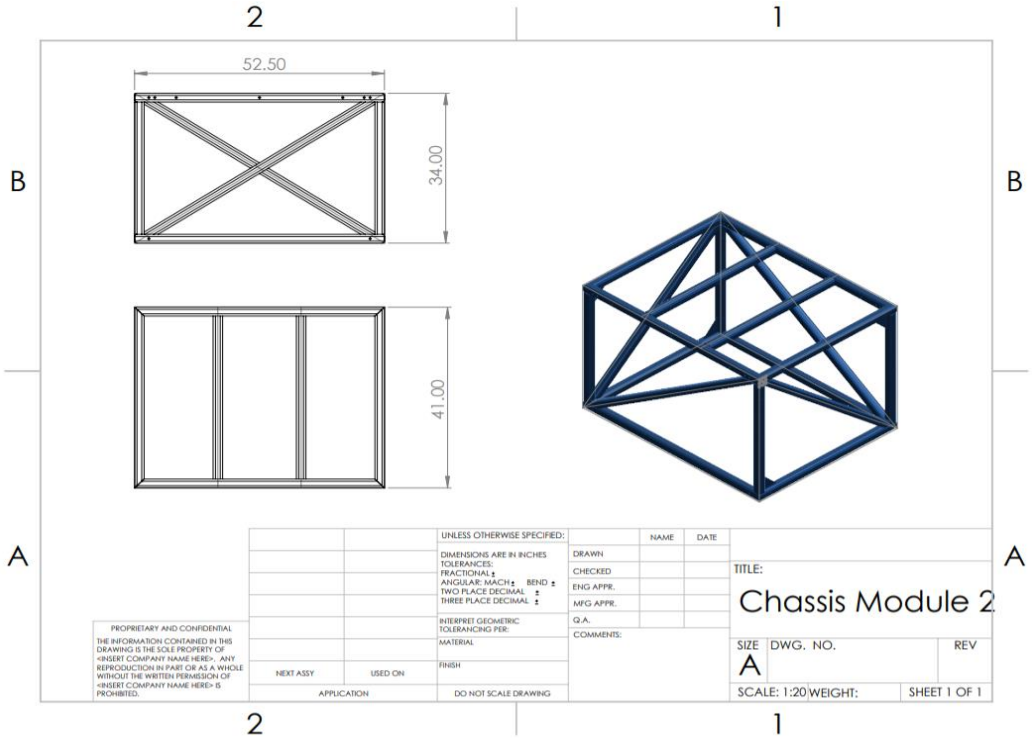

Figure B5: Chassis Module 2

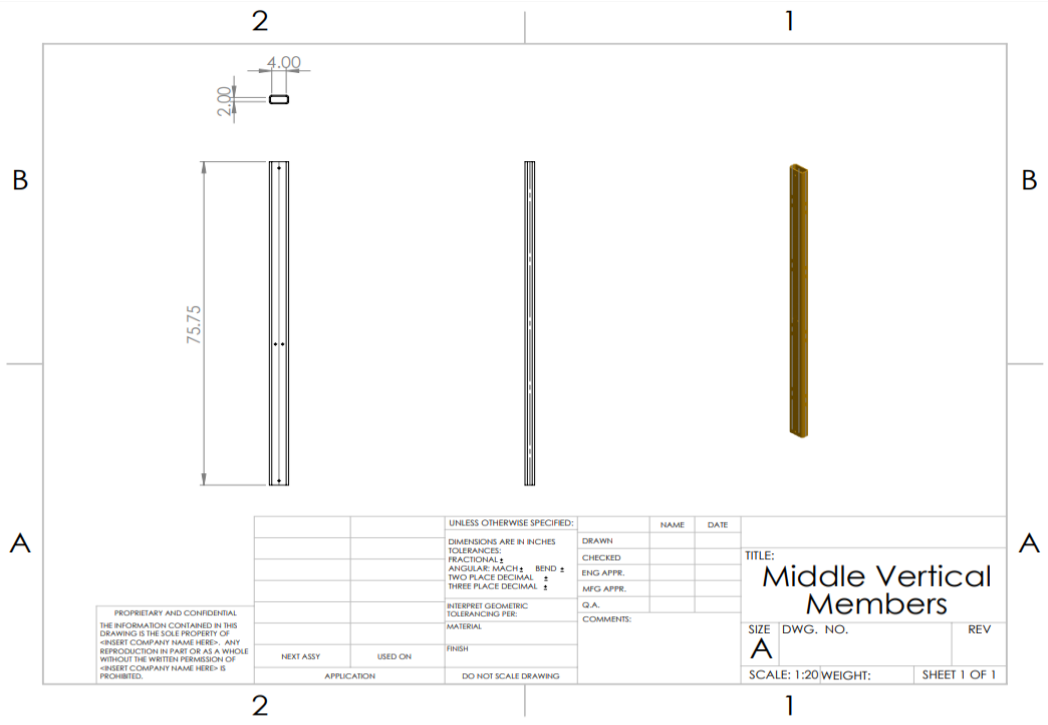

Figure B6: Middle Vertical Members

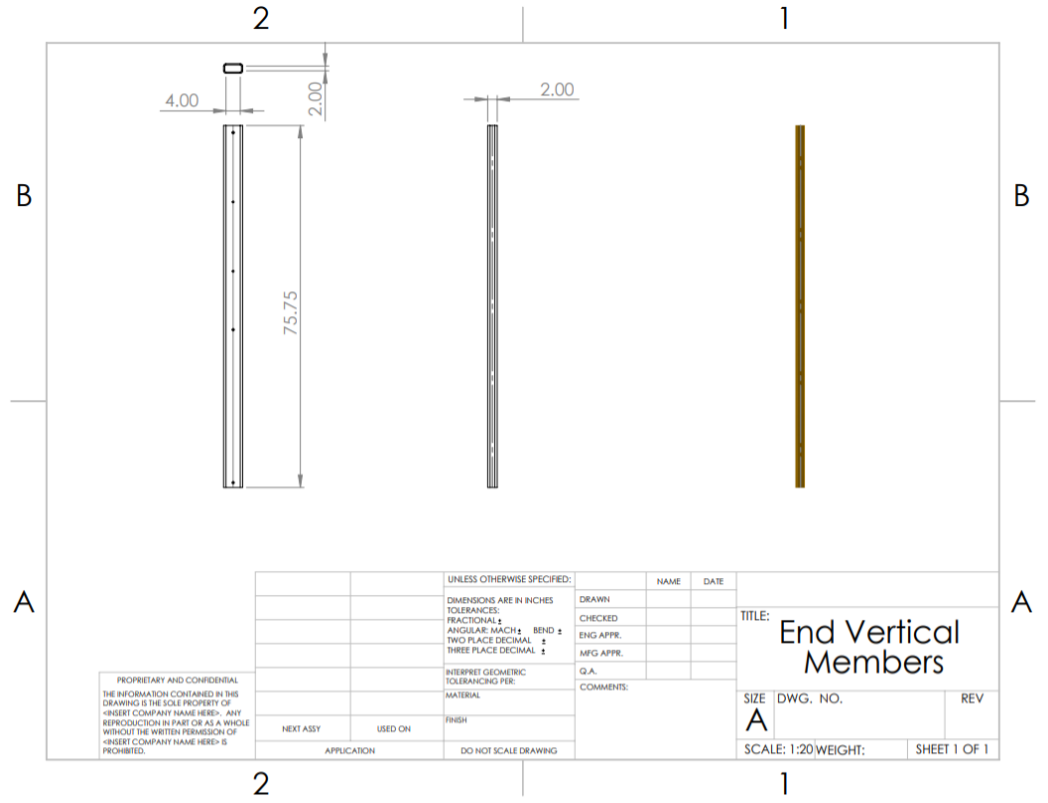

Figure B7: End Vertical Members

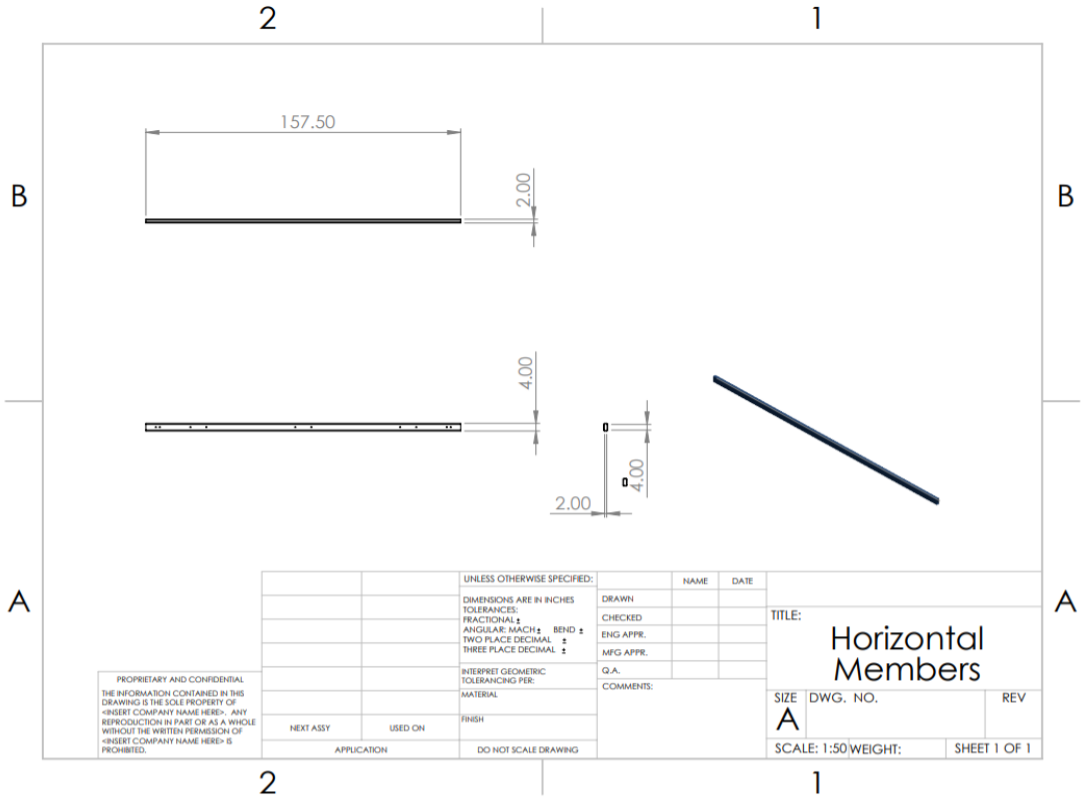

Figure B8: Horizontal Members

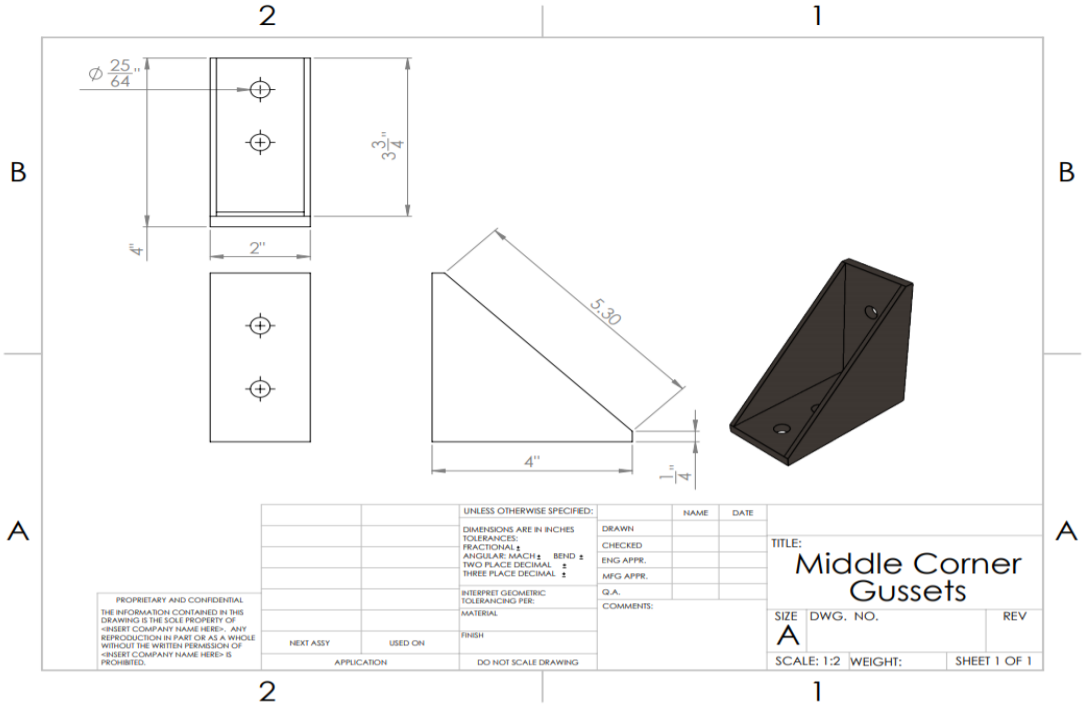

Figure B9: Middle Corner Gussets

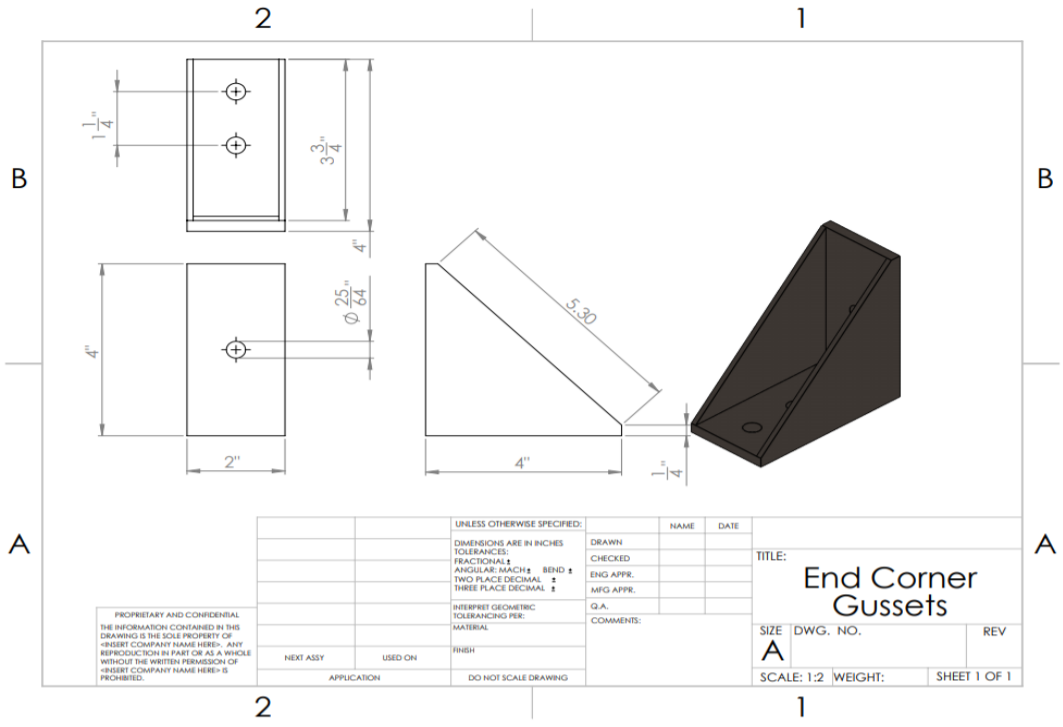

Figure B10: End Corner Gussets

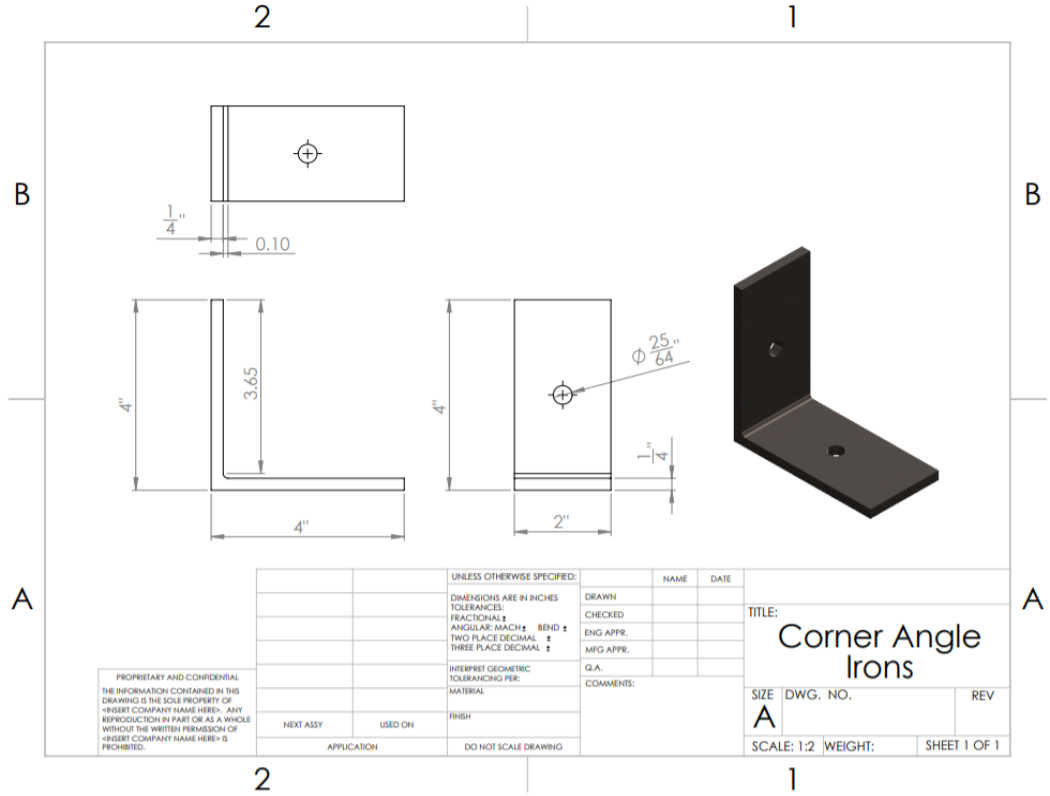

Figure B11: Corner Angle Irons

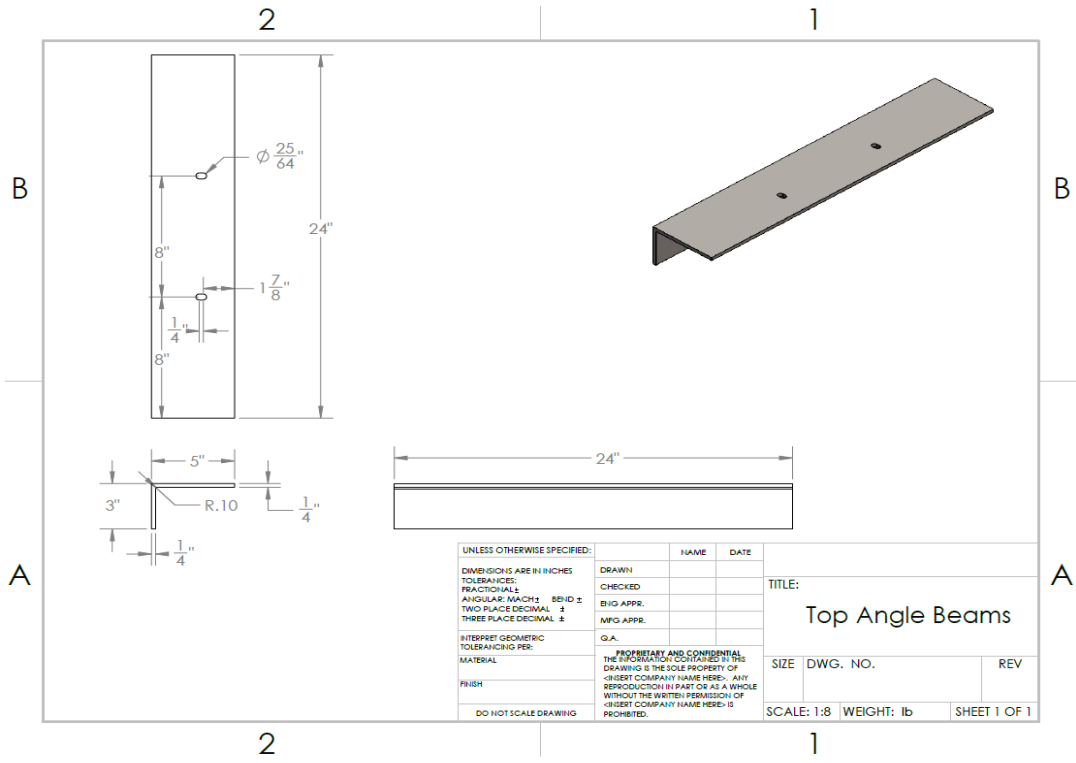

Figure B12: Top Angle Beams

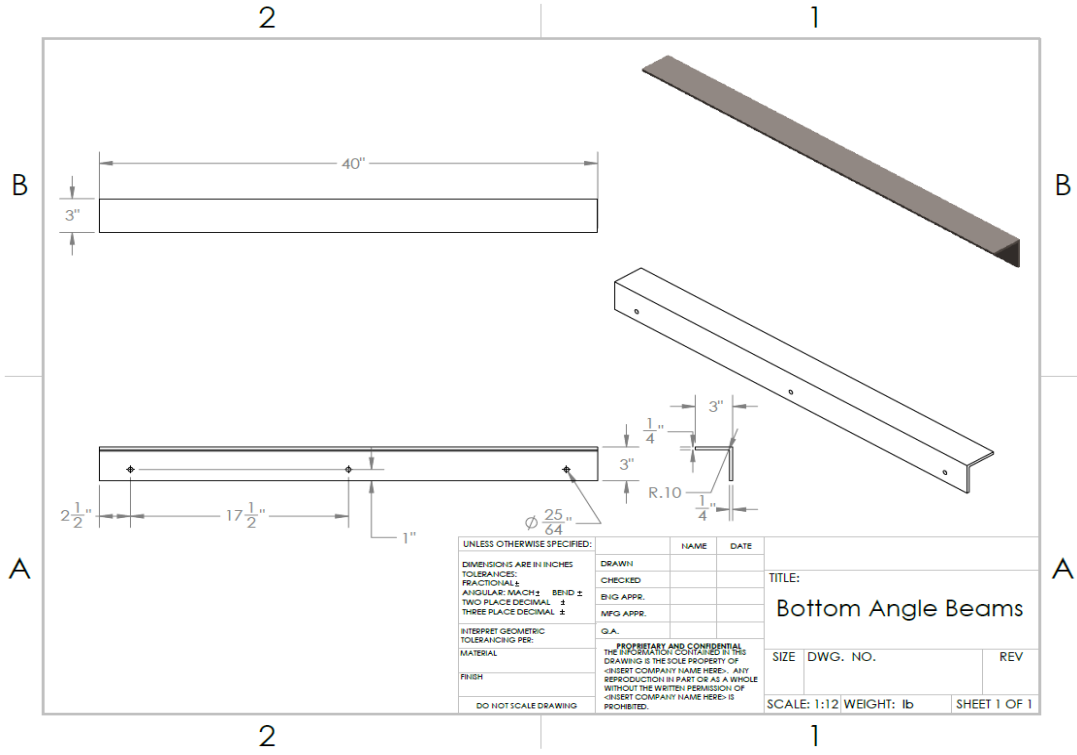

Figure B13: Bottom Angle Beams

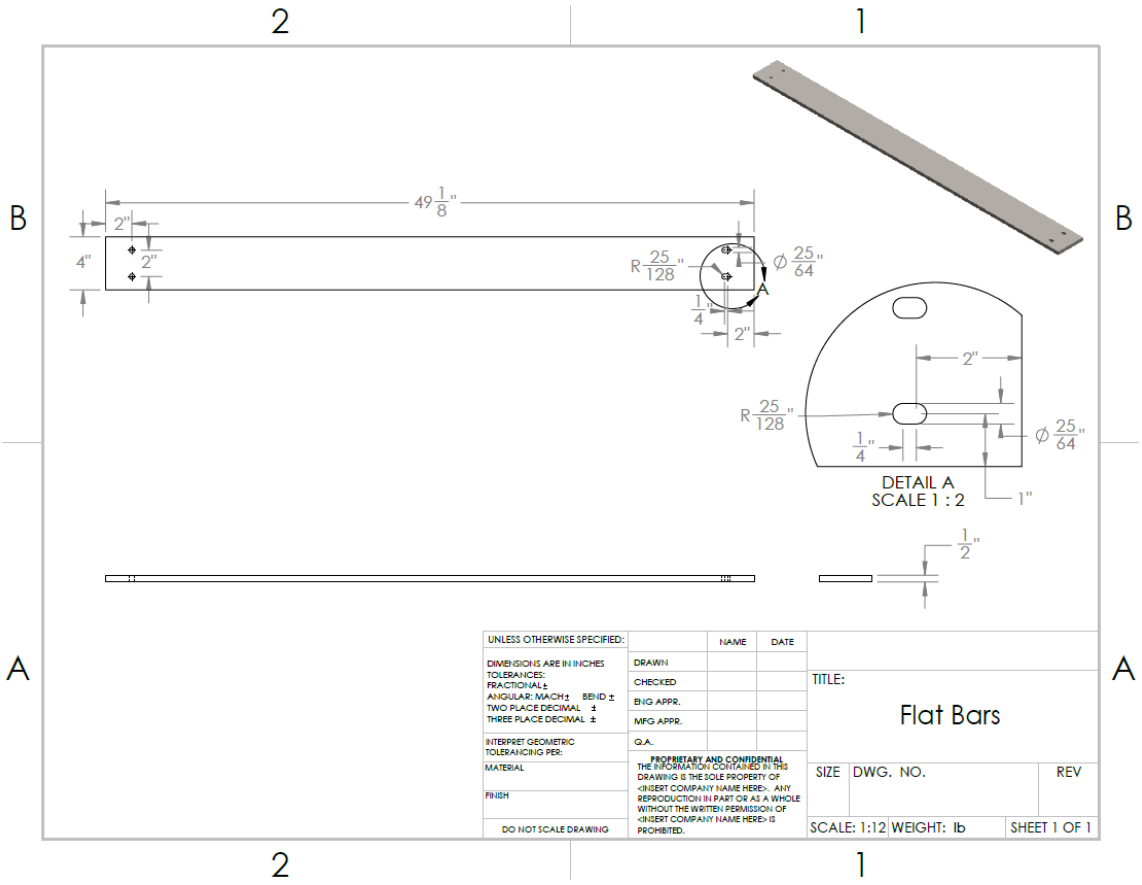

Figure B14: Flat Bars

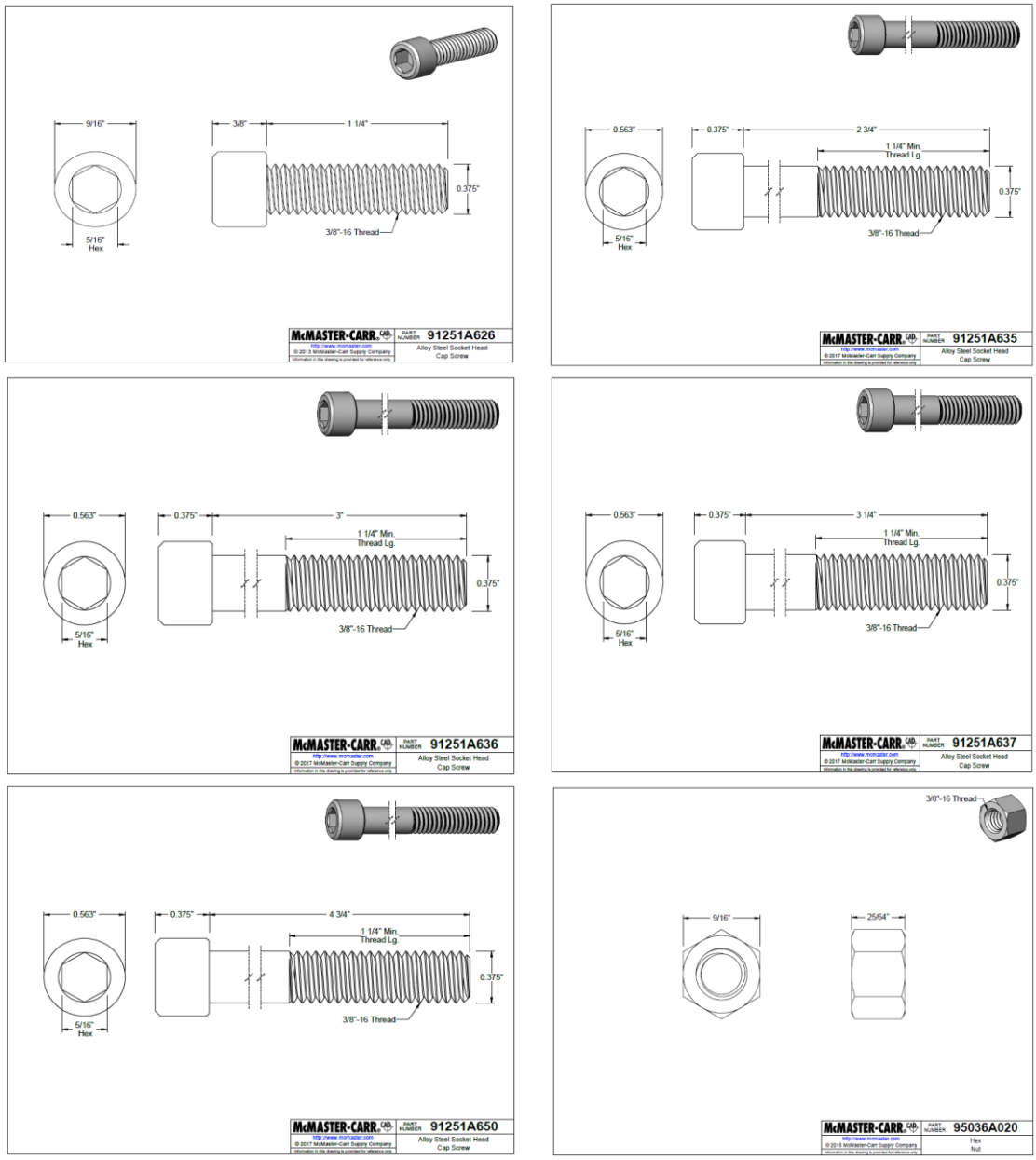

Figure B15: Bolts, Nuts, and Washers for Test Channel

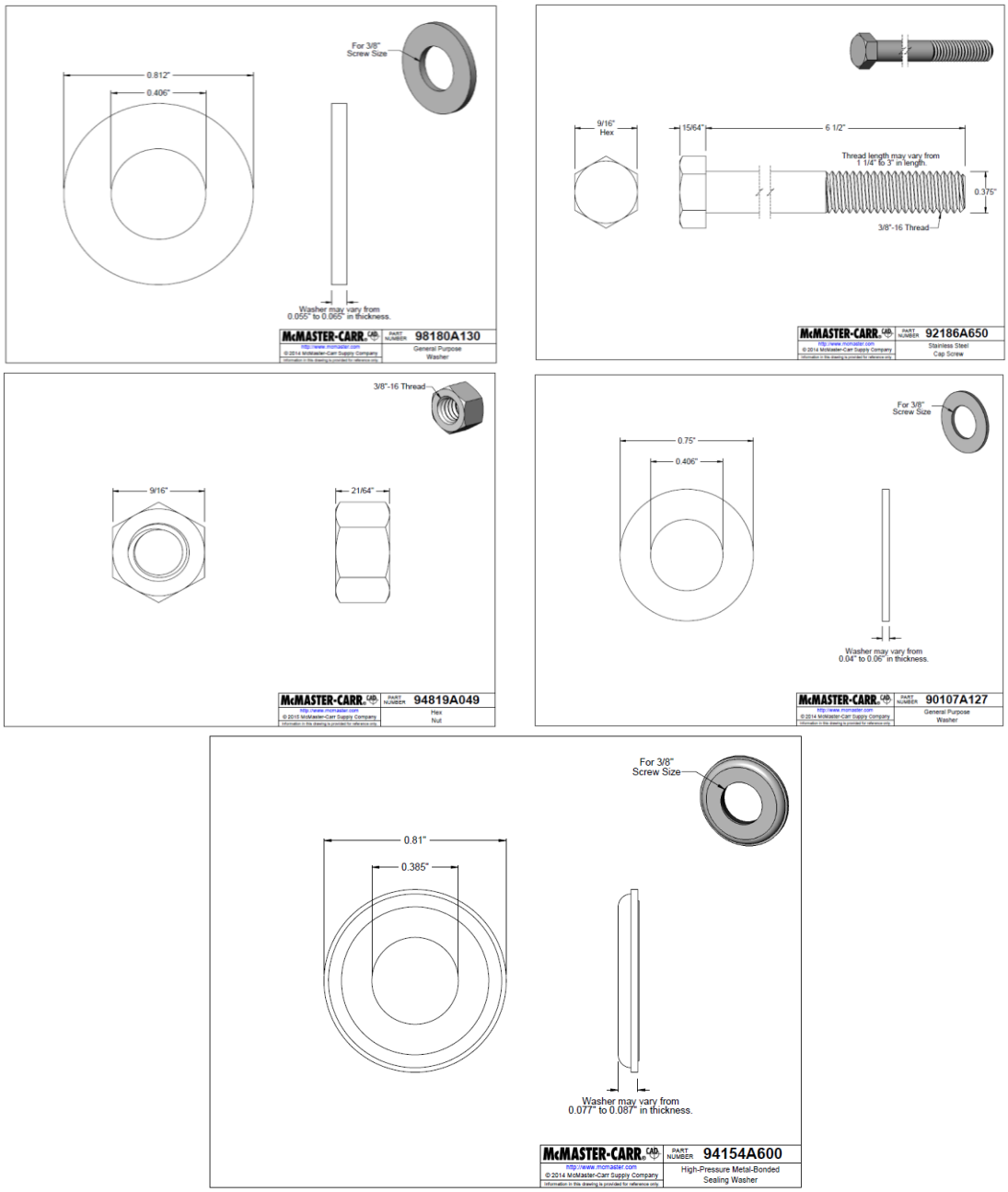

Figure B15 continued: Bolts, Nuts, and Washers for Test Channel

Appendix C: End Tank

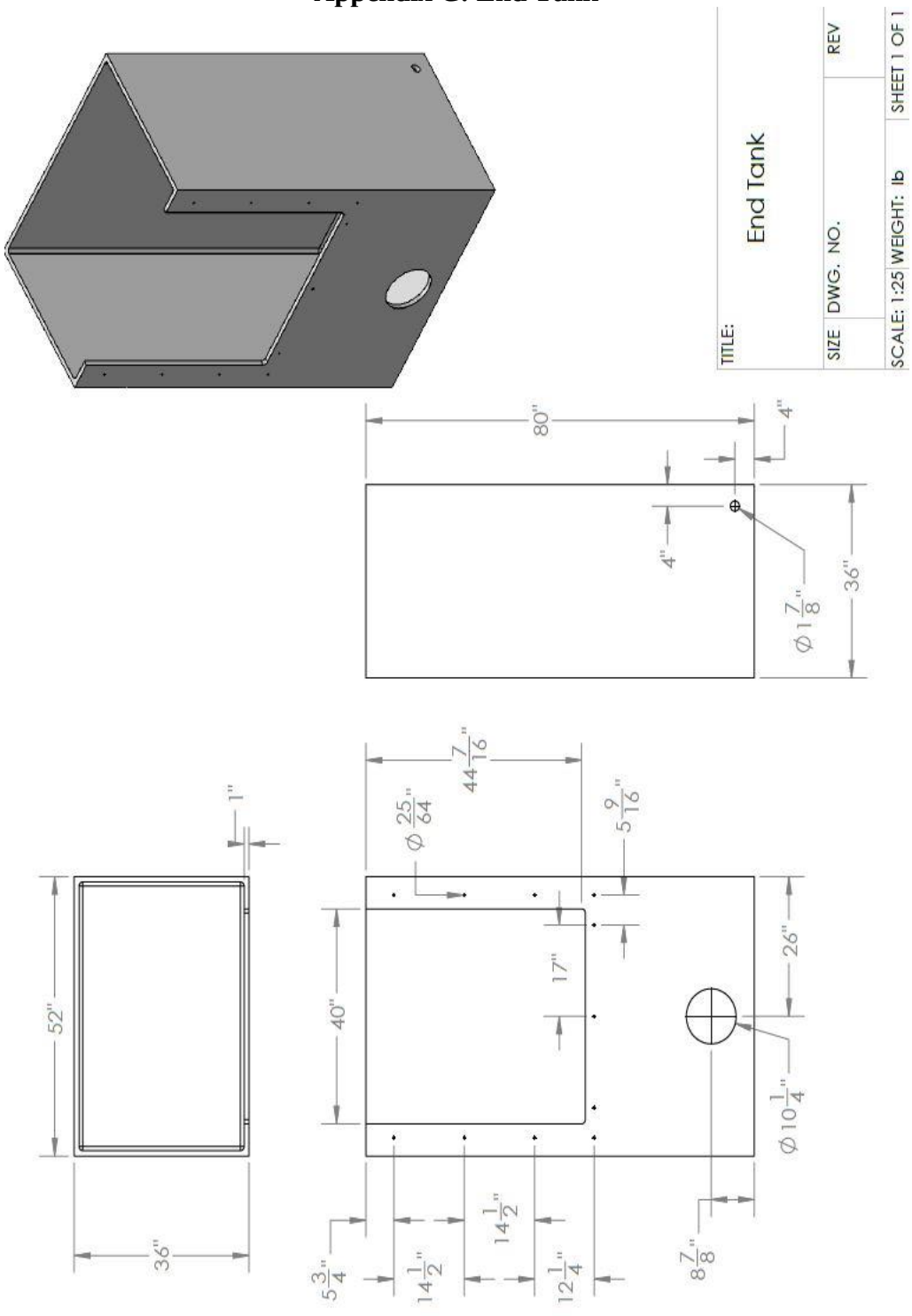

Figure C1: End Tank

APPENDIX D: Miscellaneous Components

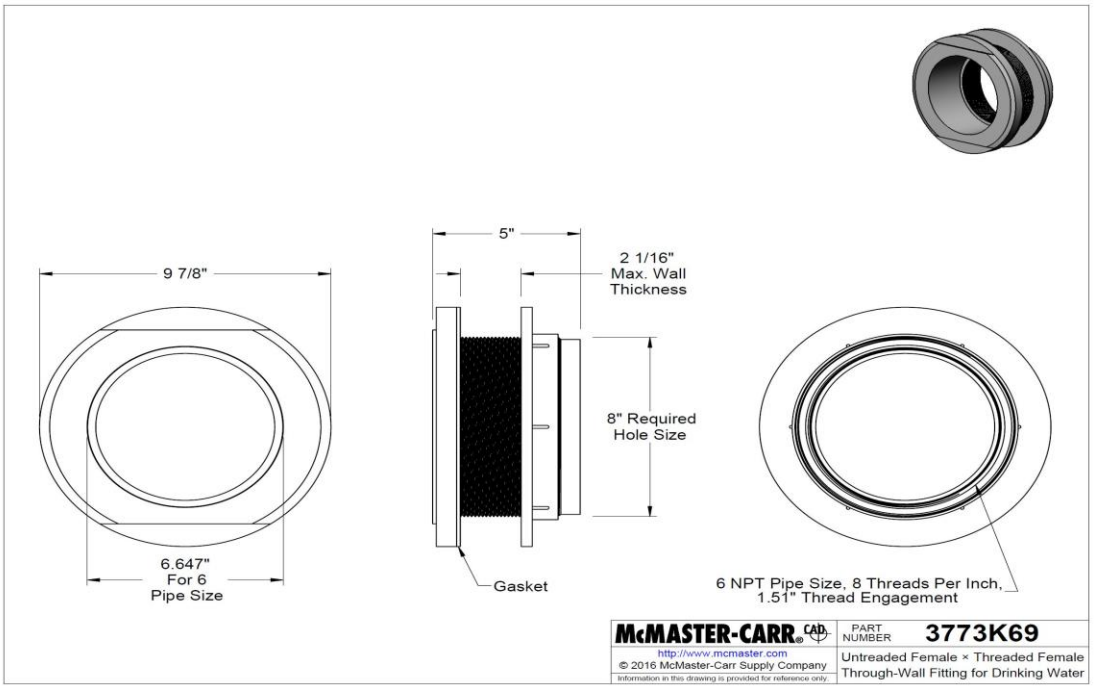

Figure D1: 6” Bulkhead Fitting

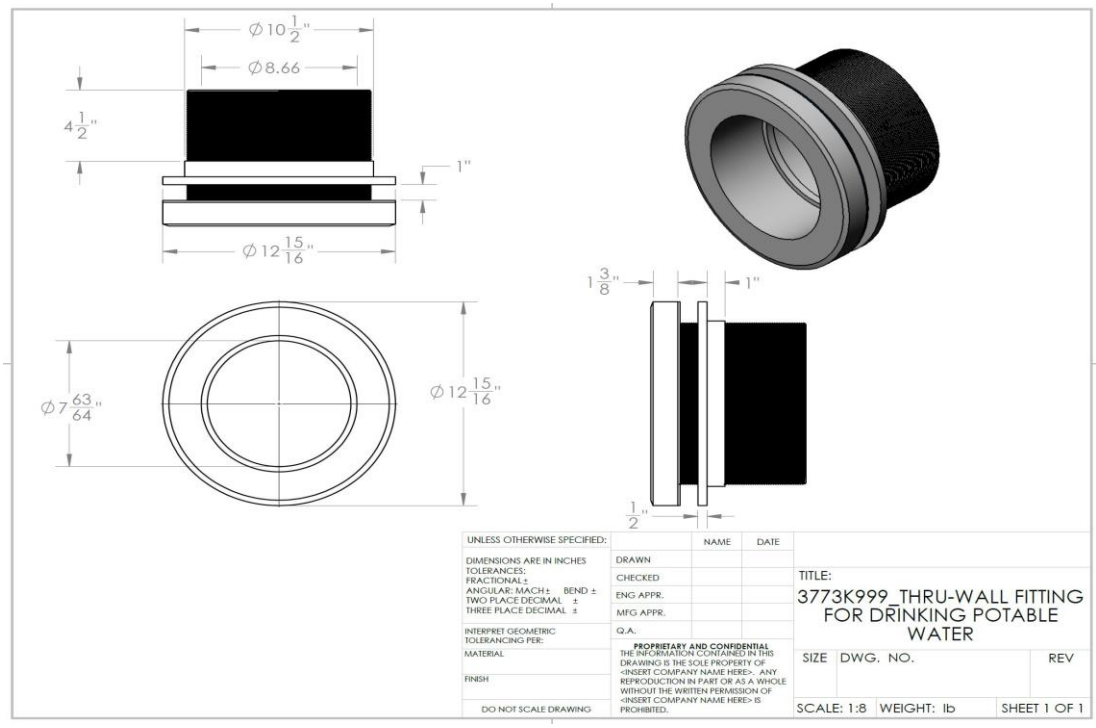

Figure D2: 8” Bulkhead Fitting

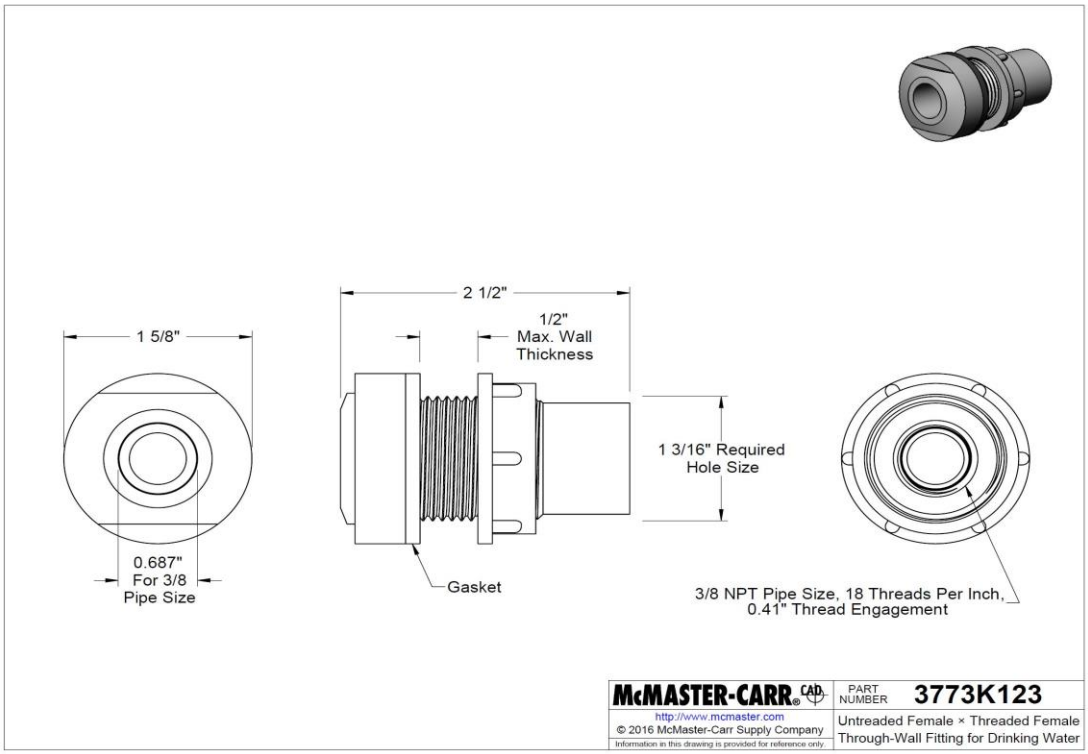

Figure D3: 1" Bulkhead Fitting

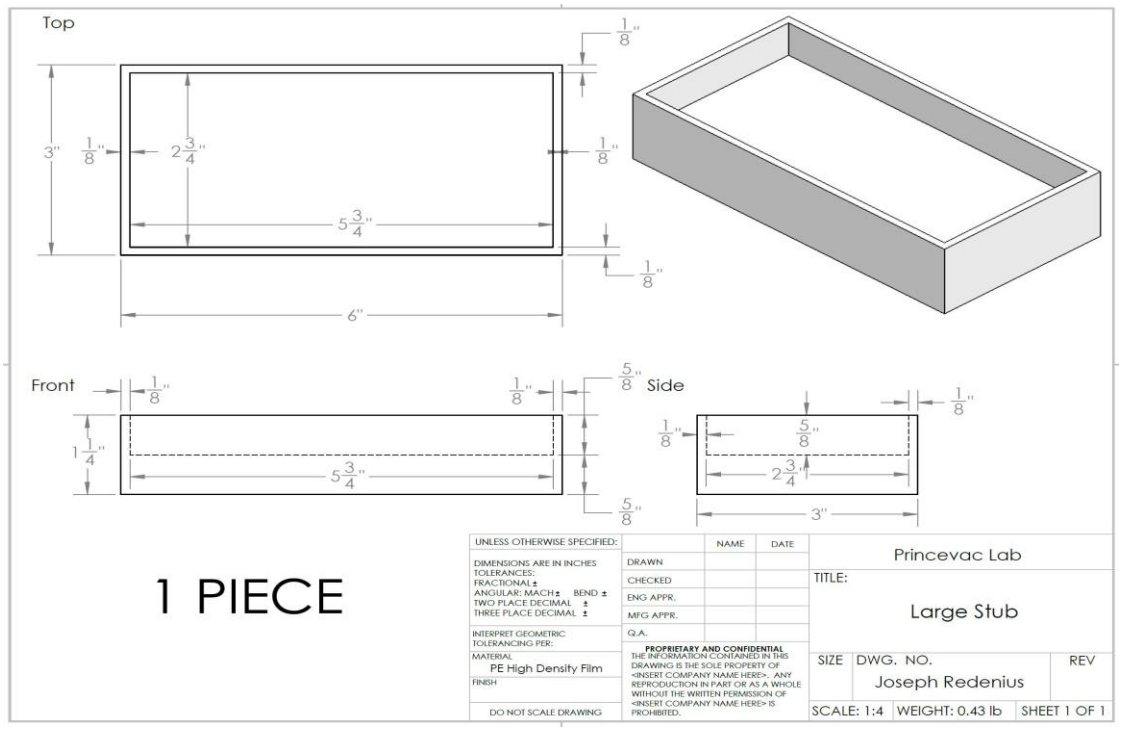

Figure D4: Pump Platform 1

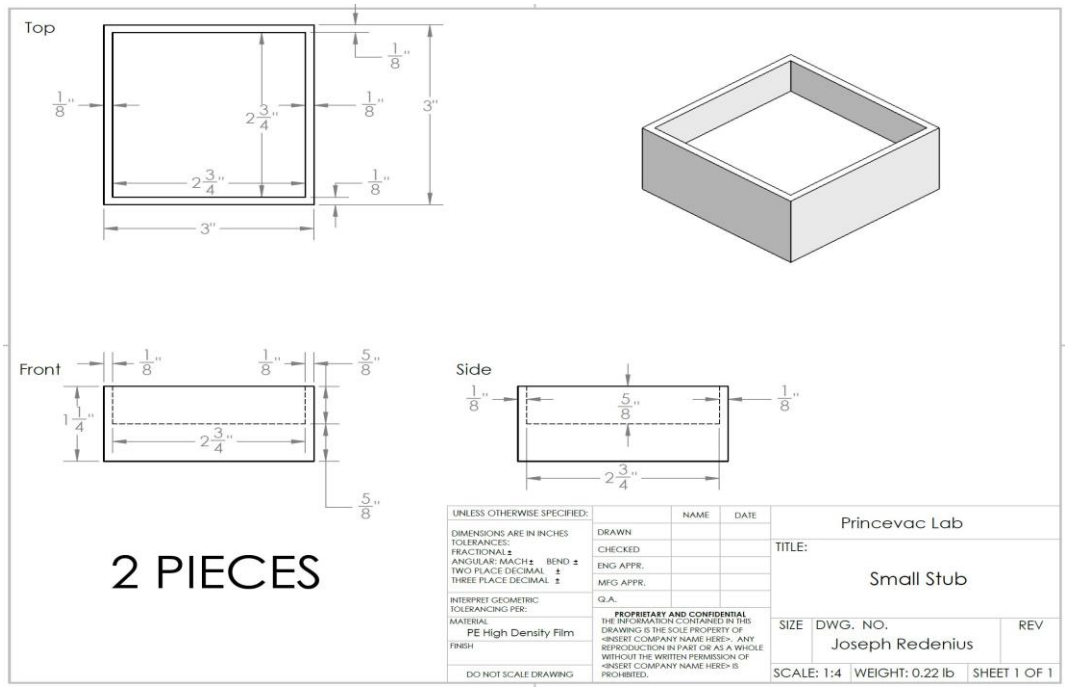

Figure D5: Pump Platform 2

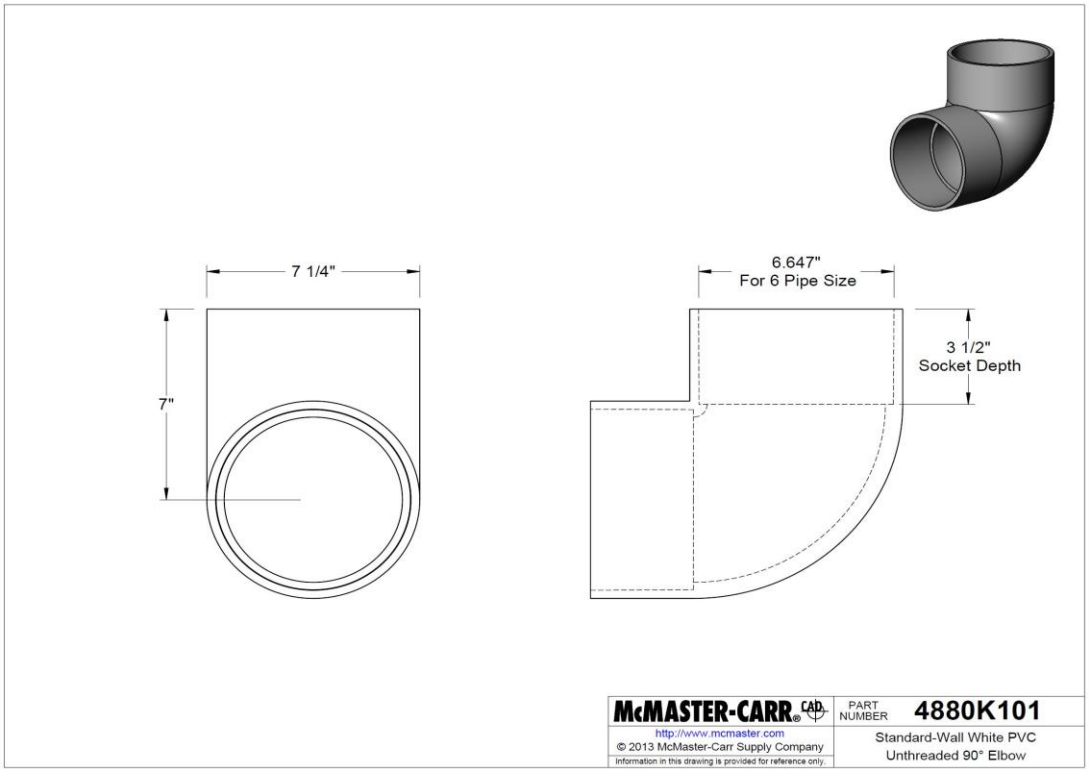

Figure D6: 6” PVC Elbow

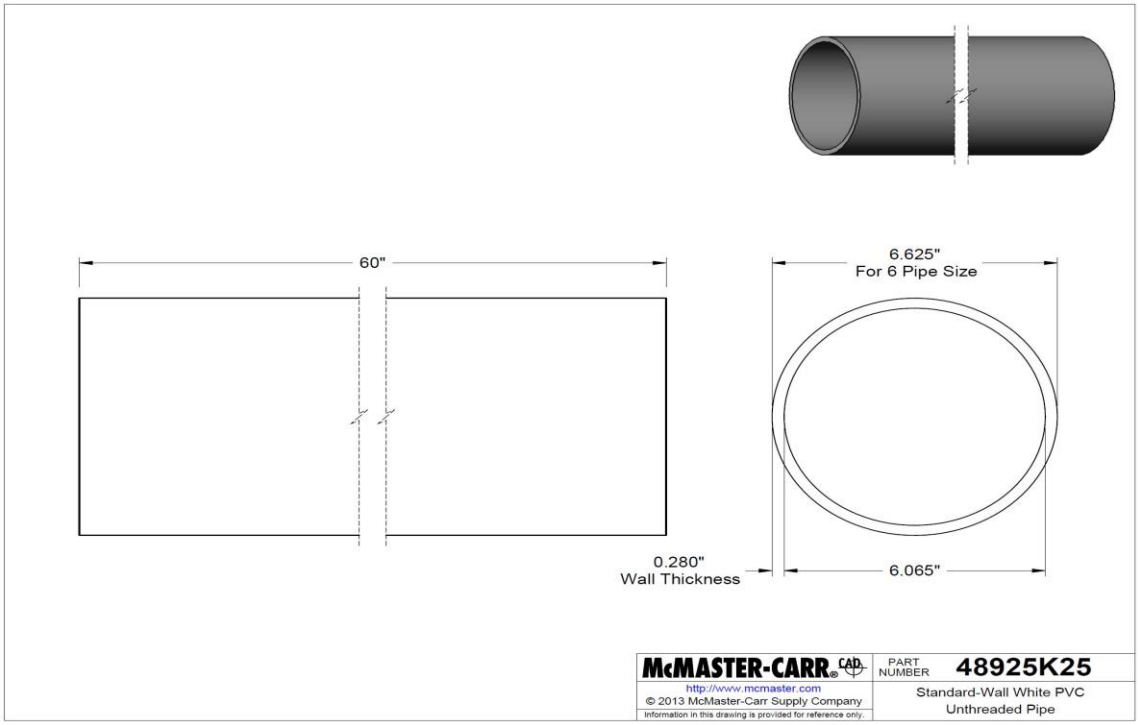

Figure D7: 6” PVC Pipe, Length Varied

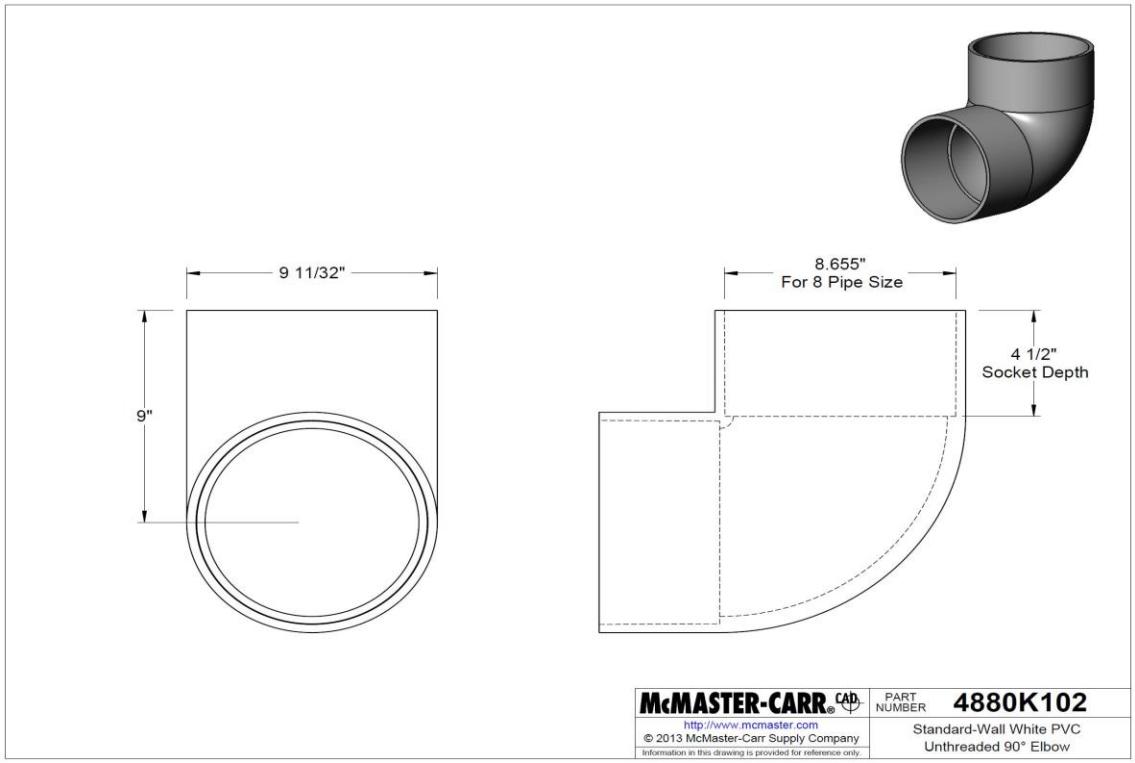

Figure D8: 8” PVC Elbow

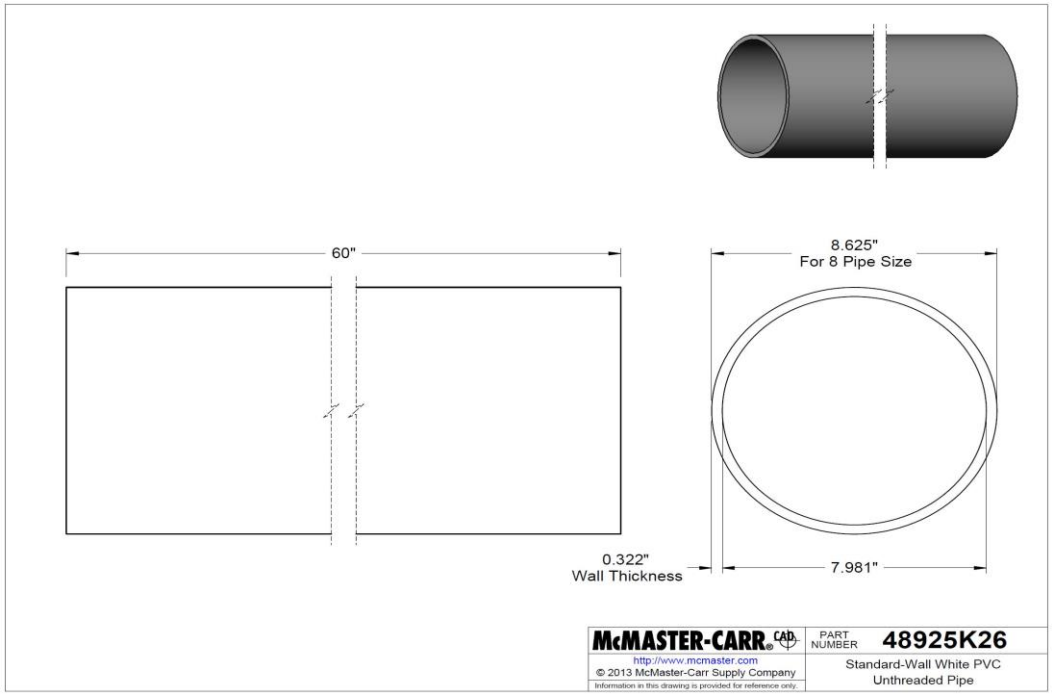

Figure D9: 8” PVC Pipe, Length Varied

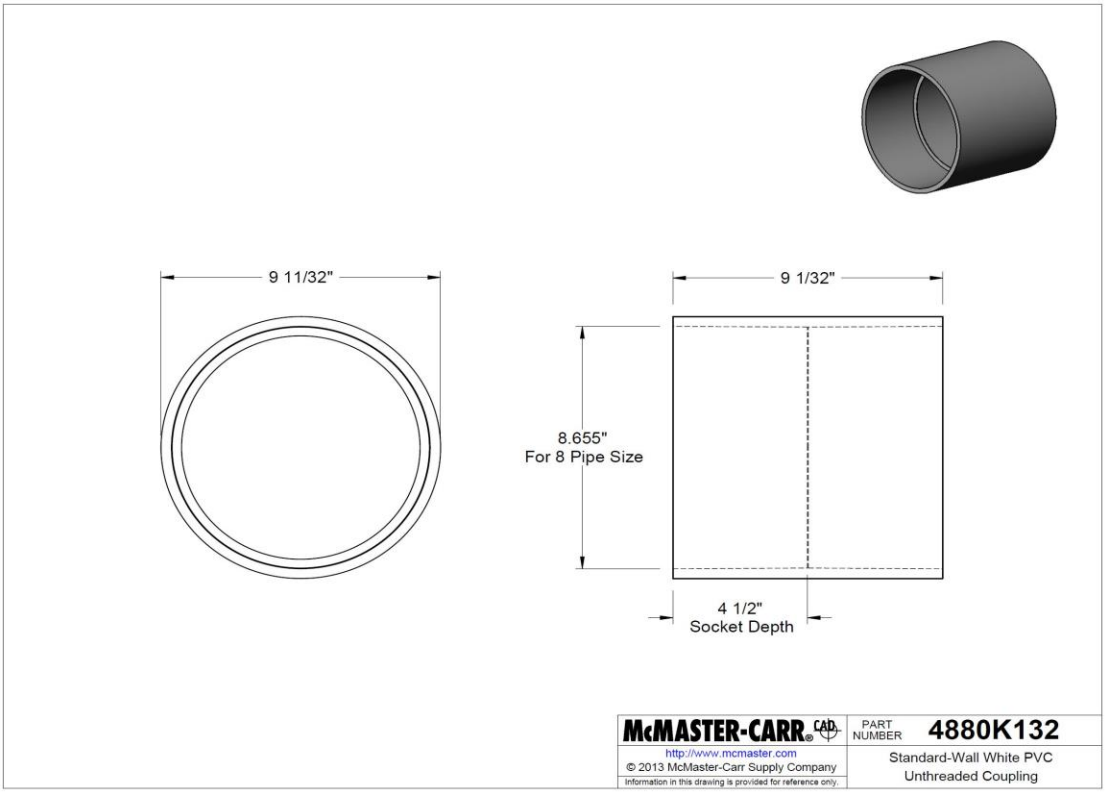

Figure D10: 8” PVC Pipe Coupler

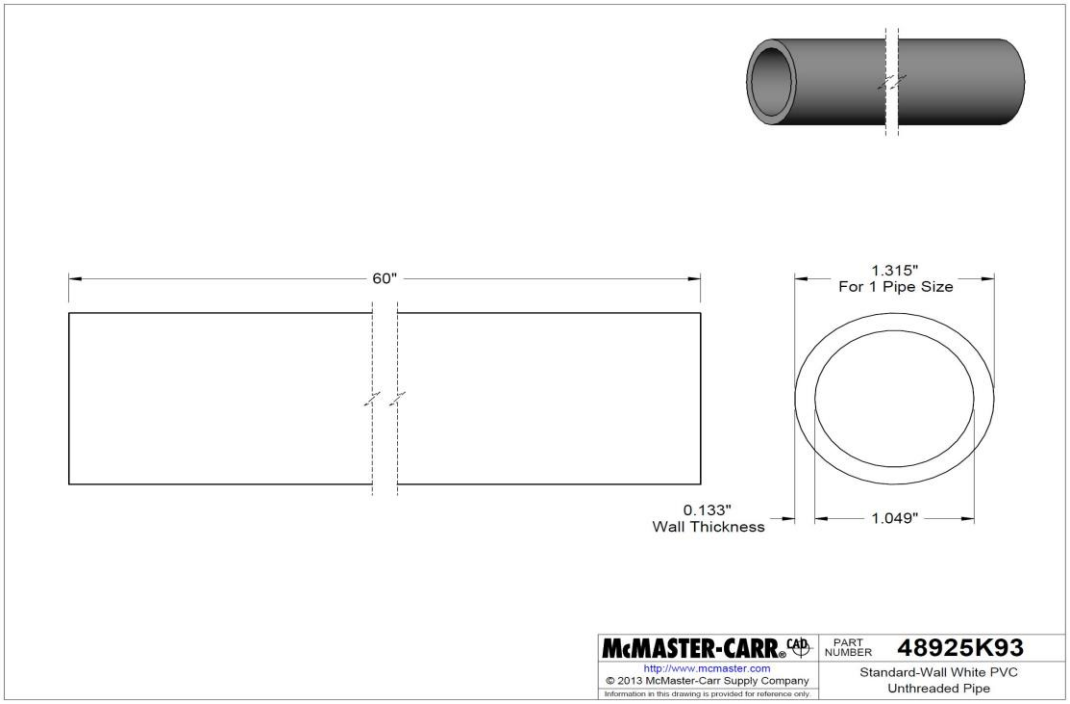

Figure D11: 1” PVC Pipe, Length Varied

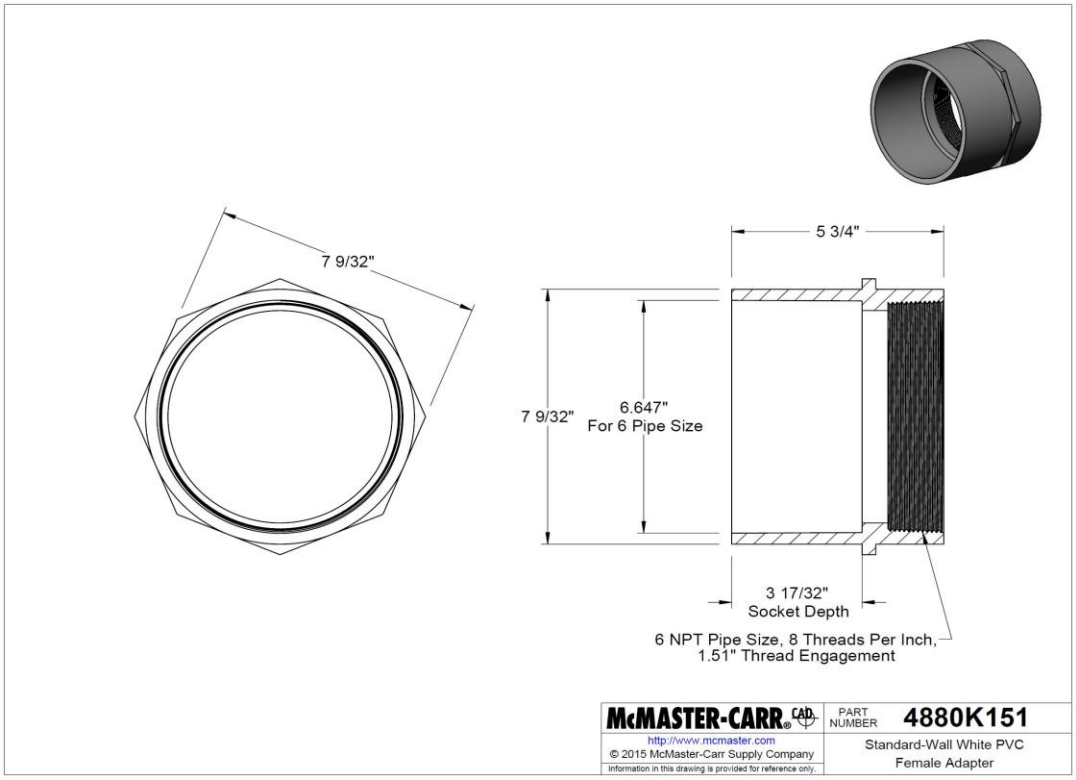

Figure D12: 6” PVC Female Adapter

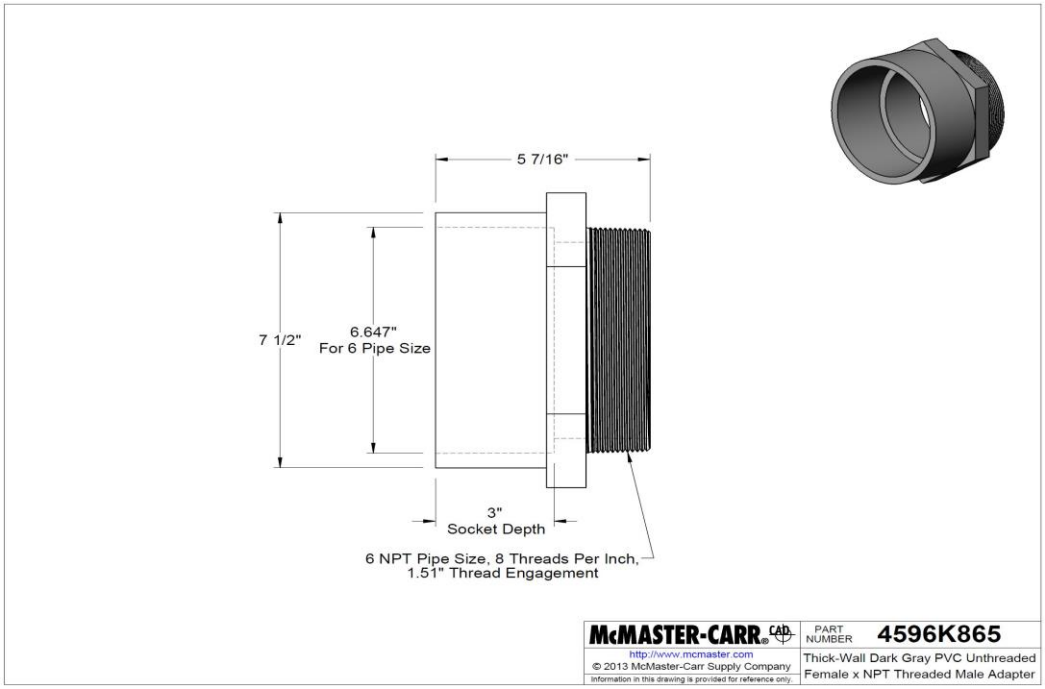

Figure D13: 6” PVC Male Adapter

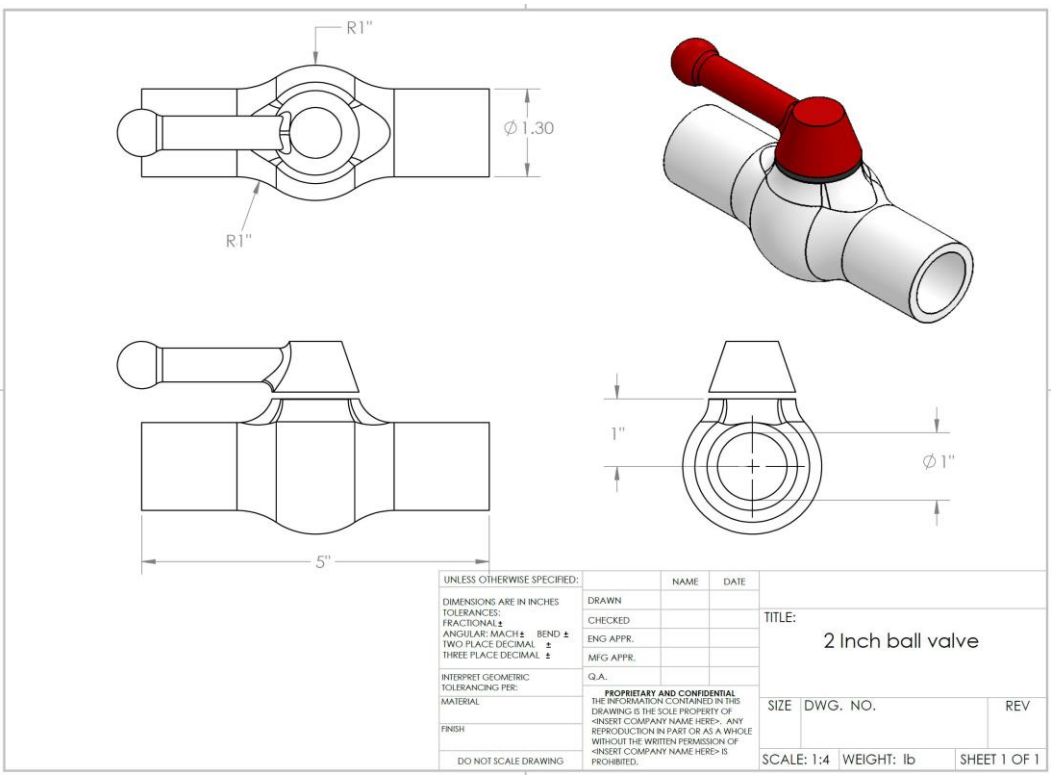

Figure D14: 2” PVC Ball Valve

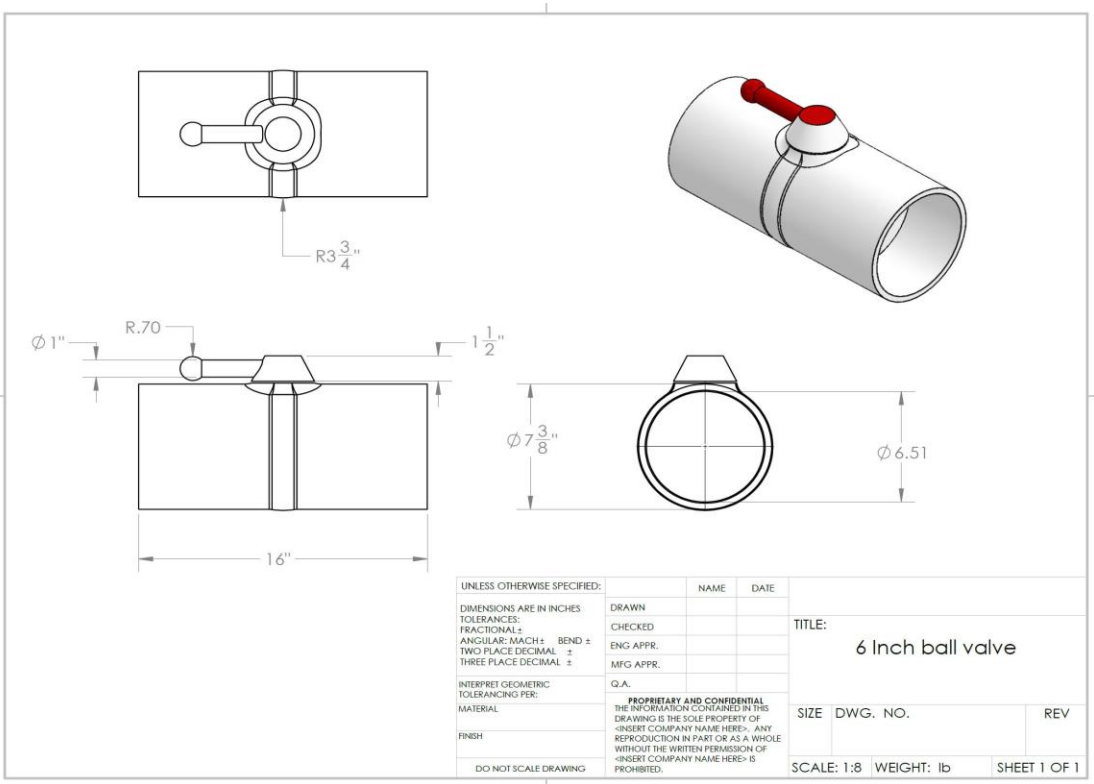

Figure D15: 6" PVC Ball Valve

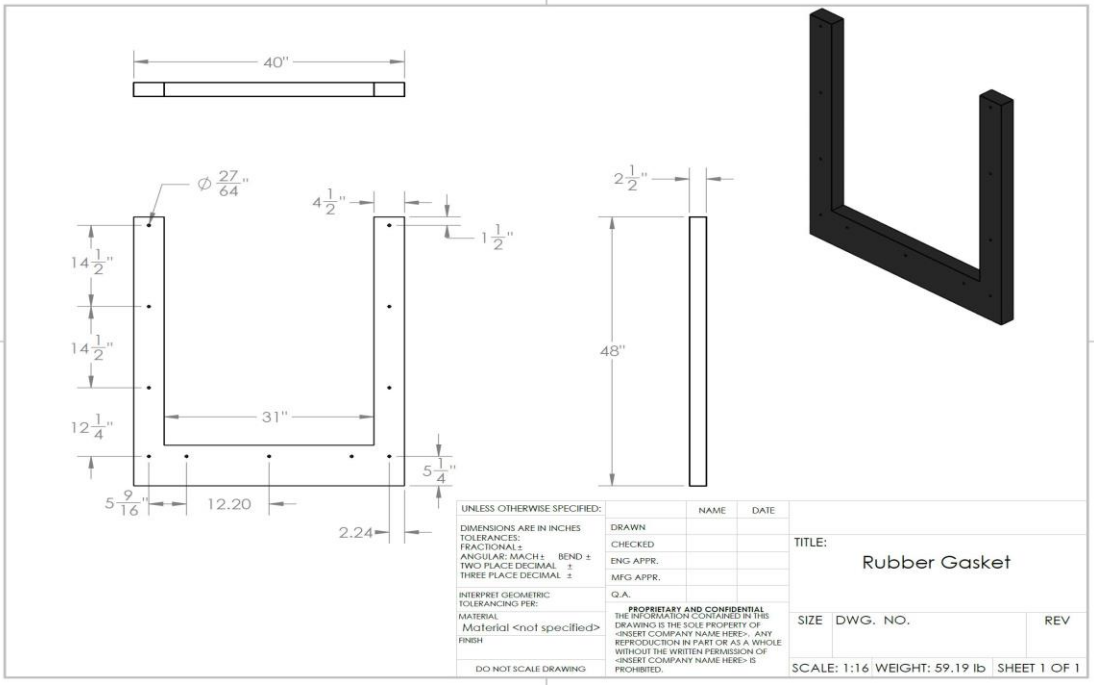

Figure D16: Rubber Gasket for tank-channel connection

CARRY MANUFACTURING, INC.
STAINLESS STEEL AXIAL FLOW SUBMERSIBLE PUMPS
STANDARD 6" DISCHARGE 316 STAINLESS STEEL MODELS

HORIZONTAL PUMP ONLY

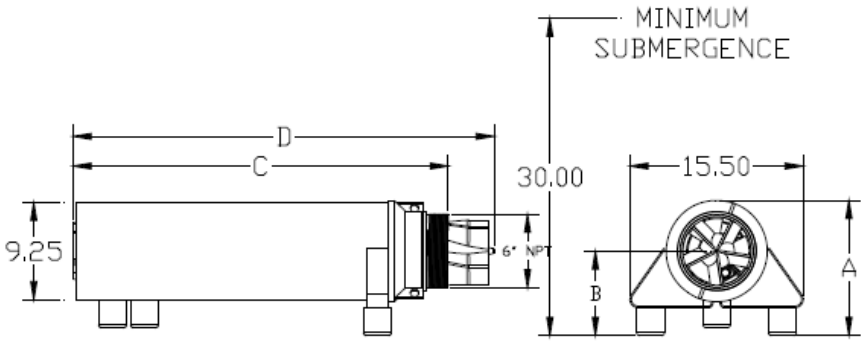

Dimensions (in inches)	Voltage	Weight (pounds)	A-Height	B-Discharge Midpoint	C-Pump Length	D-Overall Length
5HP/1PH	230	157	11.625	7.625	25.625	29.625
5HP/3PH	200, 230, 460 or 575	141	11.625	7.625	23.125	27.125
7.5HP/1PH	230	173	12.875	8.875	28.125	32.125
7.5HP/3PH	200, 230, 460 or 575	148	12.875	8.875	24.375	28.375
10HP/1PH	230	190	12.875	8.875	30.875	34.875
10HP/3PH	200, 230, 460 or 575	158	12.875	8.875	24.625	28.625
15HP/1PH	230	203	12.875	8.875	32.875	36.875
15HP/3PH	200, 230, 460 or 575	180	12.875	8.875	28.125	32.125

Figure D17: Carry Manufacturing Pump

Appendix E – Density Stratification

An interesting phenomenon in fluid dynamics is density stratification. Density stratification is the vertical variation of water density due to temperature, pressure, and salinity (Lee & Chu, 2003). If sufficiently deep enough, layers of water consist of cold, heavier fluid at the bottom and warm, lighter fluid near the surface. Earth's oceans are a great example of water stratification. Figure E1 shows a typical temperature and salinity profile of the ocean. There are three primary layers: surface/mixing layer, the pycnocline (strong density gradients), and the deep water.

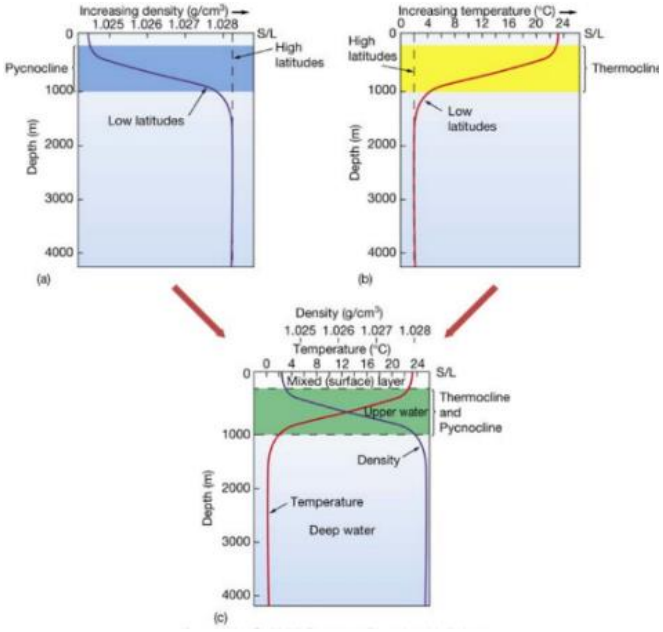

Figure E1: Visual of density gradient in halocline and thermocline.[2]

Both the surface layer and deep water have minimal changes in temperature and salinity, so the density is often constant. The pycnocline is an area of interest because its density gradient profiles (halocline for salinity and thermocline for temperature) act as a

[2] http://www.iupui.edu/~g115/mod07/lecture08.html - Copyright 2005 Pearson Prentice Hall, Inc.

barrier to nutrient and heat exchange between layers of water. The Brunt–Väisälä frequency , or buoyancy frequency, is an important parameter in this region.

$$N = \sqrt{-\frac{g}{\rho_a}\frac{\delta\rho}{\delta z}} \tag{E1}$$

The buoyancy frequency *N* is a measure of an object or fluid parcel's density and gravity driven oscillations. If *N* is greater than 0, a fluid parcel initially displaced from its original position will oscillate back and forth, creating internal waves, until oscillations are dampened out. A frequency less than zero indicates an unstable environment and the parcel will accelerate away from its original position. Figure E2 presents a simple schematic of this motion.

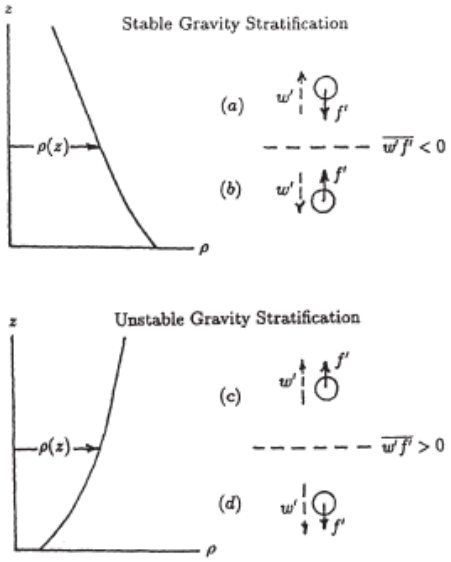

Figure E2: Fluid parcel perturbation.[3]

Density gradients in the pycnocline have been shown to act as barriers to water circulation, heat transfer, and nutrient mixing, but they are often overcome by turbulent

[3] Lee, J.H. W., & Chu, V.H. (2003). *Turbulent Jets and Plumes: A Lagrangian Approach.* Pg. 143

shear forces (Fernando, 2002). However, it remains to be seen if these gradients have an effect on organism movement (Lalli and Parsons, 2002). Wilhelmus and Dabiri (2014) showed that jets produced by brine shrimp have a profound effect on turbulent mixing in constant density environments when stimulated by light, potentially on par with surface wind and wave mixing. A density stratified water experiment may provide information regarding whether or not organisms can swim through a gradient, and if they can, to what extent their turbulent jets have on buoyancy-driven internal wave generation.

To explore vertical movement of microorganisms, similitude of density gradients must be modeled and achievable in the tank. Typical ocean values of N, converted to frequency f, range from 0.2 – 6 cycles/hour (a period of 600-18000 seconds/cycle). These gradients can be formed via several methods. Interdiffusion is the only method that does not require any external influence. Sharp boundary layers initially form between water layers, but this slowly achieves a linear gradient over a long period of time. To achieve density gradient profiles quicker, Oster (1965) proposed the double-tank method that consists of controlled flow rates and mechanical stirring of water in three tanks. Economidou and Hunt (2009) proposed two models: 1) a nonlinear profile creation by Oster's method and 2) a free drain approach, where three tanks are vertically aligned and flow through each tank is gravity driven to create various density profiles. Another process involves large scale centrifugal driven density gradients, commonly used in biology to separate cell structures for studying. This is done by mechanical rotation at angular velocities greater than 1000 revolutions per second. Figure E3 shows a schematic of each model.

(a)

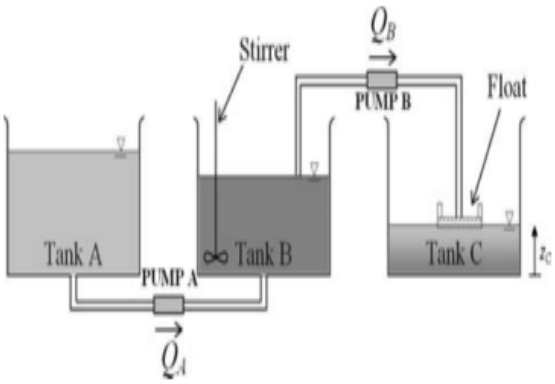

(b)

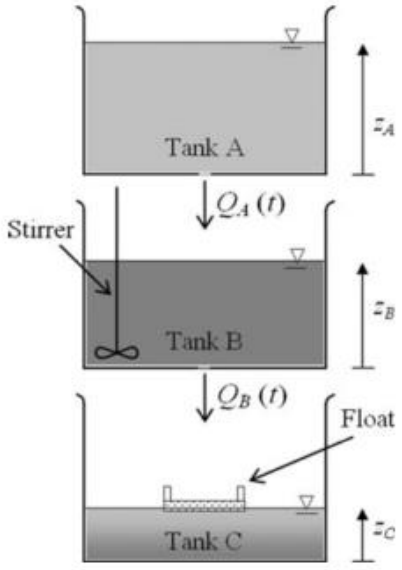

(c)

Figure E3: (a) Interdiffusion (left three) and centrifugal rotation.[4] (b) Oster's forced drain approach. (c) Free drain approach.[5]

Each method has its benefits and drawbacks, and selecting one to use depends on dimensional constraints, safety precautions, desired density profiles, and experimental time constraints. Interdiffusion is the simplest method with no dimensional constraints and no

[4] Oster, G. (1965). *1965 Scientific American, Inc.* p. 72
[5] Economidou, M., & Hunt, G.R. (2009). Density stratified environments: the double-tank method. *Exp Fluids*. p. 454, 457.

safety concerns to account for. This is best used for creating sharp boundaries with no density gradient but not recommended for gradient formation as the process takes days or even weeks to unfold. Centrifugal driven stratification is not recommended due to the high rotational speeds required. With potentially 773 gallons of water to mix, an extremely powerful stirrer would be required, and the forces exerted on the tank walls could lead to unwanted splashing and potential damage to components.

Oster's double tank method and Economidou's free drain approach are both promising options. Although both require a mechanical stirrer, the volume being mixed is half of that used with centrifugal rotation. For the double tank approach, time constraints depend on the flow rate, which may or may not be faster than gravity induced filling. Both methods have been proven to offer linear and nonlinear density gradients. However, the free drain model requires that three tanks be vertically aligned and spaced in a specific manner. Limited ceiling space and the complexity of the setup make this option unfeasible to pursue. The Oster double tank method allows both settling tanks of the water channel to work in conjunction via mechanical pumps and stirrers in a relatively safe manner to quickly model linear density gradients and is therefore recommended.

For simplification, the same notation from Figure E3 (b) will be used. The double tank method requires that fresh water from Tank A contain the same volume as the saltwater from Tank B. One immediate issue that arises with the double tank method is the three tank requirement. With an installed ball valve, the water channel can essentially be split into two tanks. A third tank can be formed by adding a partition in the polypropylene tank to create two tanks. Tank A and Tank B would thus both be in the

settling tank. Another solution is to simply purchase a tank with the required dimensions. More research is recommended in this area to consider all options.

Oster found that a linear gradient profile can be achieved by pumping fresh water from Tank A at exactly half the rate the mixed saltwater from Tank B is pumped into Tank C (the transparent tank of the water channel).

$$Q_A = \frac{1}{2} Q_B \tag{E2}$$

A mass and volume balance between the three tanks give the linear density gradient as:

$$\frac{\delta \rho}{\delta z} = \frac{1}{2}\left(\rho_A - \rho_{B,i}\right)\frac{A_c}{V_{B,i}} \tag{E3}$$

where ρ_A is the density of the fresh water in Tank A, $\rho_{B,i}$ is the initial density of the salt water in Tank B, A_C is the cross sectional area of Tank C, and $V_{B,i}$ is the initial volume of water in Tank B. $V_{B,i}$ must have the same initial volume as Tank A, $V_{A,i}$. A stirring mechanism must be provided in Tank B for homogeneity.

Excluding the volume occupied by both sides of the piping system, the summation of $V_{A,i} + V_{b,i}$ is the total volume of water to be occupied by the transparent tank. The partition method would halve the total volume of water occupied by the settling tank, and gradients profiles would extend only up to 19" inside Tank C (assuming the polypropylene settling tank is filled up the test section entrance). It is therefore recommended that a third external tank be assembled and act as Tank A or Tank B. This way, gradient profiles can extend up to 38".

Combining E2 and E3, the buoyancy frequency can be written as:

$$N = \sqrt{-g \frac{A_c}{V_{B,i}} \left(\frac{\rho_A - \rho_{B,i}}{\rho_A + \rho_{B,i}} \right)} \tag{E4}$$

The current design does not allow for any variation in the Tank C area. Utilization of the settling tank is limited by its height up to the water channel, hence the 38" gradient. This could be resolved by implementing the same method to be used for enclosing the transparent tank. Another option may be to add a specified flow rate with the same density ρ_A to Tank A and perform a mass and density balance with the added flow rate to calculate conditions for a linear gradient. With the current tank dimensions and setup, A_c and $V_{B,i}$ are known, and the relative density difference can be plotted versus buoyancy frequency and oscillation period (Figures E4-E6).

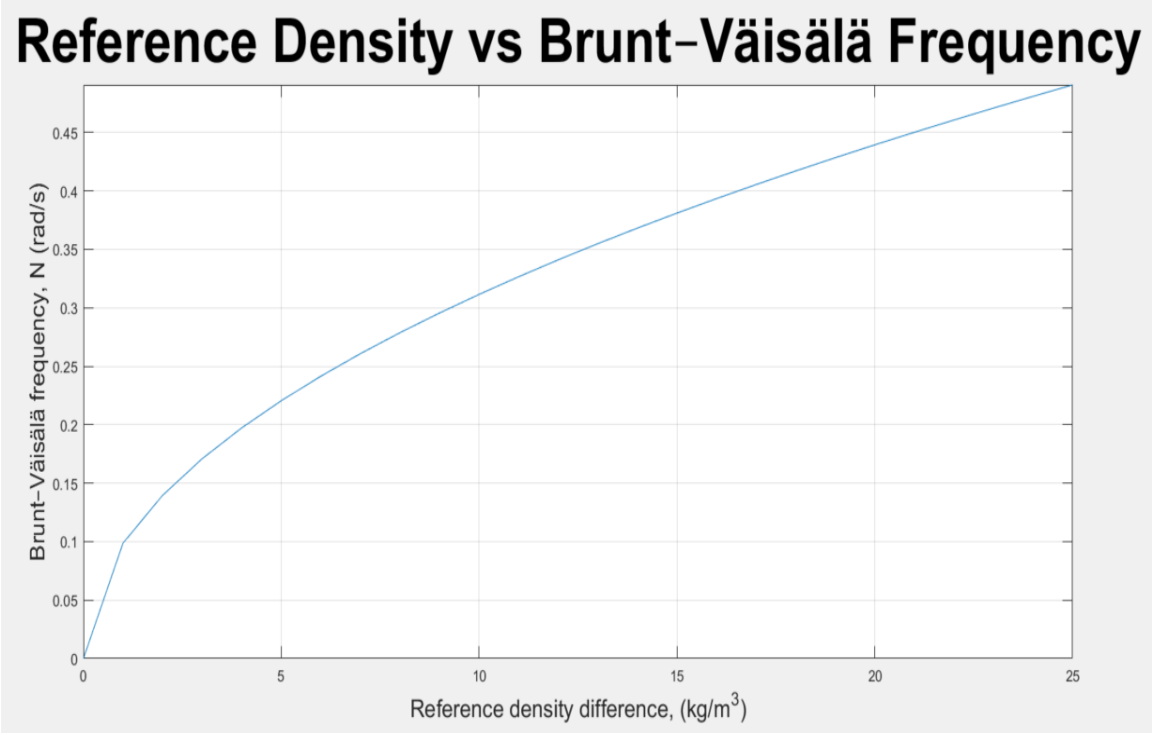

Figure E4: Reference density vs Buoyancy frequency (radians/second).

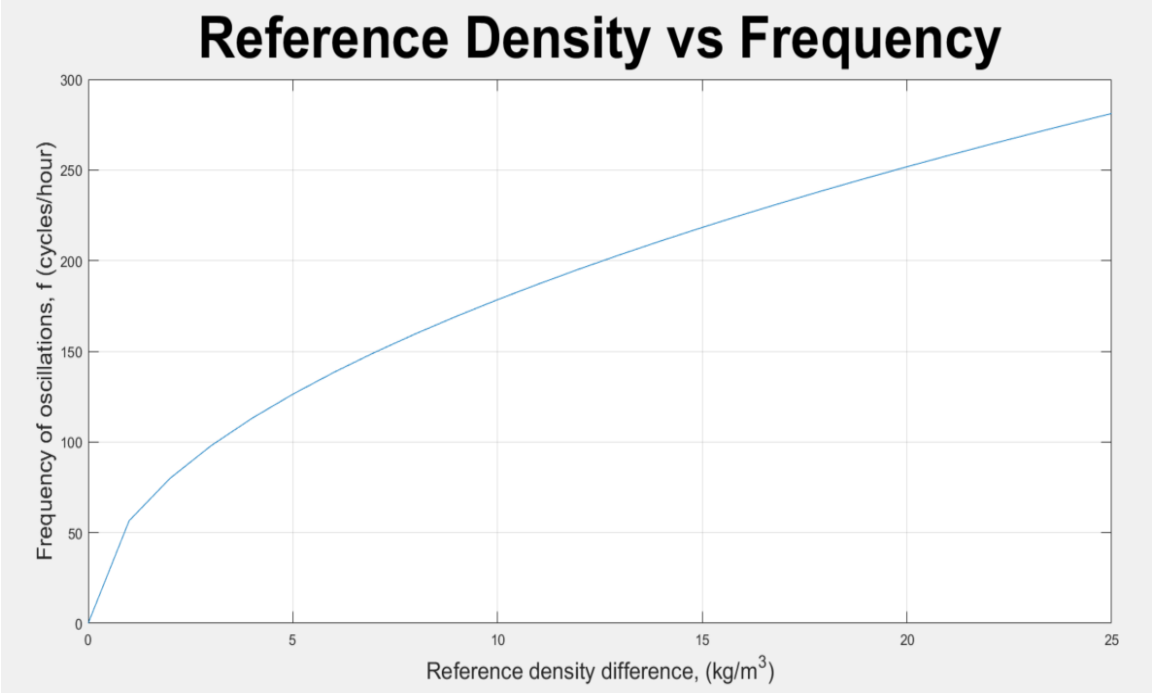

Figure E5: Reference density vs Buoyancy frequency (cycles/hour).

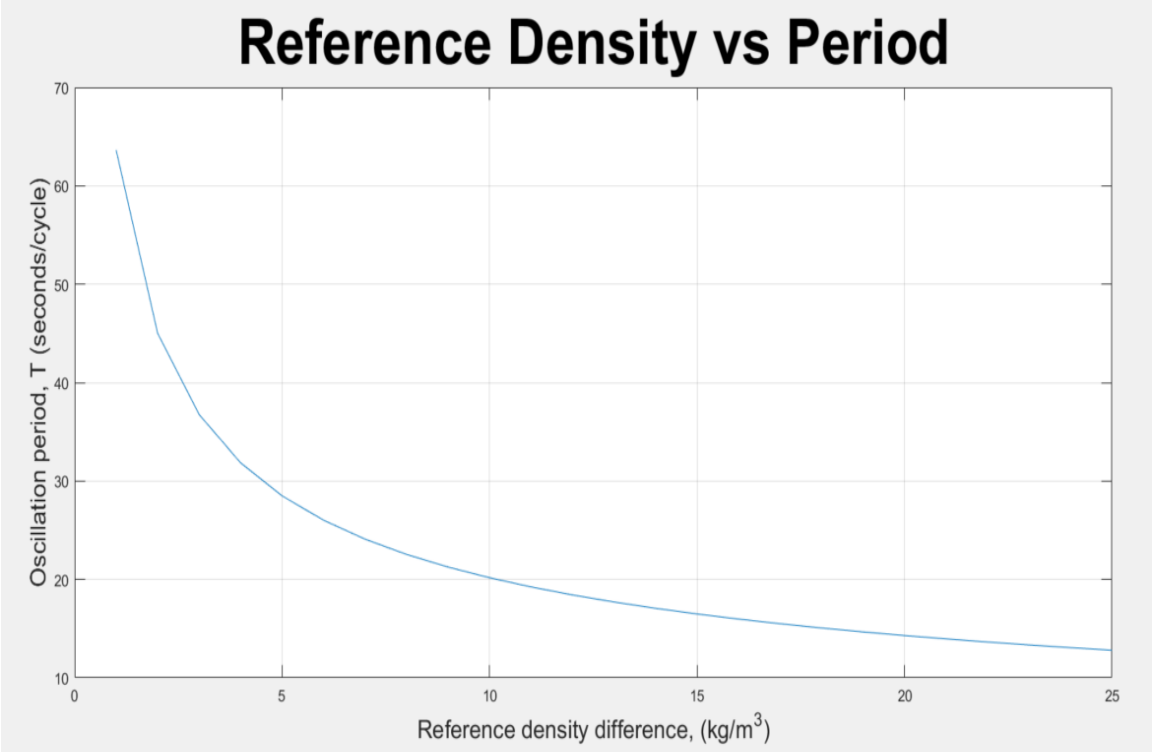

Figure E6: Reference density vs Period (seconds/cycle).

The density of water is a function of salinity, temperature, and pressure.

$$\rho = \rho(S, T, P) \tag{E5}$$

Pressure is often omitted from oceanic buoyancy models to isolate variables. At a relatively small depth compared to the ocean, pressure can be neglected in the transparent tank.

$$\rho = \rho(S, T) \tag{E6}$$

A recommended measurement method goes as follows. First, one should take salinity and temperature measurements of the homogenous mixtures for ρ_A and $\rho_{B,i}$. This may be done by salinometers or refractometers, the former being more precise. Measurements may then be used to calculate salinity and temperature with updated mathematical relationships from the United Nations Educational, Scientific and Cultural Organization (UNESCO). These can be found in Millero & Huang's "The density of seawater as a function of salinity and temperature" (2009). Once the Tank C water is stratified, tracer particles should be added for PIV measurements. Particles should be of a known density within the range of the gradient.

```
clear all
clc
close all

% Density variation based on pure fresh water (1000 kg/^m3 or 62.4 lbf/ft^3)
% and average salinity of ocean (1025 kg/m^3 or 63.99 lbf/ft^3)
%SI units
%g=9.81 m/s2, Ac=1.745 m2, VBi = 0.8778 m3, rhoA=1000 kg/m^3, rhoBi= 1025
kg/m^3
% same SI or USCS units to get rad/s
g=9.81;
Ac=1.745;
VBi=0.8778;
rhoA=1000;
rhoBi=[rhoA:1:1025]; % Variation of densities from rhoA to rhoBi
sigmat=rhoBi-rhoA; %Relative density difference
%--------------------------------------------------
N = sqrt(-g*(Ac/VBi).*(rhoA-rhoBi)./(rhoA+rhoBi)); % Buoyancy Frequency
f = N./(2*pi); % Cycles per second
T = 1./f; % Period
f = f.*3600; %Cycles per hour
%--------------------------------------------------
figure(1);
plot(sigmat,N);
ylim([0 max(N)]);
xlabel('Reference density difference, (kg/m^3)','fontsize', 16);
ylabel('Brunt–Väisälä frequency, N (rad/s)','fontsize', 16);
title('Reference Density vs Brunt–Väisälä Frequency','fontsize', 40);
grid on;

figure(2);
plot(sigmat,f);
xlabel('Reference density difference, (kg/m^3)','fontsize', 16);
ylabel('Frequency of oscillations, f (cycles/hour)','fontsize', 16);
title('Reference Density vs Frequency','fontsize', 40);
grid on;

figure(3);
plot(sigmat,T);
xlabel('Reference density difference, (kg/m^3)','fontsize', 16);
ylabel('Oscillation period, T (seconds/cycle)','fontsize', 16);
title('Reference Density vs Period', 'fontsize', 40);
grid on;
```

Appendix F: Channel Flow

Open channel flow consists of constant atmospheric pressure along the water surface, gravity driven motion, and turbulent flow unaffected by surface tension. The Reynolds number for open channel flow is given by:

$$\mathrm{Re} = \frac{UR_h}{\nu} \begin{cases} \mathrm{Re} < 500 & \text{laminar} \\ 500 < \mathrm{Re} < 2000 & \text{transitional} \\ 2000 < \mathrm{Re} & \text{turbulent} \end{cases} \tag{F1}$$

where U is the mean free stream velocity, R_h is the hydraulic radius, and ν is the kinematic viscosity. The hydraulic radius for an open rectangular channel is given by

$$R_h = \frac{A}{P} = \frac{b \cdot h}{b + 2h} \tag{F2}$$

with b as the flow width (set at 40" for the redesigned water channel) and h as the flow depth in the channel.

To determine the channel's Reynolds number, both U and R_h depend on what the user requires. The current pump installed has a maximum flow rate of 1500 gallons per minute (gpm) (3.34 ft^3/s). From a Bernoulli friction loss balance of the circulating flow system, accounting for minor losses and friction losses, the pump must overcome approximately 7.36 feet of head. The pump's performance curve shown in Figure F1 indicates that the theoretical maximum flow rate the pump can produce is approximately 1425 gpm (3.17 ft^3/s). Keeping this volumetric flow rate constant, the free stream velocity U in the channel is dependent on the depth the channel is filled up to. Plots of U vs h and Re vs h are displayed in Figure F2 and Figure F3, respectively.

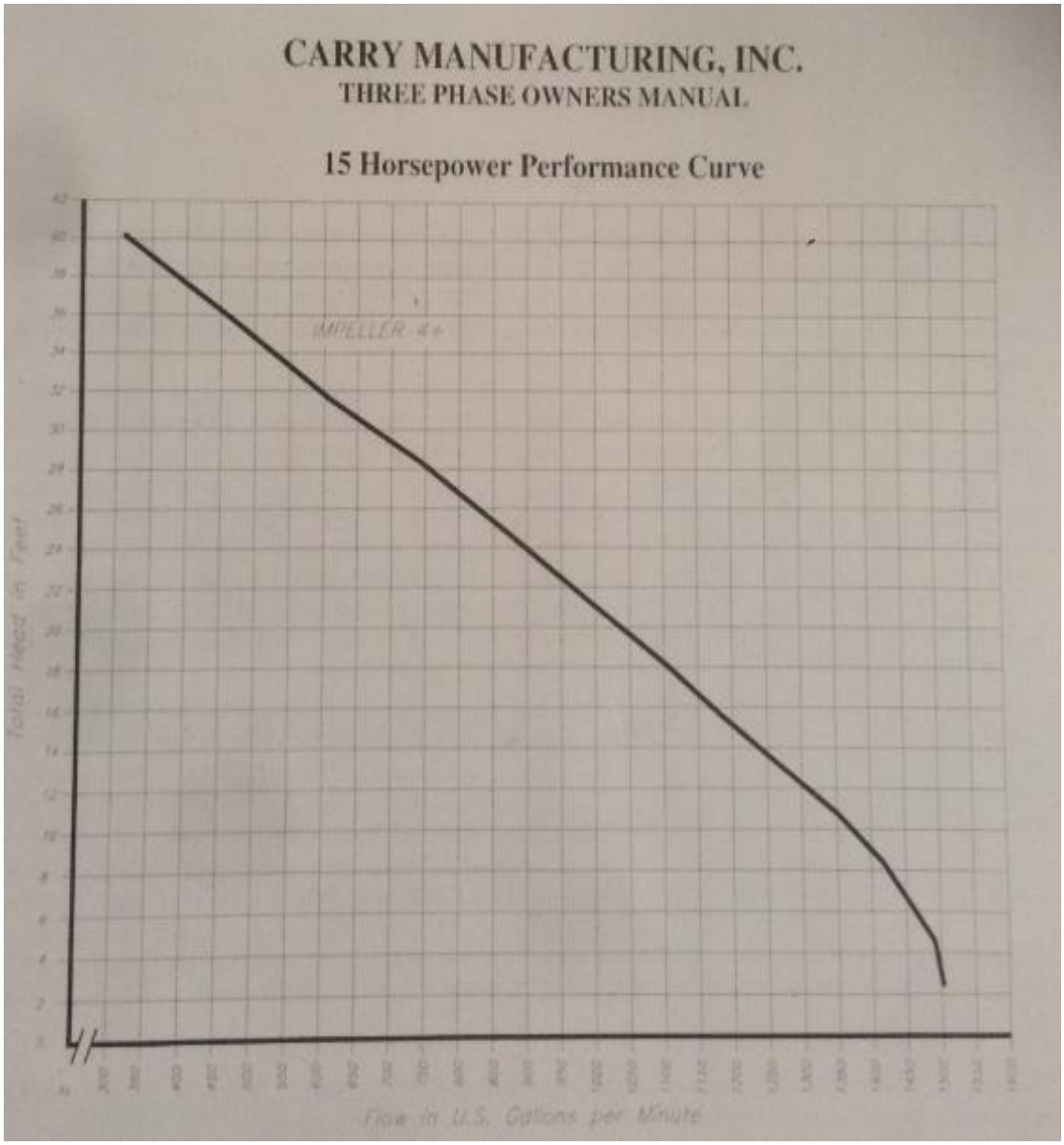

Figure F1: Carry Manufacturing Pump Performance Curve

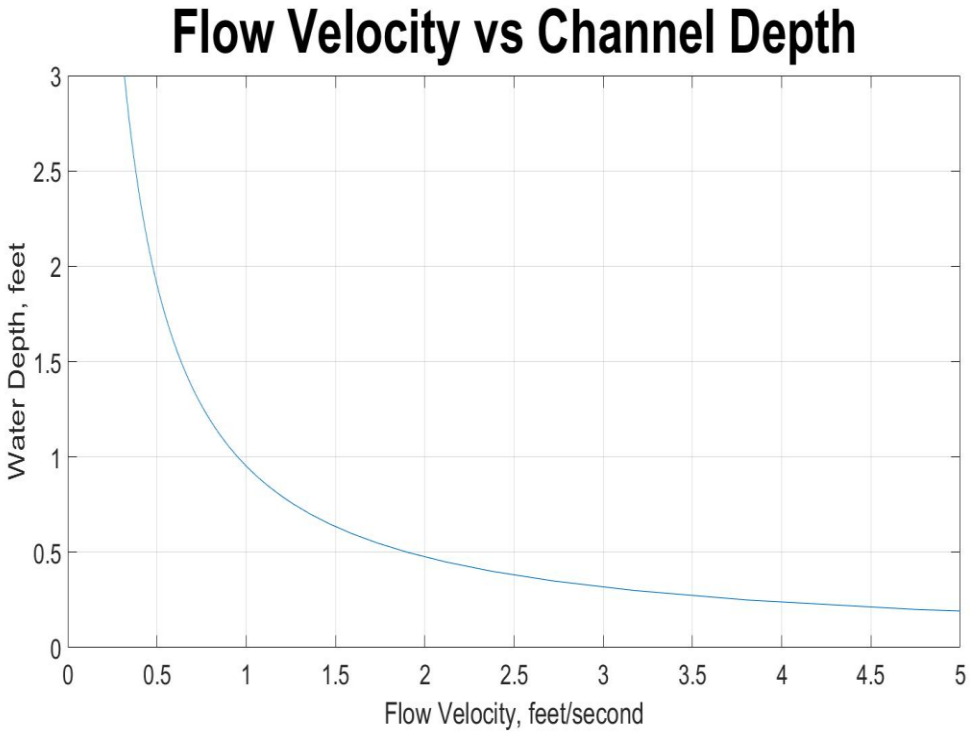

Figure F2: Channel depth vs. free stream velocity relationship.

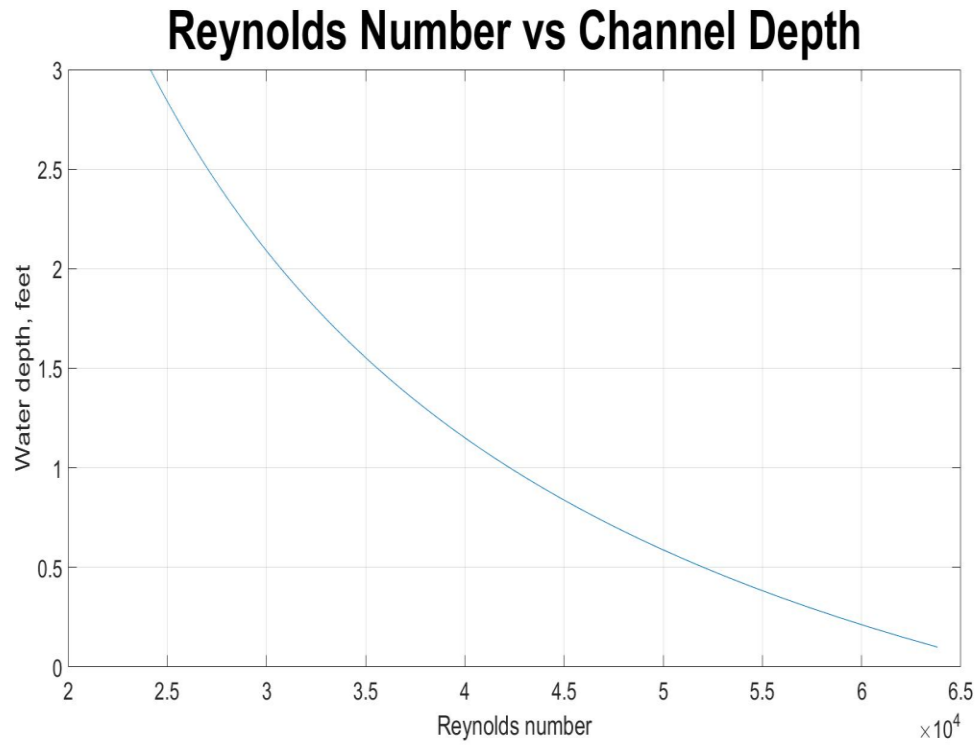

Figure F3: Channel depth vs. Reynolds number relationship.

Fluid experimentation often requires creating streamlines and fully conditioned flow in order to gather useful data. Honeycomb profiles and/or perforated screens/meshes are recommended to be added since the sharp entrance will induce flow separation eddy formation. This flow conditioning will help eliminate vortices and non-axial (turbulent intensity) fluctuations. If needed, screens or profiles can also be added at the test section outlet to reduce backflow. For testing and flow verification, PIV experimentation or a hot wire anemometer setup is recommended to determine flow velocity based off the channel depth to verify at what length a flow is fully conditioned.

Along with the channel flow, one needs to account for pump cavitation to eliminate potential damage and allow for proper operation, meaning that the net positive suction head allowed ($NPSH_a$) must always be larger than the pump's suction head requirement ($NPSH_r$). $NPSH_r$ is usually given by the pump manufacturer in graph form, and usually increases squarely with the flow rate for turbulent flow. Excluding the static head, which is dependent on the user defined depth, the system $NPSH_a$ was calculated to be approximately 32.87 feet. Unfortunately, the manufacturer of the pump did not provide a $NPSH_r$ curve or data, but instead recommended a minimum submergence of 20 inches. Since the height from the top of the pump to the bottom of the test channel is 21.25 inches, the minimum submergence is met for any water depth in the channel. Contacting the pump manufacturer, they stated that they did not have any $NPSH_r$ curves, but they had updated their minimum submergence requirement for the specific pump to 36 inches at a flow rate of 1500 gpm. If this requirement were to be followed, the test channel would need to be filled up to 14.75 inches.

The water channel setup indicates that cavitation will not be an issue as long as the recommended water depth is reached. However, air in the pump and pipes must still be flushed out before powering on the pump. This can be done by closing the ball valve and filling only one tank up to the channel height, then opening the ball valve to allow the water to push water and air out into the other tank.

```
clear all
clc
close all

%USCS units

g = 32.174; %ft/s^2
h = [0.1:0.05:3]; %water depth/height, feet
b = 3.33; %channel width, feet
A = h.*b; %flow area, feet^2
Q = 3.17; %volumetric flow rate, ft^3/s
V = Q./A; %velocity, ft/s

Perimeter = b + 2*h; %perimeter, feet
Rh = A./Perimeter; %hydraulic radius, feet
nu = 1.407E-5; %kinematic viscosity, ft^2/s
Re = (V.*Rh)./nu; %Reynolds number
%---------------------------
%subplot(2,1,1);
figure(1)
p1 = plot(V,h);
xlim([0 5]);
x1 = xlabel('Flow Velocity, feet/second');
y1 = ylabel('Water Depth, feet');
t1 = title('Flow Velocity vs Channel Depth');
set(x1,'fontsize',16);
set(y1,'fontsize',16);
set(gca,'fontsize',18);
set(t1,'fontsize',40);
%set(p1,'Xtick',0:0.25:max(V),'Ytick',0:0.5:max(h));
grid on;

%subplot(2,1,2)
figure(2);
p2 = plot(Re,h);
x2 = xlabel('Reynolds number');
y2 = ylabel('Water depth, feet');
t2 = title('Reynolds number vs Channel Depth');
set(x2,'fontsize',16);
set(y2,'fontsize',16);
set(gca,'fontsize',18);
set(t2,'fontsize',40);
%set(p2,'Xtick',0:0.5E4:max(Re),'Ytick',0:0.5:max(h));
grid on
```

Appendix G: Material Properties

Table G1: Transparent Tank Component Mechanical Properties

Transparent Tank	Material	Elastic Modulus E (psi)	Yield Strength σ_y (psi)	Tensile Strength σ_{uts} (psi)	Compressive Strength σ_{ucs} (psi)	Poisson's Ratio ν	Density, ρ (lbf/ft^3)
90 Degree Angle Beams	316 Stainless Steel	$28 \cdot 10^6$	30,000	75,000		0.26	490
Gussets	Low Carbon Steel	$29 \cdot 10^6$	36,000	58,000		0.26	490
Vertical and Horizontal Beams	Carbon Steel	$29 \cdot 10^6$	45,700	58,000		0.29	486
Bolts, Nuts, Washers	18-8 Stainless Steel	$28 \cdot 10^6$	40,000	70,000			
Glass	Tempered	$10 \cdot 10^6$	10,000	> 10000 psi	> 10,000 psi	0.23	156
Base	PVC	411,000	7,500	7,500	7,500	0.4	88
Acrylic	Plexiglass	450,000	10,500	10,500	16,000	0.35	74.25

Table G2: Test Channel Component Mechanical Properties

Test Channel	Material	Elastic Modulus E (psi)	Yield Strength σ_y (psi)	Tensile Strength σ_{uts} (psi)	Poisson's Ratio ν	Density ρ (lbf/ft^3)
Chassis	Carbon Steel	$29 \cdot 10^6$	45,700	58,000	0.29	486
Vertical Beams	Carbon Steel	$29 \cdot 10^6$	45,700	58,000	0.29	486
Horizontal Beams	Carbon Steel	$29 \cdot 10^6$	45,700	58,000	0.29	486
Flat Bars	1018 Alloy Steel	$29 \cdot 10^6$	53,700	63,800	0.29	491
90 Degree Angle Beam (Middle and Top)	HR Steel	$29 \cdot 10^6$	36,000	58,000	0.26	490
Gussets	HR Steel	$29 \cdot 10^6$	36,000	58,000	0.26	490
Glass	Annealed					156
Glass	Tempered	$10 \cdot 10^6$	10,000	> 10000 psi	0.23	156
Bolts - Support Frame	Black-oxide alloy steel	$29 \cdot 10^6$	153,000	170,000		
Bolts - Tank Connection	316 Stainless Steel	$28 \cdot 10^6$	30,000	70,000		
Washers - Support Frame	Grade 8 Steel	$29 \cdot 10^6$	130,000	150,000		
Washers - Tank Connection	316 Stainless Steel	$28 \cdot 10^6$	30,000	70,000		
Nuts - Support Frame	Grade 9 Cadmium Yellow-Chromate	$29 \cdot 10^6$	140,650	180,000		
Nuts - Tank Connection	316 Stainless Steel	$28 \cdot 10^6$	30,000	70,000		

Table G3: Plastic Tank, Sealant, and Rubber Mechanical Properties

Plastic End Tank	Material	Elastic Modulus, E (psi)	Yield Strength, σ_y (psi)	Tensile Strength, σ_{uts} (psi)	Poisson's Ratio, ν	Density, ρ (lbf/ft^3)
Settling Tank at Outlet	Polypropylene Copolymer	195,000	3,400			56.784
Miscellaneous						
Sealant	GE Silicone Type 2, GE Silicone 100% for Plastics and Plastic Sheets	N/A	N/A	N/A	N/A	N/A
Rubber Gasket/Rubber	Neoprene	N/A	N/A	900	0.49	76.75
Rubber Adhesive	High Contact Neoprene Adhesive 1357, Pliobond 25 VOC Compliant	N/A	N/A	N/A	N/A	N/A

Appendix H: Standard Operating Procedure

Bourns Hall B140: Water Channel Maintenance
STANDARD OPERATING PROCEDURE

Type of SOP: ☒ Process ☐Hazardous Chemical ☐ Hazard Class

1. HAZARD OVERVIEW

Cleaning and maintenance will often require physically entering the channel. Any sign of water leakage from any location requires immediate attention. In case of a catastrophic failure, potential harm to students and water damage to equipment is assessed. Water filling/draining and pump maintenance and setup is also reviewed.

2. PERSONAL PROTECTIVE EQUIPMENT (PPE)

a. Foot Protection
Closed toe shoes only. Non slippery footwear.

b. Hand Protection
At a minimum, wear a nitrile chemical-resistant glove if dealing with cleaning supplies or silicone addition/removal.

3.

3. PROTOCOL/PROCEDURES

a. Silicone Removal/Reapplication
i. Put on appropriate PPE. Primary need are gloves.
ii. Wet the area to be scraped with water. Scrape parallel to glass with minimal force, ensuring not to scratch glass. Extra precaution is needed here.
iii. Add new layer of silicone on tank, smother down.
iv. Recommended wait time before water testing is 24 hours.

b) Filling/Draining Water Channel
i. Close the two small ball valves and the large one for the piping system. The glass tank is to be filled first.
ii. Fill using faucets. Ensure plastic tubing is stable and will not flail. Future recommendation should ensure a more stable method.
iii. Once water level reaches test section, open large ball valve to flush out air.
iv. Continue filling until desired height is reached.
v. Drain by opening smaller ball valves. If instruments need to be rolled on the other side of the water channel, PVC might need to be replaced with flexible tubing.

c. Pump Startup
    1. Before turning on the main power, water depth in water channel must be at a minimum at the same height as the horizontal annealed glass of the test section. Priming the pump.
    2. Turn main power switch on.
    3. Variable Frequency Drive (VFD) will start where previously left off.
    4. Ensure pump calibrated with appropriate measurement tools.
    5. Check that cavitation is not occurring (water height). If so, either slow pump impeller speed or add more water to the system.

4. SPECIAL HANDLING PROCEDURES AND STORAGE REQUIREMENTS

a. Instrument implementation/modifications that will be added must have a separate SOP in place in terms of installation and removal if required or deemed a hazard to the safety of the water channel or people.

5. SPILL AND INCIDENT PROCEDURES

Mop up water leaks and spills to prevent falls. If leaking, immediately flush system for analyzing leaking joints.
Medical Emergency - Dial 911 and EH&S 951-827-5528

Refer to "Injuries and Medical Treatment" Flipchart posted in the laboratory.

6. WASTE DISPOSAL

All waste must be disposed through the EH&S Hazardous Waste Program. Staff dealing with hazardous waste disposal should have completed UCR Hazardous Waste Management training-http://ehs.ucr.edu/training/online/hwm/indexlms.html

General silicone waste disposal guidelines: Throw excess silicone and rubber in common waste.

7. PRIOR APPROVAL/REVIEW REQUIRED

All work with water channel must be pre-approved by the Principal Investigator prior to use and all training must be well documented. In addition, the following shall be completed:

- Documented specific training and specific training on the techniques and processes to be used.
- Read and understand the relevant Safety Data Sheet.
- Demonstrate competence to perform work.

A review of this SOP and re-approval is required when there are any changes to procedures, personnel, equipment, or when an incident or near miss occurs.

8. DESIGNATED AREA

N/A

9. SAFETY DATA SHEETS

Online SDS can be found at https://ehs.ucr.edu/services/msds.html

10. DETAILED PROTOCOL

When working in the lab, a laboratory worker must:

1. Not work alone;
2. Be cognizant of all of the SDS and safety information presented in this document;
3. Follow all related SOPs in the laboratory SOP bank (PPE, drill techniques, waste disposal, etc. as appropriately modified by any specific information in the SDS information presented in this document);
4. Discuss ALL issues or concerns regarding the water channel with the PI prior to its use.

If there is an unusual or unexpected occurrence when using this material(s), the occurrence must be documented and discussed with the Principal Investigator or Lab Supervisor and others who might be using the stratification tank. Unusual or unexpected occurrences might include glass breakage or failure and water leakage.

_____

Principal Investigator or Lab Supervisor SOP Approval

Print name _____Signature_____

Approval Date: